STEM CELLS

The fountain of bone growth

Bone elongation requires the maintenance of a growth plate of cartilage. Two studies have now identified stem cells specific to this structure that give rise to both cartilage cells and bone-marrow stem cells. SEE LETTER P.234

MANUELA WUELLING & ANDREA VORTKAMP

The growth of long bones in young mammals (including children) is driven by the growth plate, a zone of cartilage that separates each end of the bone from the main shaft. The growth plate contains three distinct types of cartilage cell (chondrocyte). Round chondrocytes in the resting zone of the growth plate differentiate into flat, proliferating chondrocytes that form columns along the bone's longitudinal axis. These cells later become hypertrophic chondrocytes that cease to proliferate and are replaced by bone and bone marrow. Consequently, growth-plate chondrocytes need to be replenished continuously and the stem cells that fuel this process have long been sought. On page 234, Newton *et al.*[1] and, previously, Mizuhashi *et al.*[2] have identified a type of skeletal stem cell in the resting zone of mouse bones that gives rise to all types of growth-plate chondrocyte, as well as some of the long-lived stem cells of the bone-marrow stroma (non-blood-lineage cells).

Both groups tracked the descendants of individual chondrocytes by genetically modifying the cells to express various fluorescent proteins. The authors identified slowly dividing cells in the resting zone that give rise to monoclonal (originating from a single cell) columns of proliferating and hypertrophic chondrocytes that span the entire growth plate (Fig. 1).

The newly identified cells expressed stem-cell markers and had the potential to differentiate into multiple cell types. Furthermore, when labelled in juvenile mice, the cells continued to generate columns of chondrocytes into adulthood. Newton *et al.* also investigated how the cells divide, and found that they are maintained as dormant cells, but occasionally undergo an asymmetric cell division that produces one self-renewing cell and another cell that is prone to differentiation. Together, these observations demonstrate the stem-cell character of the newly identified cells and support the hypothesis that rare, asymmetric stem-cell divisions refill the chondrocyte pool of the growth plate, which is expanded further by the transient proliferation of the stem cells' daughter cells (flat chondrocytes).

How diverse are the stem cells identified in the two studies? Newton *et al.* labelled chondrocytes that express type II collagen. Such cells are likely to include the population of cells expressing parathyroid hormone-related protein (PTHrP) that were tracked by Mizuhashi and colleagues. Notably, although resting-zone stem cells clearly belong to the chondrocyte lineage, Mizuhashi and colleagues found that they express a comparable set of stem-cell markers and undergo a maturation process similar to that of bone-marrow stem cells. The mechanisms that regulate the sequence of differentiation of both stem-cell types are, however, still to be deciphered.

Where do the resting-zone stem cells come from? Embryonic bone growth, like postnatal bone growth, is driven by the proliferation of chondrocytes, followed by hypertrophic differentiation and the replacement of chondrocytes by bone. The process results in an ossified bone shaft that is flanked by cartilage at both ends. Newton *et al.* labelled embryonic chondrocytes and found that some develop into resting-zone stem cells. These experiments also revealed that, before birth, individual columns of proliferating and hypertrophic chondrocytes have a multiclonal origin, rather than being derived from a single, self-renewing stem cell. This observation implies that embryonic and postnatal bone growth is organized in surprisingly different ways.

How do cells derived from embryonic chondrocytes acquire a stem-cell character? Both studies show that the manifestation of self-renewing potential is linked to the generation of secondary ossification centres (areas

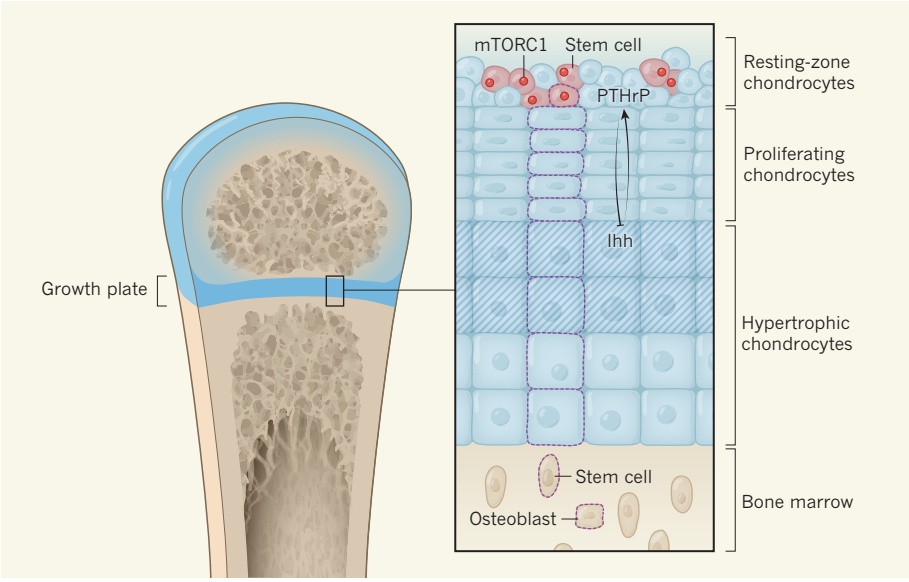

Figure 1 | How long bones grow. The postnatal growth plate of a bone, which is made of cartilage, is located between the end of the bone and its shaft (cartilage shown in blue, ossified tissue in brown). The growth plate can be divided into a resting zone that contains round cartilage cells (chondrocytes); a zone that is formed by columns of flat, proliferating chondrocytes; and a zone comprising large (hypertrophic), non-proliferating chondrocytes. Newton *et al.*[1] show that the resting zone contains stem cells (red) that form monoclonal (originating from a single cell) columns of flat and hypertrophic chondrocytes, some of which become bone-forming cells (osteoblasts) or stem cells of the bone-marrow stroma (which are not from the blood-cell lineage). One resting-zone stem cell and the descendants of that single cell have a dashed outline. The mammalian target of rapamycin complex 1 (mTORC1) signalling pathway maintains the self-renewal potential of resting-zone stem cells. Parathyroid hormone-related protein (PTHrP), produced in the resting zone, and the protein Indian hedgehog (Ihh), produced by early-differentiated hypertrophic chondrocytes (cross-hatched cells), interact to regulate the proliferation and differentiation of growth-plate chondrocytes, including resting-zone stem cells.

where bone tissue forms) at the ends of bones soon after birth. Newton *et al.* investigated the mammalian target of rapamycin complex 1 (mTORC1) pathway, which has been reported to regulate stem-cell function[3]. They found that chondrocyte-specific activation of mTORC1 signalling leads to a shift from asymmetric to symmetric stem-cell divisions, and consequently to an increased number of stem cells in the resting zone. These observations strongly support a role for mTORC1 in regulating the self-renewal potential of resting-zone stem cells.

Both groups also analysed the role of the protein Indian hedgehog (Ihh), a member of the Hedgehog family of growth factors that is expressed in early-differentiated hypertrophic chondrocytes. Ihh has been shown to induce the expression of PTHrP in resting-zone chondrocytes, which in turn inhibits the premature initiation of hypertrophy in proliferating cells[4]. Additionally, both Ihh and PTHrP activate chondrocyte proliferation[3].

Newton *et al.* and Mizuhashi *et al.* provide evidence that the inhibition of Hedgehog signalling reduces the length of chondrocyte columns. Newton and colleagues also observed increased proliferation and the expression of genes targeted by Hedgehog proteins in resting-zone cells after activation of the Hedgehog pathway. These findings suggest that Hedgehog signalling has a role in controlling the stem-cell character of resting-zone cells.

However, given that Ihh regulates PTHrP expression directly, the observed changes in chondrocyte-column length and cell proliferation might also be a consequence of altered PTHrP levels. Furthermore, when Newton *et al.* inhibited Hedgehog signalling and activated the mTORC1 pathway simultaneously, some stem cells moved from the resting zone into the proliferating zone without differentiating into flat cells. Together, these observations support a role for Ihh in regulating stem-cell proliferation rather than stem-cell identity. Given that the interaction between Ihh and PTHrP signalling is complex, it will be challenging to distinguish clearly between the roles of Ihh as a regulator of stem-cell proliferation, PTHrP expression and the induction and maintenance of 'stemness'.

The model of how cartilage is replaced by bone has changed substantially in the past few years. Previously, hypertrophic chondrocytes were thought to die and then be replaced by bone-forming cells called osteoblasts. However, more recent fate-mapping studies have shown that a fraction of hypertrophic chondrocytes differentiate into bone-forming osteoblasts or long-lived stem cells and progenitor cells of the bone-marrow stroma[5–7]. Mizuhashi *et al.* now demonstrate that cells that are descendants of resting-zone stem cells contribute to the bone-marrow stroma. Therefore, such stem cells seem to follow an unusual path of differentiation, transforming from stem cells of the chondrocyte lineage into differentiated chondrocytes, and then into multilineage stem cells of the bone-marrow stroma.

Future investigations should clarify how many of the postnatal bone-marrow stem cells descend from resting-zone stem cells, and whether these postnatal cells differ functionally from other bone-marrow cells. Given that bone-marrow-derived skeletal stem cells are required for bone turnover and fracture repair throughout a person's life, deciphering the specific features of the chondrocyte-derived population will be of high clinical relevance.

The identification of a growth-plate-specific skeletal stem cell is an important step towards understanding human skeletal growth and associated diseases, but many questions remain. Follow-up studies need to determine which mechanisms besides Hedgehog and mTORC1 signalling induce and maintain the stem-cell character of these cells, which type of embryonic chondrocyte evolves into a resting-zone stem cell, and how the induction of that process is linked to the formation of secondary ossification centres.

Further studies also need to clarify how the differentiation of stem cells in the resting zone is regulated, and which components of the chondrocyte-specific extracellular matrix (the network of proteins and sugar molecules that surrounds cells) are required to generate a stem-cell niche. Finally, given that some hypertrophic chondrocytes differentiate into osteoblasts and bone-marrow stem cells, whereas others die[5–7], it is tempting to ask whether the fate of hypertrophic cells is already determined by the distinct subtypes of resting-zone stem cell from which they originate. ■

Manuela Wuelling *and* **Andrea Vortkamp**
are at the Centre for Medical Biotechnology, Department of Developmental Biology, University Duisburg-Essen, 45141 Essen, Germany.
e-mails: manuela.wuelling@uni-due.de; andrea.vortkamp@uni-due.de

1. Newton, P. T. *et al. Nature* **567**, 234–238 (2019).
2. Mizuhashi, K. *et al. Nature* **563**, 254–258 (2018).
3. Ito, K. & Suda, T. *Nature Rev. Mol. Cell Biol.* **15**, 243–256 (2014).
4. Ohba, S. *J. Dev. Biol.* **4**, E20 (2016).
5. Park, J. *et al. Biol. Open* **4**, 608–621 (2015).
6. Yang, L., Tsang, K. Y., Tang, H. C., Chan, D. & Cheah, K. S. *Proc. Natl Acad. Sci. USA* **111**, 12097–12102 (2014).
7. Zhou, X. *et al. PLoS Genet.* **10**, e1004820 (2014).

This article was published online on 27 February 2019.

INFORMATION SCIENCE

Machine learning in quantum spaces

Ordinary computers can perform machine learning by comparing mathematical representations of data. An experiment demonstrates how quantum computing could use quantum-mechanical representations instead. SEE LETTER P.209

MARIA SCHULD

Machine learning and quantum computing have their staggering levels of technology hype in common. But certain aspects of their mathematical foundations are also strikingly similar. On page 209, Havlíček *et al.*[1] exploit this link to show how today's quantum computers can, in principle, be used to learn from data — by mapping data into the space in which only quantum states exist.

One of the first things one learns about quantum computers is that these machines are extremely difficult to simulate on a classical computer such as a desktop PC. In other words, classical computers cannot be used to obtain the results of a quantum computation. The reason is that a lot of numbers are required to describe each internal step of the computation. Consider the multi-step procedure that many people learn at school for dividing large numbers. If this were a quantum computation being simulated on a classical computer, every intermediate step could easily need more numbers to describe it than there are atoms in the observable Universe.

The state of a quantum system when described by a collection of numbers is known as a quantum state. And if a quantum state is associated with many values, it is said to 'live' in a large space. For certain quantum computers that are based on continuous variables, such spaces can even be infinitely large.

Machine learning, by comparison, analyses data that live in much smaller spaces — that is, the data are described by many fewer values. For example, a photograph that contains one million pixels records just three million numbers to describe the amount of red, green and blue in each pixel. A prominent task of machine learning could be to guess the content of the image, or to produce similar images. However, a well-established theory in machine learning called kernel methods[2] treats data in a way that has a similar feel to how quantum theory deals with data.

In a nutshell, kernel methods carry out

LETTER

https://doi.org/10.1038/s41586-018-0662-5

Resting zone of the growth plate houses a unique class of skeletal stem cells

Koji Mizuhashi[1], Wanida Ono[1], Yuki Matsushita[1], Naoko Sakagami[1], Akira Takahashi[1], Thomas L. Saunders[2], Takashi Nagasawa[3], Henry M. Kronenberg[4] & Noriaki Ono[1]*

Skeletal stem cells regulate bone growth and homeostasis by generating diverse cell types, including chondrocytes, osteoblasts and marrow stromal cells. The emerging concept postulates that there exists a distinct type of skeletal stem cell that is closely associated with the growth plate[1–4], which is a type of cartilaginous tissue that has critical roles in bone elongation[5]. The resting zone maintains the growth plate by expressing parathyroid hormone-related protein (PTHrP), which interacts with Indian hedgehog (Ihh) that is released from the hypertrophic zone[6–10], and provides a source of other chondrocytes[11]. However, the identity of skeletal stem cells and how they are maintained in the growth plate are unknown. Here we show, in a mouse model, that skeletal stem cells are formed among PTHrP-positive chondrocytes within the resting zone of the postnatal growth plate. PTHrP-positive chondrocytes expressed a panel of markers for skeletal stem and progenitor cells, and uniquely possessed the properties of skeletal stem cells in cultured conditions. Cell-lineage analysis revealed that PTHrP-positive chondrocytes in the resting zone continued to form columnar chondrocytes in the long term; these chondrocytes underwent hypertrophy, and became osteoblasts and marrow stromal cells beneath the growth plate. Transit-amplifying chondrocytes in the proliferating zone—which was concertedly maintained by a forward signal from undifferentiated cells (PTHrP) and a reverse signal from hypertrophic cells (Ihh)—provided instructive cues to maintain the cell fates of PTHrP-positive chondrocytes in the resting zone. Our findings unravel a type of somatic stem cell that is initially unipotent and acquires multipotency at the post-mitotic stage, underscoring the malleable nature of the skeletal cell lineage. This system provides a model in which functionally dedicated stem cells and their niches are specified postnatally, and maintained throughout tissue growth by a tight feedback regulation system.

We first defined the formation of PTHrP^{+} chondrocytes in the growth plate using a *Pthrp-mCherry* (*Pthrp* is also known as *Pthlh*) knock-in reporter allele (Extended Data Fig. 1a, see also Supplementary Information). During the fetal stage, PTHrP–mCherry^{+} cells were mitotically active and localized within the Sox9^{+} perichondrial region (Extended Data Fig. 1b). Although this pattern continued at birth (Fig. 1a), a distinct group of PTHrP–mCherry^{+} chondrocytes appeared in the central area of the growth plate that is devoid of proliferation at postnatal day (P)3 (Extended Data Fig. 1c). These PTHrP–mCherry^{+} chondrocytes increased markedly in number between P6 and P9, and occupied a well-defined zone in the growth plate (Fig. 1b–d, Extended Data Fig. 1c); these chondrocytes were less proliferative than their counterparts in the proliferating zone (EdU^{+}; 6.1 ± 2.3% of mCherry^{+} cells versus 30.5 ± 3.2% of proliferating chondrocytes at P9, $n = 3$ mice). Therefore, PTHrP–mCherry^{+} chondrocytes in the resting zone ('resting chondrocytes') develop in the postnatal growth plate, which is closely associated with the formation of secondary ossification centres. Flow cytometry analysis revealed that PTHrP–mCherry^{+} cells were exclusively found in the CD45^{neg} cell population in the growth plate (Fig. 1e), and were completely absent in the CD45^{neg} population in bone and bone marrow cells (Extended Data Fig. 2a). PTHrP–mCherry^{+} cells in the growth plate did not express Col1a1(2.3kb)-GFP (Extended Data Fig. 2b), which indicates that PTHrP–mCherry is specifically expressed by growth-plate chondrocytes but not by osteoblasts or bone marrow stromal cells. We next asked whether PTHrP–mCherry^{+} resting chondrocytes express a panel of cell-surface markers for transplantable skeletal stem and progenitor cells[3]—particularly three subsets of skeletal stem and progenitor populations (integrin alpha V (CD51)$^{+}$Thy-1 (CD90)$^{-}$); mouse skeletal stem cells (mSSCs) (CD105^{-}CD200^{+}), pre-bone, cartilage and stromal progenitors (pre-BCSPs) (CD105^{-}CD200^{-}), and bone, cartilage and stromal progenitors (BCSPs) (CD105^{+}). A large majority of CD45^{-}Ter119^{-}CD31^{-} growth-plate cells—including both mCherry^{-} and mCherry^{+} fractions—were in a CD51^{+}CD90^{-} skeletal stem and progenitor population (Fig. 1f, left panels). Among CD45^{-}Ter119^{-}CD31^{-}CD51^{+}CD90^{-}mCherry^{+} cells, 49.2 ± 8.4%, 23.4 ± 8.4% and 27.4 ± 16.5% were CD105^{-}CD200^{+} (mSSCs), CD105^{-}CD200^{-} (pre-BCSPs) and CD105^{+} (BCSPs), respectively (Fig. 1f, right panels; see also Extended Data Fig. 2c, d). Conversely, 41.6 ± 4.4%, 31.7 ± 6.2% and 53.4 ± 16.9% of mSSCs, pre-BCSPs and BCSPs, respectively, were positive for PTHrP–mCherry (Extended Data Fig. 2e). Therefore, PTHrP–mCherry^{+} resting chondrocytes represent a substantial subset of immunophenotypically defined skeletal stem and progenitor cells in the growth plate.

We next determined whether PTHrP^{+} resting chondrocytes behave as stem cells in vivo, by using a *Pthrp-creER* bacterial artificial chromosome transgenic line (L909, Extended Data Fig. 3a; see also Supplementary Information, Supplementary Methods and Extended Data Fig. 10 for establishment of this system and validation of tamoxifen-negative controls). Analysis of *Pthrp*$^{mCherry/+}$*;Pthrp-creER;R26R*^{ZsGreen} mice revealed that ZsGreen^{+} cells largely overlapped with mCherry^{+} cells shortly after a tamoxifen pulse at P6 (Extended Data Fig. 3b–d). The percentage of CD105^{+} cells within the ZsGreen^{+} cell population was significantly lower than that within the mCherry^{+} cell population (Extended Data Fig. 3e), which indicates that *Pthrp-creER* preferentially marks an immature subset of PTHrP–mCherry^{+} cells. An EdU label-exclusion assay of *Pthrp-creER;R26R*^{tdTomato} mice pulsed with tamoxifen at P6 revealed that a large majority of tdTomato^{+} cells were resistant to EdU incorporation (Extended Data Fig. 3f, EdU^{+}; 7.7 ± 2.0% of tdTomato^{+} cells versus 61.1 ± 11.5% of proliferating-zone chondrocytes, $n = 3$ mice), which demonstrates that *Pthrp-creER* specifically marks resting chondrocytes (Extended Data Fig. 3g). These PTHrP^{+} resting chondrocytes did not express Grem1[4] (Extended Data Fig. 3h). Subsequently, we traced the fate of PTHrP^{+} resting chondrocytes labelled on P6 (hereafter, PTHrP^{CE}-P6 cells) in vivo. After remaining within the resting zone at P12 (Fig. 2a; see also Extended Data Fig. 3g), PTHrP^{CE}-P6 cells first formed short columns (composed of <10 cells) (Fig. 2b, arrowhead) and subsequently formed longer columns (composed of >10 cells) that originated from the

[1]University of Michigan School of Dentistry, Ann Arbor, MI, USA. [2]Transgenic Animal Model Core, University of Michigan Medical School, Ann Arbor, MI, USA. [3]Laboratory of Stem Cell Biology and Developmental Immunology, Graduate School of Frontier Biosciences, Osaka University School of Medicine, Suita, Japan. [4]Endocrine Unit, Massachusetts General Hospital and Harvard Medical School, Boston, MA, USA. *e-mail: noriono@umich.edu

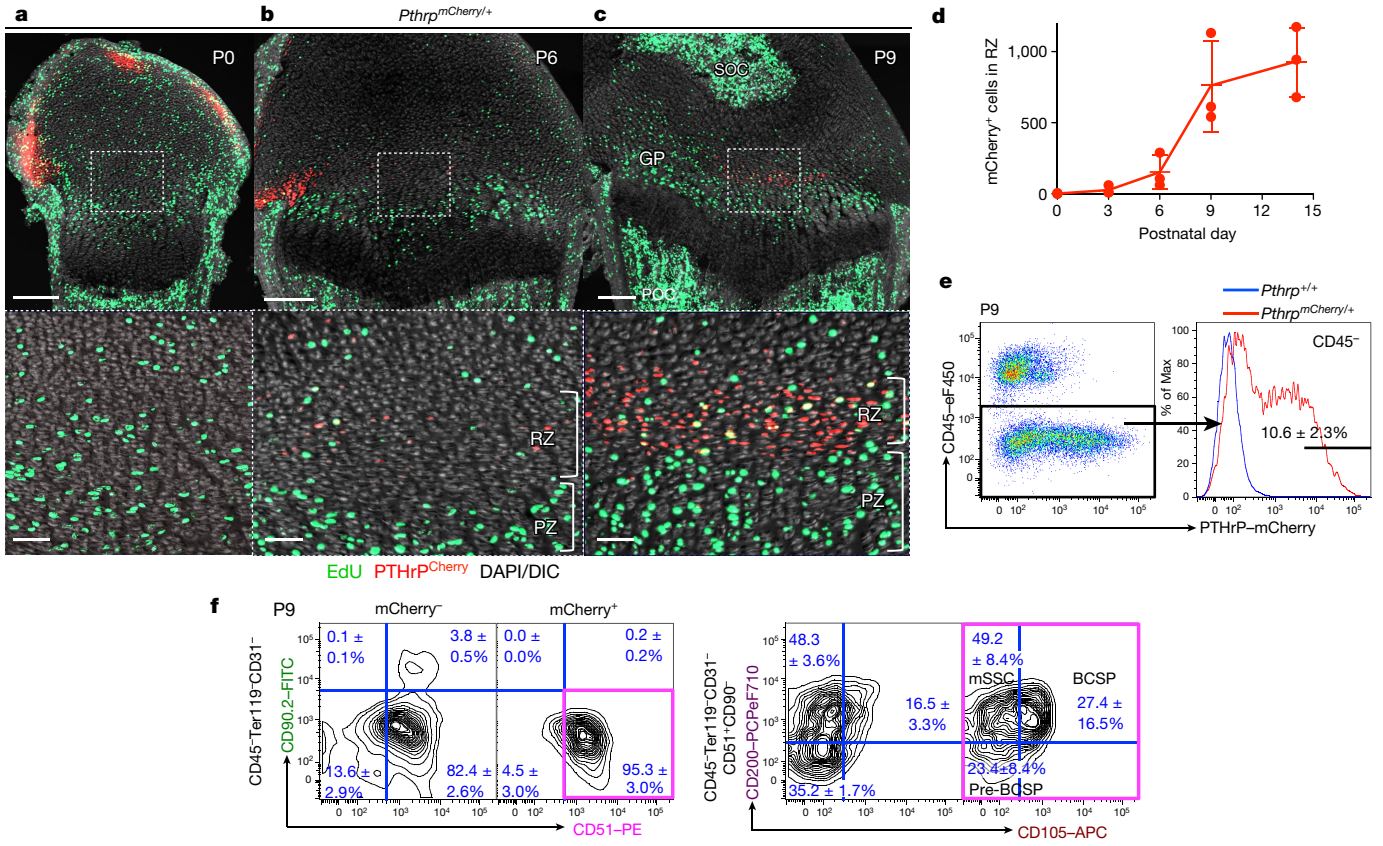

Fig. 1 | Formation of PTHrP–mCherry$^+$ chondrocytes in the resting zone of the growth plate. a–c, *Pthrp*$^{mCherry/+}$ distal-femur growth plates with EdU administration shortly before analysis. Bottom panels show magnified views of central growth plates. RZ, resting zone; PZ, proliferating zone; GP, growth plate; POC, primary ossification centre; SOC, secondary ossification centre. Grey, DAPI and DIC. Scale bars, 200 μm (top panels), 50 μm (bottom panels). **d**, Quantification of mCherry$^+$ cells. $n = 3$ mice per group, data are presented as mean ± s.d. **e**, Flow cytometry analysis of *Pthrp*$^{mCherry/+}$ growth-plate cells. $n = 8$ mice, data are presented as mean ± s.d. **f**, Skeletal stem and progenitor cell-surface-marker analysis of *Pthrp*$^{mCherry/+}$ growth-plate cells. mCherry$^-$, mCherry$^-$ fraction of *Pthrp*$^{mCherry/+}$ cells; mCherry$^+$, mCherry$^+$ fraction of *Pthrp*$^{mCherry/+}$ cells. Magenta box, CD45$^-$Ter119$^-$CD31$^-$CD51$^+$CD90$^-$mCherry$^+$ fraction. $n = 3$ mice per group, data are presented as mean ± s.d.

resting zone, at around P18 (Fig. 2c, arrows). After a month of chase, PTHrP^{CE}-P6 cells constituted the entire column from the resting zone to the hypertrophic zone (Fig. 2d). The number of tdTomato$^+$ resting chondrocytes transiently increased during the first week of chase and decreased thereafter, owing to the formation of columnar chondrocytes (Fig. 2e). The number of short tdTomato$^+$ columns peaked at P18 and decreased thereafter, whereas long tdTomato$^+$ columns appeared at P18 and continued to increase until P36 (Fig. 2f). Thus, *Pthrp-creER*$^+$ resting chondrocytes stay within the resting zone for the first week, and establish columnar chondrocytes starting from the second week of chase. Analysis of *Pthrp-creER;R26R*^{Confetti} mice revealed that each column was marked by its unique colour (CFP, YFP or tdTomato, Fig. 2g), which demonstrates that single *Pthrp-creER*$^+$ resting chondrocytes can give rise to multiple types of chondrocytes. Additional analysis of *Col2a1-creER;R26R*^{Confetti} mice further supported the existence of clonal cell populations (Extended Data Fig. 4a). Together, these findings support the notion that individual PTHrP$^+$ resting chondrocytes are multipotent and can clonally establish columnar chondrocytes in the growth plate.

To investigate whether *Pthrp-creER*$^+$ resting chondrocytes undergo self-renewing asymmetric divisions, we performed an EdU label-retention assay. Analysis of PTHrP^{CE}-P6 cells with serial pulses of EdU revealed that, after three weeks of chase, these cells gradually diluted the EdU signal as they differentiated towards the hypertrophic zone (Fig. 2h). Further, PTHrP^{CE}-P6 cells in the resting zone expressed PTHrP–mCherry, whereas those in the proliferating zone lost this expression (Fig. 2i). Therefore, *Pthrp-creER*$^+$ chondrocytes maintain themselves in the resting zone as PTHrP$^+$ cells and become the source of columnar chondrocytes in the growth plate, by providing the transit-amplifying progeny. Analysis of *Pthrp-creER;R26R*^{tdTomato} mice after being pulsed at various preceding pre-natal and early post-natal time points revealed that *Pthrp-creER*$^+$ chondrocytes started to be formed within the resting zone at embryonic day (E)17.5 (Extended Data Fig. 4b–e); a tamoxifen pulse on a later day laterally expanded the domain of tdTomato$^+$ cells. However, once they were marked, tdTomato$^+$ cells did not expand laterally upon further chase (Extended Data Fig. 4f,g), which indicates that PTHrP$^+$ resting chondrocytes are dedicated—at least to some degree—to making columnar chondrocytes longitudinally. Additional analysis of *Dlx5-creER;R26R*^{tdTomato} mice revealed that chondrocytes in the proliferating and hypertrophic zone could only form short columns (<10 cells) that eventually disappeared from the growth plate (Extended Data Fig. 5a–d), indicating that *Dlx5-creER*$^+$ proliferating chondrocytes are not the source of columnar chondrocytes in the growth plate.

During an extended chase period, PTHrP^{CE}-P6 cells continued to form columnar chondrocytes within the growth plate for at least a year after the pulse (Fig. 3a–c for *Col1a1(2.3kb)-GFP*; Extended Data Fig. 6a–d for *Cxcl12-GFP*[12]): the number of tdTomato$^+$ columns in the growth plate gradually decreased until six months after the pulse, and reached a plateau thereafter (Fig. 3d). A majority of tdTomato$^+$ columns extended beyond the hypertrophic layer and continued into the primary spongiosa and the metaphyseal bone marrow, an area beneath the growth plate[13]. These chondrocytes became Cxcl12–GFP$^+$ stromal cells beneath tdTomato$^+$ columns (Extended Data Fig. 6e), and reticular cells near trabecular bones (Fig. 3a, bottom). These chondrocytes also became Col1a1(2.3kb)–GFP$^+$ osteoblasts on the trabecular surface

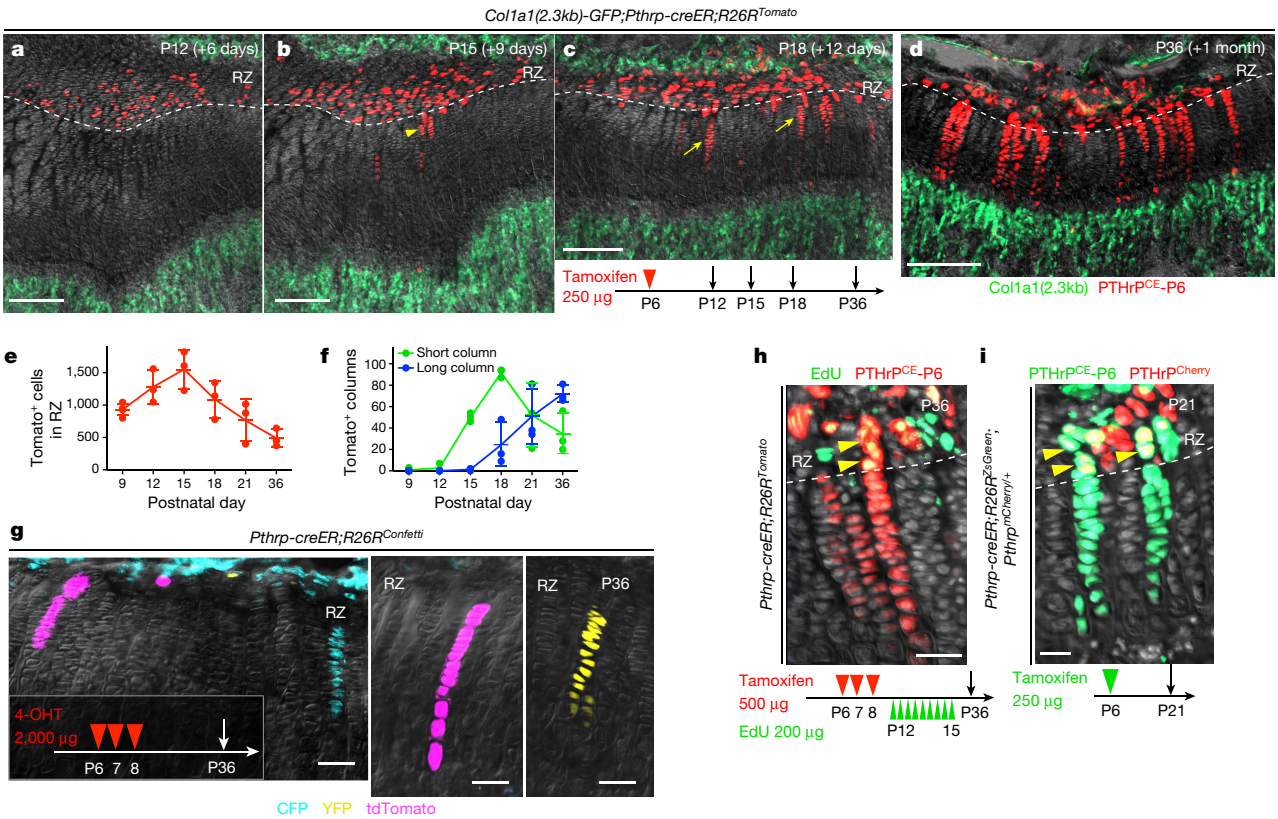

Fig. 2 | *Pthrp-creER*$^+$ resting chondrocytes are the source of columnar chondrocytes. a–d, Cell-fate analysis of *Pthrp-creER*$^+$ resting chondrocytes. *Col1a1(2.3kb)-GFP;Pthrp-creER;R26R*^{tdTomato} (pulsed on P6) distal-femur growth plates. Arrowhead, short column (<10 cells); arrows, long columns (>10 cells). Scale bars, 200 μm. **e**, **f**, Quantification of tdTomato$^+$ cells in resting zone (red line) (**e**) and columns in growth plate, short columns (<10 cells, green line) and long columns (>10 cells, blue line) (**f**). $n = 5$ (P9), $n = 3$ (P12–P36) mice per group, data are presented as mean ± s.d. **g**, In vivo clonal analysis of *Pthrp-creER*$^+$ resting chondrocytes. *Pthrp-creER;R26R*^{Confetti} distal-femur growth plates (pulsed on P6, P7 and P8). 4-OHT, 4-hydroxytamoxifen. Scale bars, 50 μm. $n = 3$ mice. **h**, EdU label-retention assay of *Pthrp-creER;R26R*^{tdTomato} distal-femur growth plates (pulsed on P6, P7 and P8). Arrowheads, EdU-retaining tdTomato$^+$ cells. Scale bars, 50 μm. $n = 3$ mice. **i**, PTHrP–mCherry expression in *Pthrp-creER;R26R*^{ZsGreen}*;Pthrp*$^{mCherry/+}$ distal-femur growth plates (pulsed on P6). Arrowheads, PTHrP–mCherry$^+$ZsGreen$^+$ cells. Scale bars, 20 μm. Grey, DAPI and DIC. $n = 3$ mice.

(Fig. 3a, bottom) and in the primary spongiosa (Fig. 3b, bottom). The number of Cxcl12–GFP$^+$tdTomato$^+$ stromal cells and Col1a1(2.3kb)–GFP$^+$tdTomato$^+$ osteoblasts increased for the first three months of chase; subsequently, the number of Col1a1(2.3kb)–GFP$^+$tdTomato$^+$ osteoblasts decreased, whereas the number of Cxcl12–GFP$^+$tdTomato$^+$ stromal cells reached a plateau (Fig. 3e). These cells did not become bone marrow adipocytes in the presence of a high-fat diet that contained a PPAR-γ agonist rosiglitazone (LipidTOX$^+$, 0 out of 443 cells examined; Extended Data Fig. 6f). Therefore, a subset of *Pthrp-creER*$^+$ resting chondrocytes can continue to reproduce themselves within the resting zone in the long term; their descendants first differentiate into hypertrophic chondrocytes within the growth plate, and then become multiple types of cells beyond the growth plate, such as osteoblasts and bone marrow stromal cells—but not adipocytes—in vivo.

We next performed a colony-forming assay to test whether *Pthrp-creER*$^+$ resting chondrocytes behave as skeletal stem cells in cultured conditions[14,15]. PTHrP^{CE}-P6 cells formed distinct and large tdTomato$^+$ colonies (>50 cells) composed of small Sox9$^+$ spherical cells (about 20 μm in diameter) (Extended Data Fig. 7a, b). By contrast, Dlx5$^+$ proliferating chondrocytes labelled on P7 failed to form tdTomato$^+$ colonies (Extended Data Fig. 7b, right), which indicates that *Pthrp-creER*$^+$ resting chondrocytes uniquely possess the capacity to form colonies when cultured ex vivo (Extended Data Fig. 7c). We next isolated individual primary PTHrP^{CE}–tdTomato$^+$ colonies and sub-cultured them further to determine whether individual colony-forming cells can self-renew in vitro (Extended Data Fig. 7d, see also Supplementary Information). Although a small fraction of P9 PTHrP^{CE}–tdTomato$^+$ primary colonies had the ability to establish secondary colonies (17 out of 518 clones, 3.3%), none of them could survive a further passage (Extended Data Fig. 7e). By contrast, an increased fraction of P12 PTHrP^{CE}–tdTomato$^+$ colonies established secondary colonies (16 out of 98 clones, 16.3%), and a fraction of these clones (2 out of 16 clones, 12.5%) could be further passaged for at least nine generations (Fig. 4a). Thus, *Pthrp-creER*$^+$ colony-forming cells appear to acquire robust in vitro self-renewability when the secondary ossification centre actively develops. Further, individual PTHrP^{CE}–tdTomato$^+$ cells (passage 4–7) could generate Alcian blue$^+$ spheres, Alizarin red$^+$ mineralized matrix and LipidTOX$^+$ oil droplets under chondrogenic, osteogenic and adipogenic differentiation conditions, respectively (Figs. 4b, 4 out of 4 clones, 100%). Upon subcutaneous transplantation into immunodeficient mice, these cells robustly differentiated into Col1a1(2.3kb)–GFP$^+$ osteoblastic cells (Fig. 4c) and effectively gave rise to Alcian blue$^+$ and Alizarin red$^+$ matrix, but produced Oil red O$^+$ lipid droplets only ineffectively (Extended Data Fig. 7f). These findings indicate that PTHrP$^+$ skeletal stem cells are predisposed to become chondrocytes and osteoblasts in vivo, and possess a baseline potential to become adipocytes in an inductive condition in vitro.

Lastly, we set out to investigate the functional importance of PTHrP$^+$ resting chondrocytes. Inducible cell ablation experiments using *Pthrp-creER;R26*$^{lsl\text{-}tdTomato/+}$ (control) and *Pthrp-creER;R26*$^{lsl\text{-}tdTomato/iDTA}$ (hereafter, DTA) littermates revealed that *Pthrp-creER*$^+$ cells were only incompletely ablated; tdTomato$^+$ resting chondrocytes and columns were still observed in the induced tissue of DTA mice (Fig. 5a, b). Nonetheless, the height of each layer of the growth plate was altered in the induced tissue of DTA mice, in which the proliferating zone was significantly reduced in association with the

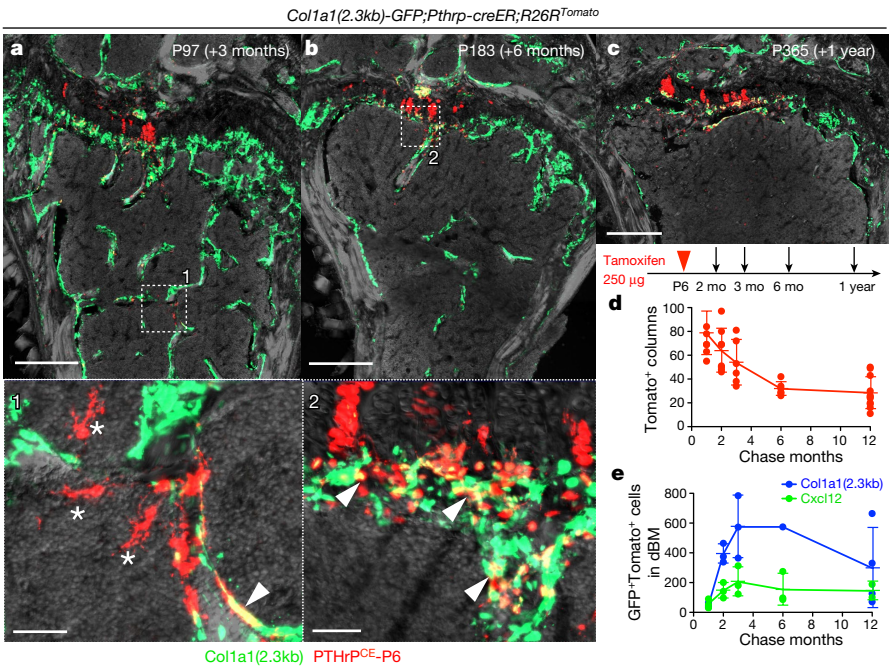

Fig. 3 | *Pthrp-creER*$^+$ resting chondrocytes behave as skeletal stem cells in vivo. a–c, Long-chase analysis of *Pthrp-creER*$^+$ resting chondrocytes. *Col1a1(2.3kb)-GFP;Pthrp-creER;R26R*^{tdTomato} distal femurs (pulsed on P6). In **a**, **b**, the bottom panel shows a magnified view of marrow space (white box in top panel). Arrowheads, Col1a1(2.3kb)–GFP$^+$tdTomato$^+$ osteoblasts; asterisks, tdTomato$^+$ reticular stromal cells. Grey, DAPI and DIC. Scale bars, 500 μm (top panels), 50 μm (bottom panels). $n = 3$ mice per group, except in **b**, $n = 1$ mouse. **d**, Quantification of tdTomato$^+$ columns in growth plate (red line) during the chase. $n = 8$ (1 month, 2 months), $n = 6$ (3 months, 6 months), $n = 11$ (12 months) mice per group, data are presented as mean ± s.d. **e**, Quantification of Col1a1(2.3kb)–GFP$^+$tdTomato$^+$ osteoblasts (blue line) and Cxcl12–GFP$^+$tdTomato$^+$ stromal cells (green line) in distal bone and bone marrow (dBM, up to 5 mm from the growth plate) during the chase. $n = 3$ (1 month, 2 months, 3 months for Col1a1(2.3kb)–GFP and Cxcl12–GFP, 6 months for Cxcl12–GFP), $n = 4$ (12 months for Col1a1(2.3kb)–GFP), $n = 2$ (12 months for Cxcl12–GFP) mice per group, data are presented as mean ± s.d., $n = 1$ (6 months for Col1a1(2.3kb)–GFP) mouse.

significant expansion of the hypertrophic and resting zones (Fig. 5c). Therefore, partial loss of PTHrP$^+$ cells in the resting zone is sufficient to alter the integrity of the growth plate by inducing premature hypertrophic differentiation of chondrocytes in the proliferating zone.

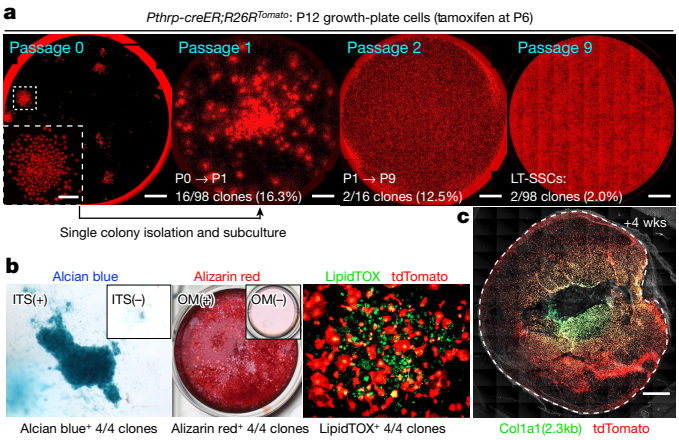

Fig. 4 | Skeletal stem cell activities of *Pthrp-creER*$^+$ resting chondrocytes ex vivo. a, Colony-forming assay and subsequent passaging of individual PTHrP^{CE}–tdTomato$^+$ colonies. Inset, magnified view of single colony. Red, tdTomato. Scale bars, 5 mm, 1 mm (inset). LT-SSCs, long-term skeletal stem cells. $n = 98$ independent experiments. **b**, Trilineage differentiation of PTHrP^{CE}–tdTomato$^+$ clones (passage 4 to 7). Chondrogenic (left), osteogenic (centre) and adipogenic (right) differentiation conditions. Insets, differentiation-medium negative controls. ITS, insulin–transferrin–selenium, OM, osteogenic differentiation medium. Four independent clones were tested. **c**, Subcutaneous transplantation of PTHrP^{CE}–tdTomato$^+$ clones into immunodeficient mice. Dotted line, contour of the plug. Grey, DIC. Scale bars, 1 mm. $n = 8$ mice.

Moreover, global manipulation of Hedgehog (Hh) signalling using Smo agonist (SAG) and antagonist (LDE225) in *Pthrp-creER;R26R*^{tdTomato} mice pulsed on P6 revealed that these regimens predominantly affected chondrocytes in the proliferating zone, without directly affecting PTHrP^{CE}-P6 cells in the resting zone (Extended Data Fig. 8a–c). Both regimens resulted in a significantly reduced number of tdTomato$^+$ columns (Fig. 5d; see also Extended Data Fig. 8d–k), indicating that uninterrupted Hh signalling is essential to maintaining the proper cell fates of PTHrP$^+$ resting chondrocytes. *Pthrp-creER*$^+$ cells directly differentiated into Col1a1(2.3kb)–GFP$^+$ osteoblasts in response to micro-perforation injury (Extended Data Fig. 8l, m), which indicates that PTHrP$^+$ skeletal stem cells lose their physiological fate in the absence of an intact proliferating zone.

Here we identified that the resting zone of the growth plate houses a unique class of skeletal stem cells, the transit-amplifying progeny of which are lineage-restricted as chondrocytes that exhibit multipotency only at the post-mitotic stage (see Extended Data Fig. 9a, b). PTHrP$^+$ cells are one of the stem-cell subgroups organized within the resting zone and—together with other as-yet unidentified cells—these cells can concertedly contribute to long-term tissue renewal. PTHrP$^+$ skeletal stem cells are dedicated to making columnar chondrocytes longitudinally, and appear to derive from PTHrP$^-$ cells. PTHrP$^+$ stem cells are highly hierarchical; approximately 2–3% of these cells acquire long-term self-renewability (Extended Data Fig. 9b). In addition, these stem cells are endowed with the ability to maintain the integrity of the growth plate, by sending a forward signal (that is, PTHrP) for transit-amplifying chondrocytes to maintain their proliferation and delay their hypertrophy in a non-cell autonomous manner. Therefore, PTHrP$^+$ stem cells can also provide the niche for transit-amplifying cells, which is compatible with a model previously proposed for the epithelium[16]. Conversely, transit-amplifying cells—which are maintained in a Hedgehog-responsive manner—appear to provide instructive cues to determine the cell fates of PTHrP$^+$ stem cells within the growth

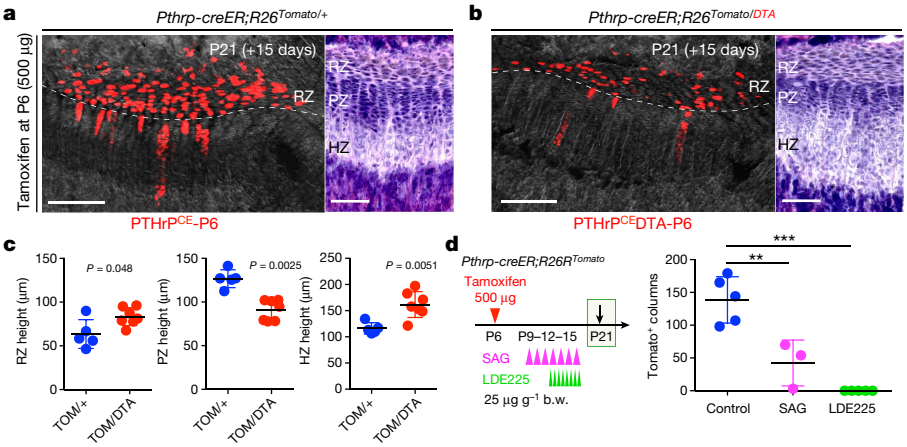

Fig. 5 | Reciprocal interactions between *PTHrP-creER*$^{+}$ resting chondrocytes and their niche. a–**c**, DTA-mediated ablation of *Pthrp-creER*$^{+}$ resting chondrocytes. **a**, *Pthrp-creER;R26*$^{lsl\text{-}tdTomato/+}$ (control). **b**, *Pthrp-creER;R26*$^{lsl\text{-}tdTomato/iDTA}$ (DTA) distal-femur growth plates (pulsed on P6). HZ, hypertrophic zone. Grey, DAPI and DIC. Right panels, haematoxylin and eosin staining. Scale bars, 200 μm (left panels) and 100 μm (right panels). **c**, Quantification of resting (left), proliferating (centre) and hypertrophic (right) zone height. TOM, tdTomato. $n = 5$ mice for control, $n = 7$ mice for DTA, data are presented as mean ± s.d., *P* values from Mann–Whitney's *U*-test, two-tailed. **d**, Pharmacological manipulation of Hedgehog signalling. Quantification of tdTomato^{+} columns in *Pthrp-creER;R26R*^{tdTomato} distal-femur growth plates (pulsed on P6). $n = 5$ (control), $n = 3$ (SAG) and $n = 5$ (LDE225) mice per group, data are presented as mean ± s.d., $^{**}P < 0.01$, $^{***}P < 0.001$. Control versus SAG, mean difference = 96.2, 95% confidence interval (41.6, 150.9); control versus LDE225, mean difference = 138.6, 95% confidence interval (91.3, 185.9); SAG versus LDE225, mean difference = 42.3, 95% confidence interval (−12.3, 97.0). One-way ANOVA followed by Tukey's multiple comparison test. b.w., body weight.

plate, which implies a reciprocal interaction between the stem cells and their progeny. We assume that PTHrP^{-} short-term precursors are the principal driver for extensive bone growth that occurs during postnatal development, reminiscent of a model proposed for haematopoietic stem cells[17,18]. It is possible that PTHrP^{+} skeletal stem cells are mainly involved in the long-term maintenance of skeletal integrity, although further details need to be clarified.

Data availability

Source Data are provided in the online version of the paper. The datasets generated during and/or analysed during the current study are available in Dryad Digital Repository (https://doi.org/10.5061/dryad.3qq5bm7).

Online content

Any methods, additional references, Nature Research reporting summaries, source data, statements of data availability and associated accession codes are available at https://doi.org/10.1038/s41586-018-0662-5.

Received: 23 September 2017; Accepted: 10 September 2018;
Published online 31 October 2018.

1. Ono, N. & Kronenberg, H. M. Bone repair and stem cells. *Curr. Opin. Genet. Dev.* **40**, 103–107 (2016).
2. Ono, N., Ono, W., Nagasawa, T. & Kronenberg, H. M. A subset of chondrogenic cells provides early mesenchymal progenitors in growing bones. *Nat. Cell Biol.* **16**, 1157–1167 (2014).
3. Chan, C. K. et al. Identification and specification of the mouse skeletal stem cell. *Cell* **160**, 285–298 (2015).
4. Worthley, D. L. et al. Gremlin 1 identifies a skeletal stem cell with bone, cartilage, and reticular stromal potential. *Cell* **160**, 269–284 (2015).
5. Kronenberg, H. M. Developmental regulation of the growth plate. *Nature* **423**, 332–336 (2003).
6. St-Jacques, B., Hammerschmidt, M. & McMahon, A. P. Indian hedgehog signaling regulates proliferation and differentiation of chondrocytes and is essential for bone formation. *Genes Dev.* **13**, 2072–2086 (1999).
7. Kobayashi, T. et al. PTHrP and Indian hedgehog control differentiation of growth plate chondrocytes at multiple steps. *Development* **129**, 2977–2986 (2002).
8. Kobayashi, T. et al. Indian hedgehog stimulates periarticular chondrocyte differentiation to regulate growth plate length independently of PTHrP. *J. Clin. Invest.* **115**, 1734–1742 (2005).
9. Chen, X. et al. Initial characterization of PTH-related protein gene-driven lacZ expression in the mouse. *J. Bone Miner. Res.* **21**, 113–123 (2006).
10. Mak, K. K., Kronenberg, H. M., Chuang, P. T., Mackem, S. & Yang, Y. Indian hedgehog signals independently of PTHrP to promote chondrocyte hypertrophy. *Development* **135**, 1947–1956 (2008).
11. Abad, V. et al. The role of the resting zone in growth plate chondrogenesis. *Endocrinology* **143**, 1851–1857 (2002).
12. Ara, T. et al. A role of CXC chemokine ligand 12/stromal cell-derived factor-1/pre-B cell growth stimulating factor and its receptor CXCR4 in fetal and adult T cell development in vivo. *J. Immunol.* **170**, 4649–4655 (2003).
13. Yang, L., Tsang, K. Y., Tang, H. C., Chan, D. & Cheah, K. S. Hypertrophic chondrocytes can become osteoblasts and osteocytes in endochondral bone formation. *Proc. Natl Acad. Sci. USA* **111**, 12097–12102 (2014).
14. Bianco, P. et al. The meaning, the sense and the significance: translating the science of mesenchymal stem cells into medicine. *Nat. Med.* **19**, 35–42 (2013).
15. Bianco, P. 'Mesenchymal' stem cells. *Annu. Rev. Cell Dev. Biol.* **30**, 677–704 (2014).
16. Pardo-Saganta, A. et al. Parent stem cells can serve as niches for their daughter cells. *Nature* **523**, 597–601 (2015).
17. Sun, J. et al. Clonal dynamics of native haematopoiesis. *Nature* **514**, 322–327 (2014).
18. Busch, K. et al. Fundamental properties of unperturbed haematopoiesis from stem cells *in vivo*. *Nature* **518**, 542–546 (2015).

Acknowledgements We thank D. Holcomb and M. Curtis of Carl Zeiss Microscopy for assistance in imaging, G. Gavrilina and W. Fillipak of the University of Michigan Transgenic Animal Model Core for assistance with transgenesis. This research was supported by NIH R01DE026666 and R00DE022564 (to N.O.), R03DE027421 (to W.O.), P01DK011794 (to H.M.K.), 2017 Fred F. Schudy Memorial Research Award from the American Association of Orthodontists Foundation (to N.O.) and University of Michigan MCubed 2.0 Grant (to N.O. and W.O.).

Reviewer information *Nature* thanks O. Klein, M. T. Longaker and the other anonymous reviewer(s) for their contribution to the peer review of this work.

Author contributions K.M. and N.O. conceived the project and designed the experiments; K.M. and N.O. performed the mouse genetic experiments with assistance from W.O., N.S. and A.T., who performed genotyping; K.M. performed histological experiments and imaging analysis; K.M. performed cell culture experiments; K.M. and N.O. performed flow cytometry experiments and analysis; Y.M. performed the surgery and cell transplantation; K.M. and N.O. analysed the data; N.O. supervised the project; T.L.S. generated the mice; T.N. provided the mice; K.M. and N.O. wrote the manuscript; T.N., W.O. and H.M.K. critiqued the manuscript.

Competing interests The authors declare no competing interests.

Additional information
Extended data is available for this paper at https://doi.org/10.1038/s41586-018-0662-5.
Supplementary information is available for this paper at https://doi.org/10.1038/s41586-018-0662-5.
Reprints and permissions information is available at http://www.nature.com/reprints.
Correspondence and requests for materials should be addressed to N.O.
Publisher's note: Springer Nature remains neutral with regard to jurisdictional claims in published maps and institutional affiliations.

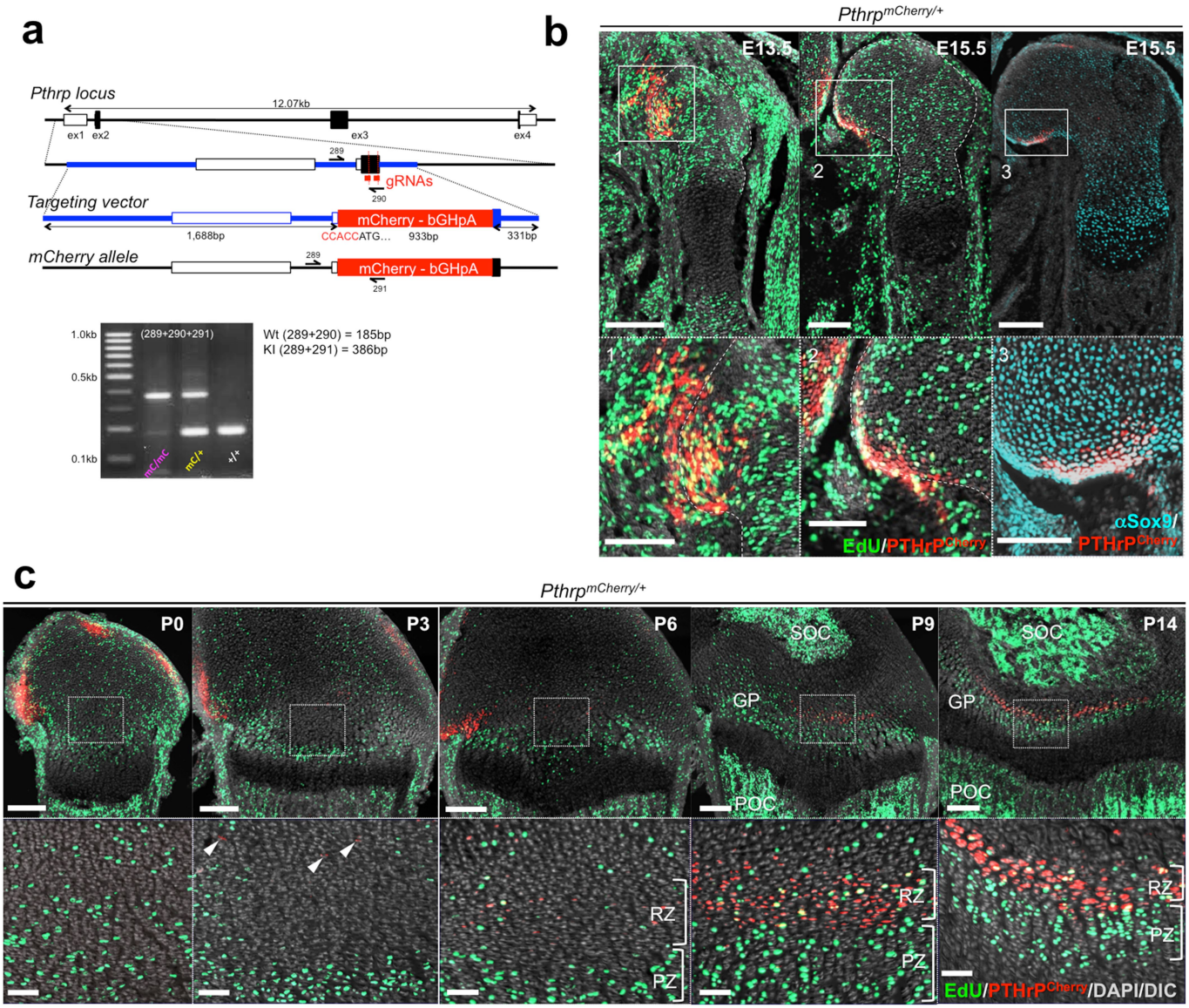

Extended Data Fig. 1 | Generation and characterization of *Pthrp-mCherry* knock-in allele. a, CRISPR–Cas9 generation of *Pthrp-mCherry* knock-in allele. Structure of the genomic *Pthrp* locus, targeting vector and knock-in allele after homologous recombination. White boxes, untranslated region; black boxes, coding region; ex, exon. Blue bars, homology arms; red bars, guide RNAs (gRNAs) as part of CRISPR–Cas9 reagents; red boxes, *Kozak-mCherry-bGHpA* cassette replacing the native start codon. Half arrows, primers; wild-type forward (289), wild-type reverse (290) and mutant reverse (291). Bottom, PCR genotyping using 289, 290 and 291 primer mix; wild-type (WT) allele, 185 bp; knock-in (KI) allele, 385 bp. At least $n = 100$ independent experiments with similar results. **b**, $Pthrp^{mCherry/+}$ fetal distal femurs with EdU administration shortly before analysis (3 h). Bottom panels show magnified views of perichondrium. Dotted lines, borders of bone anlage. Grey, DAPI and DIC. Scale bars, 200 μm (top panels), 100 μm (bottom panels). $n = 2$ (E13.5, E15.5) mice, $n = 1$ (α-Sox9) mouse. **c**, $Pthrp^{mCherry/+}$ distal-femur growth plates with EdU administration shortly before analysis (3 h). Bottom panels show magnified views of central growth plates. Arrowheads, $mCherry^{+}$ cells. Grey, DAPI and DIC. Scale bars, 200 μm (top panels), 50 μm (bottom panels).

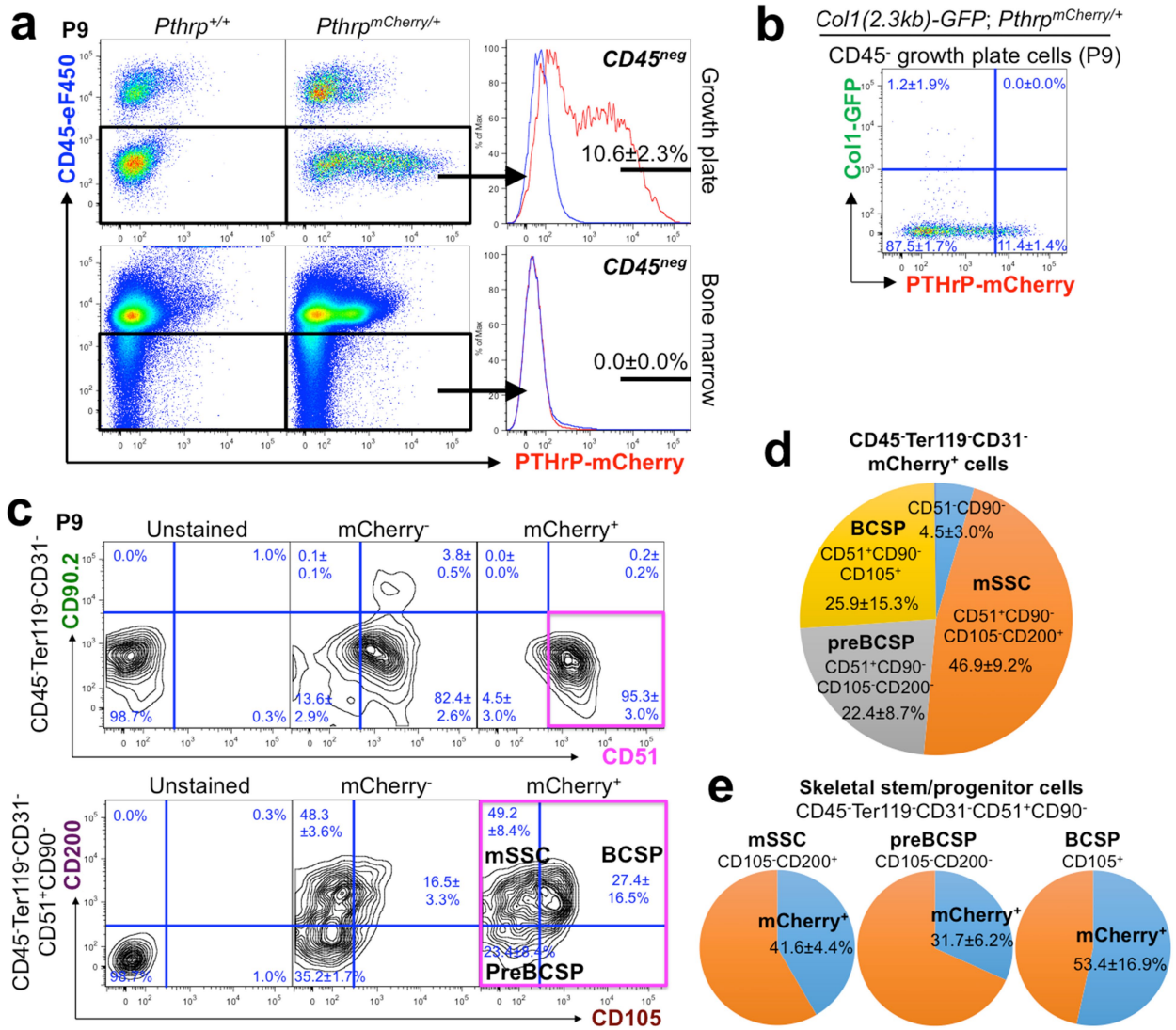

Extended Data Fig. 2 | Skeletal stem and progenitor cell-marker expression in PTHrP–mCherry^{+} resting chondrocytes. a, Flow cytometry analysis of *Pthrp*$^{mCherry/+}$ growth-plate cells (top panels) and bone-marrow cells (bottom panels). $n = 8$ mice for *Pthrp*$^{mCherry/+}$ and $n = 3$ mice for *Pthrp*$^{+/+}$, data are presented as mean ± s.d. **b**, Flow cytometry analysis of *Col1a1(2.3kb)-GFP;Pthrp*$^{mCherry/+}$ growth-plate cells. $n = 5$ mice per group, data are presented as mean ± s.d. **c**, Skeletal stem and progenitor cell-surface-marker analysis of *Pthrp*$^{mCherry/+}$ growth-plate cells. Unstained, *Pthrp*$^{+/+}$ cells mice only stained for CD45, Ter119 and CD31; mCherry^{-}, mCherry^{-} fraction of *Pthrp*$^{mCherry/+}$ cells; mCherry^{+}, mCherry^{+} fraction of *Pthrp*$^{mCherry/+}$ cells. Magenta box, CD45^{-}Ter119^{-}CD31^{-}CD51^{+}CD90^{-}mCherry^{+} fraction. $n = 3$ mice for *Pthrp*$^{mCherry/+}$, data are presented as mean ± s.d., $n = 1$ mouse for *Pthrp*$^{+/+}$. **d**, Composition of CD45^{-}Ter119^{-}CD31^{-}mCherry^{+} growth-plate cells. $n = 3$ mice per group, data are presented as mean ± s.d. **e**, Percentage of mCherry^{+} cells among mSSCs (left, CD105^{-}CD200^{+}), pre-BCSPs (centre, CD105^{-}CD200^{-}) and BCSPs (right, CD105^{+}), gated under CD45^{-}Ter119^{-}CD31^{-}CD51^{+}CD90^{-} fraction. $n = 3$ mice per group, data are presented as mean ± s.d.

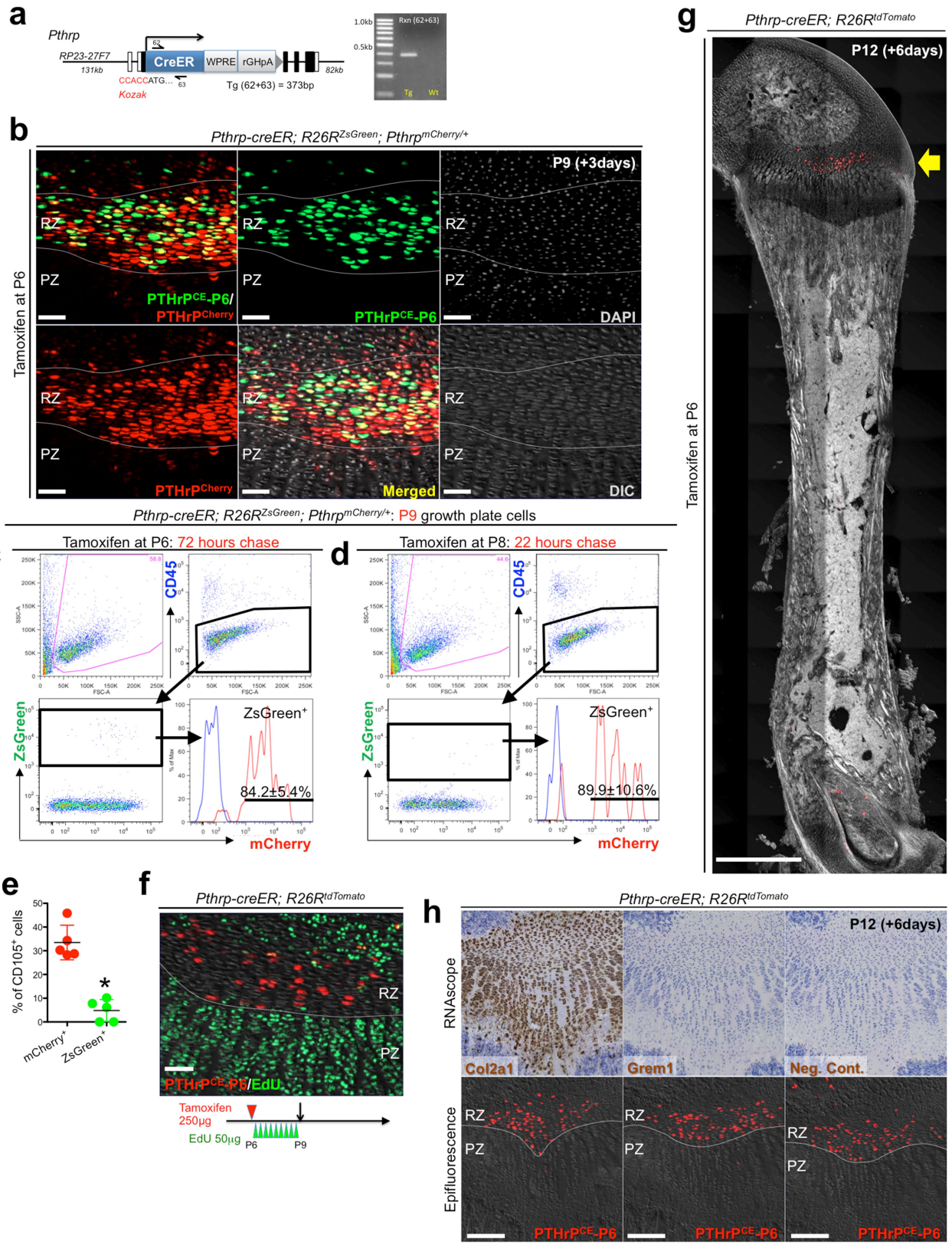

Extended Data Fig. 3 | See next page for caption.

Extended Data Fig. 3 | Generation and characterization of *Pthrp-creER* bacterial artificial chromosome transgenic line. a, Generation of *Pthrp-creER* bacterial artificial chromosome (BAC) transgenic mice. Structure of the *Pthrp-creER-WPRE-rGHpA* BAC construct. *Kozak-Pthrp-creER-WPRE-rGHpA-frt-Neo^{R}-frt* cassette containing 62-bp homology arms was recombineered into a BAC clone RP23-27F7 containing 131-kb upstream and 82-kb downstream genomic sequences of the *Pthrp* gene. *Neo^{R}* and backbone *lox* sites were removed before pronuclear injection. Half arrows, forward (62) and reverse (63) primers. Right, PCR genotyping using 62 and 63 primer mix; transgenic (Tg), 373 bp. White boxes, exons; black boxes, introns. At least $n = 100$ independent experiments with similar results. **b**, Short-chase analysis of *Pthrp-creER;R26R^{ZsGreen};Pthrp$^{mCherry/+}$* distal-femur growth plates (pulsed on P6). Scale bars, 50 μm. $n = 3$ mice. **c**–**e**, Short-chase flow cytometry analysis of *Pthrp-creER;R26R^{ZsGreen};Pthrp$^{mCherry/+}$* growth-plate cells, with tamoxifen injection at 72 h (**c**, **e**) or 22 h (**d**) in advance. Red lines, ZsGreen^{+} cells; blue lines, control cells without PTHrP–mCherry. $n = 5$ mice (72 h) or $n = 3$ mice (22 h) per group. **e**, Percentage of CD105^{+} cells within mCherry^{+} (red) and ZsGreen^{+} (green) cells. $n = 5$ mice per group, data are presented as mean ± s.d., $^{*}P = 0.012$, Mann–Whitney's *U*-test, two-tailed. **f**, *Pthrp-creER;R26R^{tdTomato}* distal-femur growth plates (pulsed on P6) at P9. EdU (50 μg) was serially injected 9 times at 8-h intervals between P6 and P9. Grey, DIC. Scale bars: 50 μm. $n = 3$ mice. **g**, Scanning of *Pthrp-creER;R26R^{tdTomato}* whole femur (pulsed on P6) at P12. Arrow, tdTomato^{+} cells localized within the resting zone of distal femur. Grey, DAPI and DIC. Scale bars, 1 mm. $n = 3$ mice. **h**, High sensitivity in situ hybridization (RNAscope) analysis of *Pthrp-creER;R26R^{tdTomato}* distal-femur growth plates (pulsed on P6) at P12. Top and bottom panels represent the identical section, before (bottom panels) and after (top panels) hybridization. Left panels, *Col2a1* (positive control); centre panels, *Grem1*; right panels, negative control. Grey, DAPI and DIC. Scale bars, 200 μm. $n = 3$ independent experiments.

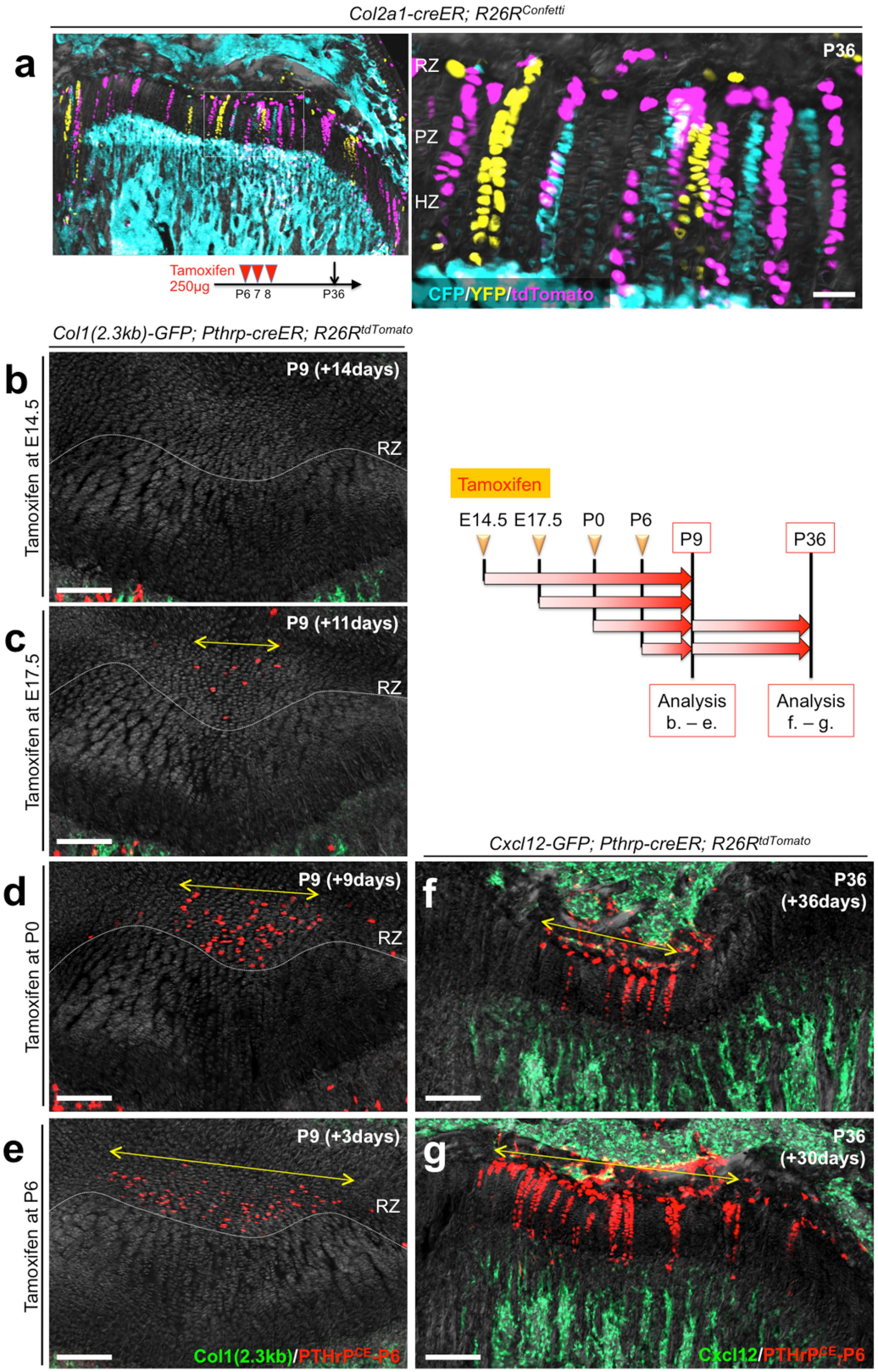

Extended Data Fig. 4 | PTHrP^{+} resting chondrocytes are functionally dedicated to columnar chondrocyte formation. a, In vivo clonal analysis of *Col2a1-creER*$^{+}$ growth-plate chondrocytes. *Col2a1-creER;R26R*^{Confetti} distal-femur growth plates (pulsed on P6, P7 and P8). Scale bars, 50 μm. $n = 2$ mice. **b**–**e**, *Col1a1(2.3kb)-GFP;Pthrp-creER;R26R*^{tdTomato} distal-femur growth plates, shown at P9 after being pulsed at various preceding time points. Yellow double-headed arrows, tdTomato^{+} domain within the resting zone. Grey, DAPI and DIC. Scale bars, 200 μm. $n = 3$ mice per group. **f**, **g**, *Cxcl12-GFP;Pthrp-creER;R26R*^{tdTomato} distal-femur growth plates, shown at P36 after being pulsed on P0 (**f**) and P6 (**g**). Yellow double-headed arrows in **f**, **g** indicate the same width as those shown in **d**, **e**. Grey, DAPI and DIC. Scale bars, 200 μm. $n = 3$ mice per group.

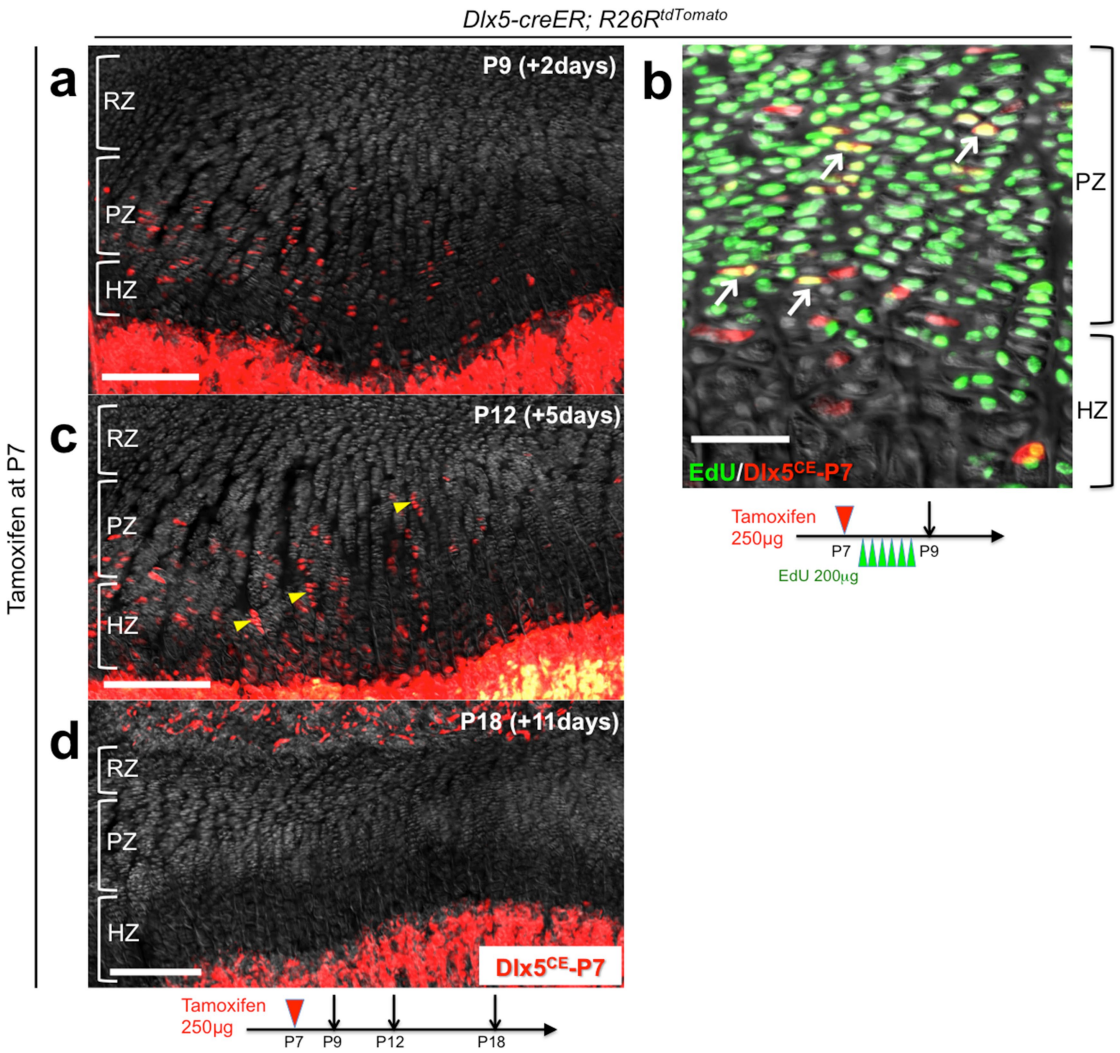

Extended Data Fig. 5 | *Dlx5-creER*$^+$ proliferating chondrocytes are not the source of columnar chondrocytes. a–d, Cell-fate analysis of *Dlx5-creER*$^+$ proliferating chondrocytes. *Dlx5-creER;R26R*^{tdTomato} distal-femur growth plates (pulsed on P7). **b**, EdU (200 μg) was serially injected 6 times at 8-h intervals, between P7 and P9. Arrows, EdU$^+$tdTomato$^+$ cells; arrowheads, short columns (<10 cells). Grey, DAPI and DIC. Scale bars, 200 μm (left panels), 50 μm (right panel). $n = 3$ mice at each time point.

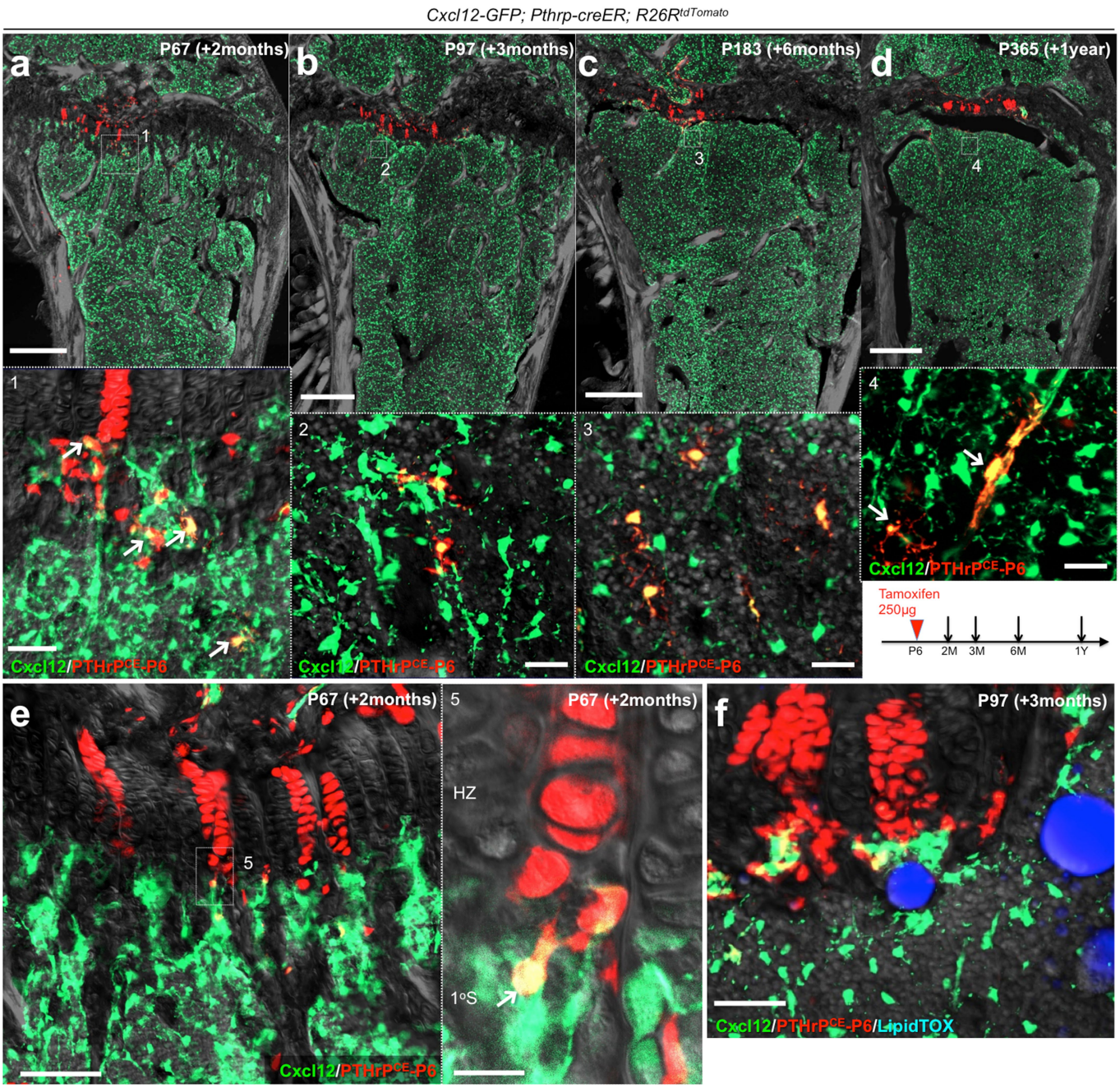

Extended Data Fig. 6 | *Pthrp-creER*$^{+}$ resting chondrocytes are precursors for bone marrow reticular stromal cells. *Cxcl12-GFP;Pthrp-creER;R26R*^{tdTomato} distal femurs (pulsed on P6). **a**–**d**, Bottom panels show magnified views of the dotted areas beneath growth plates. Arrows, Cxcl12–GFP^{+}tdTomato^{+} reticular stromal cells. **e**, Magnified view of the junction between hypertrophic layer and primary spongoisa. Arrow, Cxcl12–GFP^{+}tdTomato^{+} reticular stromal cells immediately below the hypertrophic zone. 1°S: primary spongiosa. **f**, Magnified view of the metaphyseal bone marrow. Mice were fed with high-fat diet containing rosiglitazone between P56 and P97. Grey, DAPI and DIC. Scale bars, 500 μm (**a**–**d**, **f**), 100 μm (**e**), 50 μm (bottom panels of **a**–**c**), 20 μm (bottom panel of **d**, right panel of **e**). $n = 3$ mice for each group, except $n = 2$ mice for P365.

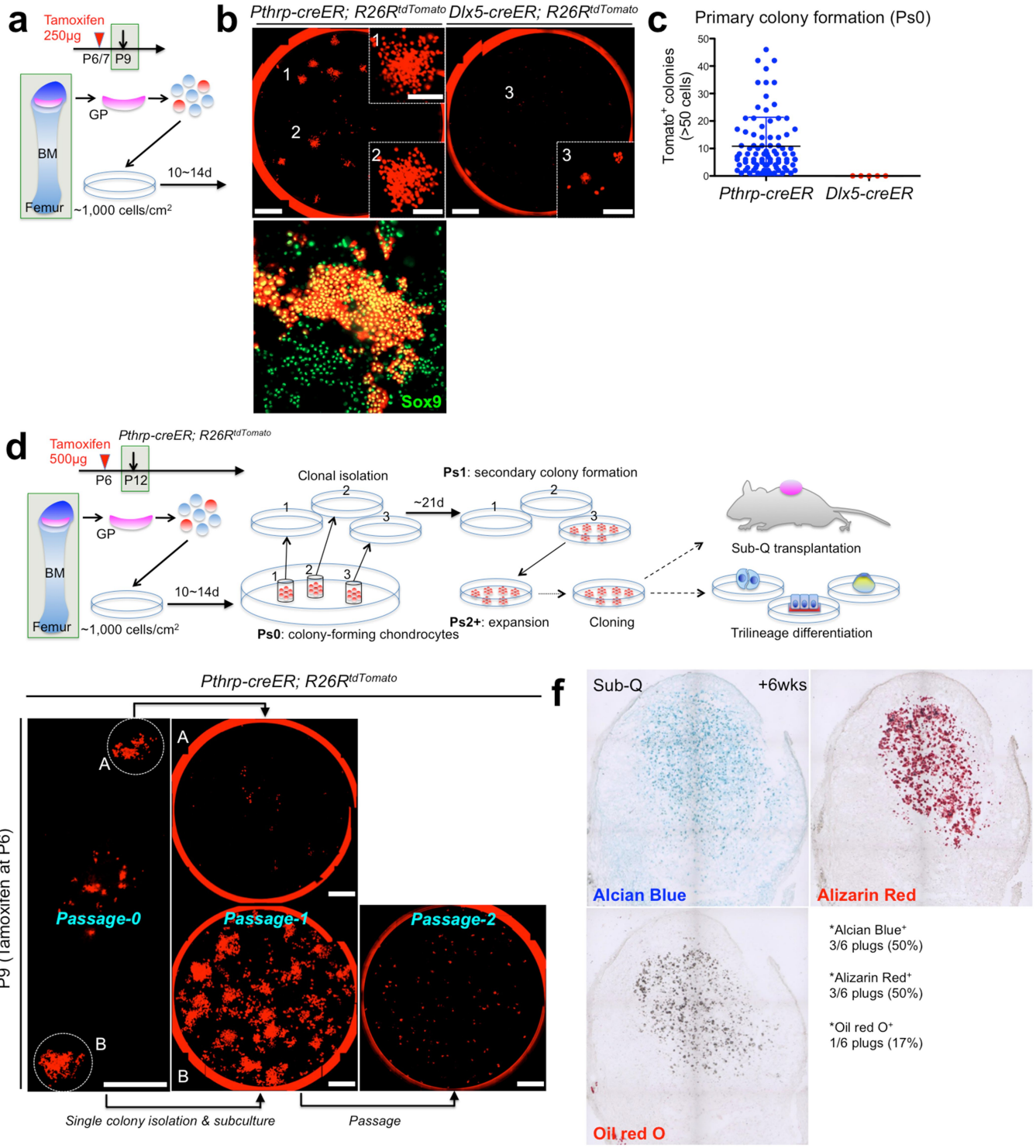

Extended Data Fig. 7 | *Pthrp-creER*$^+$ resting chondrocytes uniquely possess colony-forming capabilities ex vivo. a, Diagram of colony-forming assay. Growth-plate cells were isolated from *Pthrp-creER;R26R*^{tdTomato} (pulsed on P6) or *Dlx5-creER;R26R*^{tdTomato} (pulsed on P7) mice at P9, and cultured at a clonal density (~1,000 cells per cm^2) for 10–14 days to initiate colony formation. BM, bone marrow. **b**, Colony-forming assay. Left top, *Pthrp-creER;R26R*^{tdTomato}; right, *Dlx5-creER;R26R*^{tdTomato}. Insets 1,2 and 3 show magnified views of the corresponding areas (labelled with 1, 2, 3). Bottom left, Sox9 staining of primary *Pthrp-creER* tdTomato$^+$ colonies. Red, tdTomato. Scale bars, 5 mm (top panels), 1 mm (top panel insets), 200 μm (bottom panel). $n = 88$ mice for *Pthrp-creER;R26R*^{tdTomato}, $n = 5$ for *Dlx5-creER;R26R*^{tdTomato}. **c**, Quantification of tdTomato$^+$ colonies (>50 cells) established from *Pthrp-creER;R26R*^{tdTomato} ($n = 88$) and *Dlx5-creER;R26R*^{tdTomato} ($n = 5$) mice. Data are presented as mean ± s.d. **d**, Diagram of colony-forming assay and subsequent analyses on self-renewal, trilineage differentiation and transplantation of individual colony-forming cells. **e**, Isolation of single PTHrP^{CE}–tdTomato$^+$ colonies and subsequent subculture of isolated clones. A, exhausting clone; B, self-renewing clone establishing secondary colonies. Right, clone B did not proliferate at passage 2 upon bulk culture. Red, tdTomato. Scale bars, 5 mm. $n = 518$ independent experiments. **f**, Subcutaneous transplantation of PTHrP^{CE}–tdTomato$^+$ clones into immunodeficient mice. $n = 8$ mice.

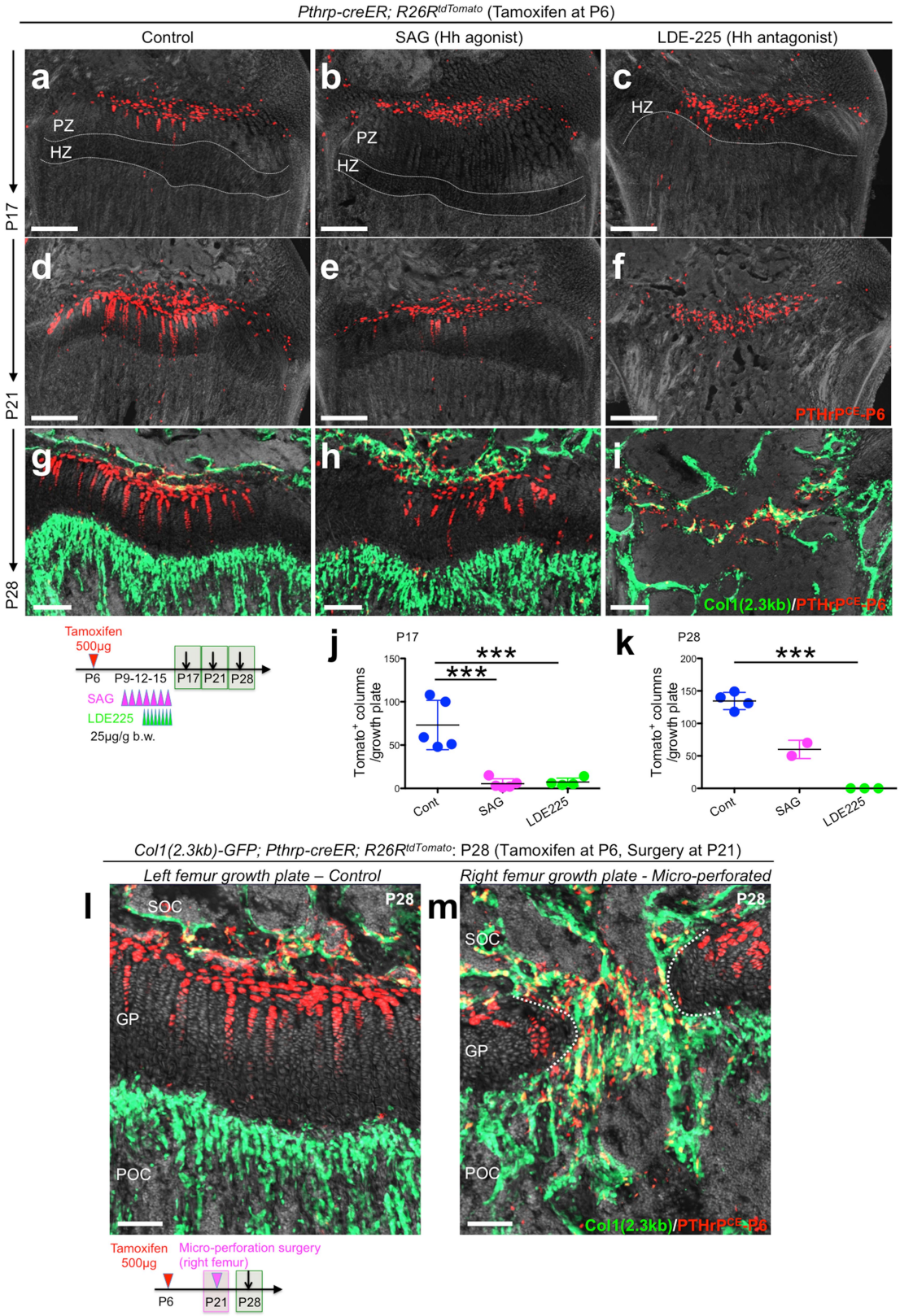

Extended Data Fig. 8 | See next page for caption.

Extended Data Fig. 8 | *Pthrp-creER*$^{+}$ resting chondrocytes form columnar chondrocytes in a Hedgehog-responsive, niche-dependent manner. a–i, Pharmacological manipulation of Hedgehog signalling. *Pthrp-creER;R26R*^{tdTomato} distal-femur growth plates (pulsed on P6). Left panels, vehicle control; centre panels, SAG (Hh agonist)-treated samples; right panels, LDE225 (Hh antagonist)-treated samples. Grey, DAPI and DIC. Scale bars, 200 μm. **j**, **k**, Quantification of tdTomato^{+} columns in *Pthrp-creER;R26R*^{tdTomato} distal-femur growth plates (pulsed on P6). P17, $n = 5$ (control), $n = 5$ (SAG), $n = 4$ (LDE225) mice per group. P28, $n = 4$ (control), $n = 3$ (LDE225) mice per group. Data are presented as mean ± s.d. P28, $n = 2$ (SAG). ***$P < 0.001$; P17 control versus SAG, mean difference = 67.8, 95% confidence interval (37.5, 98.1); P17 control versus LDE225, mean difference = 66.0, 95% confidence interval (33.9, 98.0); P17 SAG versus LDE225, mean difference = −1.85, 95% confidence interval (−33.9, 30.2); P28 control versus LDE225, mean difference = 134.5, 95% confidence interval (108.7, 160.3). One-way ANOVA followed by Tukey's multiple comparison test. **l**, **m**, Micro-perforation injury of growth plates. *Col1a1(2.3kb)-GFP;Pthrp-creER;R26R*^{tdTomato} distal femurs (pulsed on P6) at P28. Micro-perforation surgery was performed at P21. **l**, Left femur growth plate (control). **m**, Right femur growth plate (micro-perforated). Dotted line, micro-perforated area. Grey, DAPI and DIC. Scale bars, 100 μm. $n = 3$ mice.

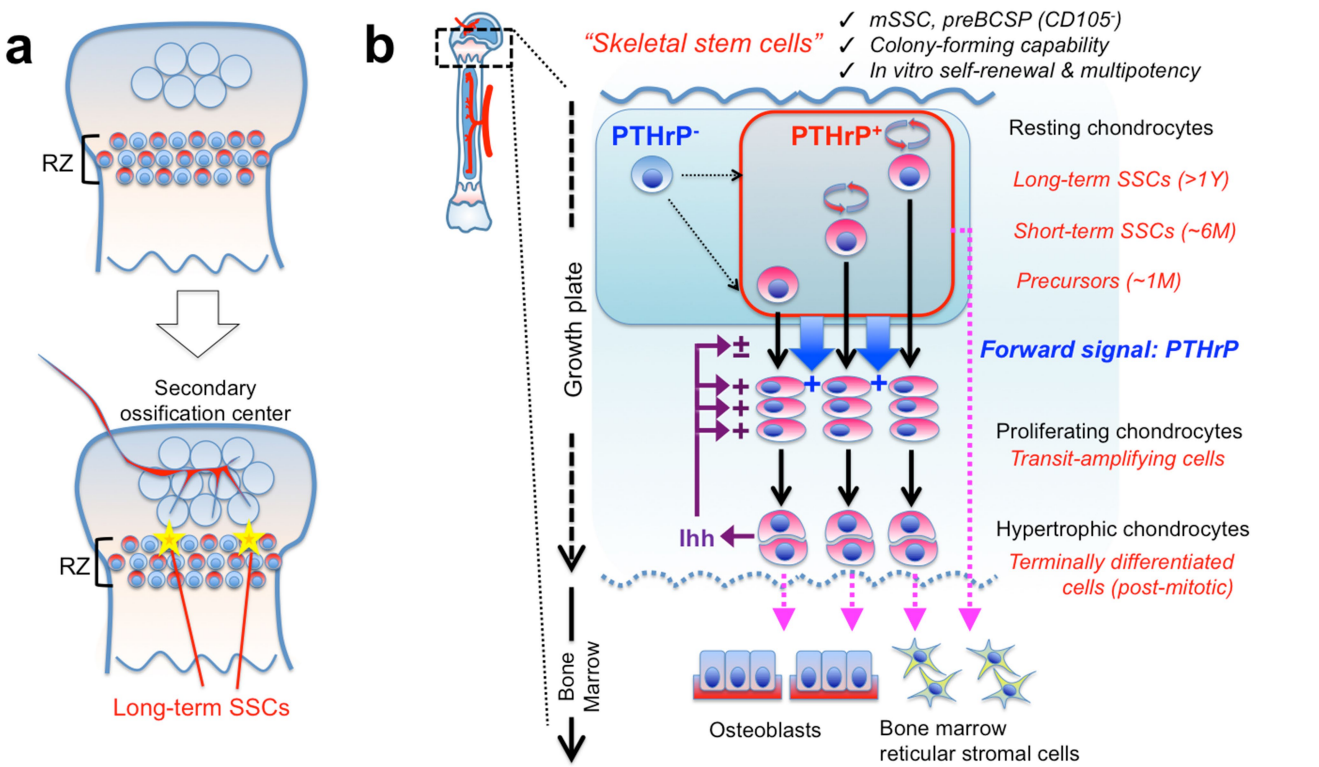

Extended Data Fig. 9 | Resting zone of the growth plate contains a unique class of skeletal stem cells. a, Formation of PTHrP$^+$ skeletal stem cells within the growth plate. A small subset of PTHrP$^+$ chondrocytes in the resting zone acquire properties as long-term skeletal stem cells in conjunction with the formation of the highly vascularized secondary ossification centre. **b**, PTHrP$^+$ skeletal stem cells are heterogeneously composed of long-term, short-term and transient populations, and undergo asymmetric divisions and maintain themselves within the resting zone. These cells may be supplemented by PTHrP$^-$ cells. PTHrP$^+$ cells perform two different functions: (1) these cells differentiate into proliferating chondrocytes, hypertrophic chondrocytes and eventually become osteoblasts and bone marrow stromal cells at the post-mitotic stage. (2) These cells send a forward signal (PTHrP) to control chondrocyte proliferation and differentiation. Indian hedgehog (Ihh) secreted by hypertrophic chondrocytes maintains the proliferation of chondrocytes and formation of columnar chondrocytes.

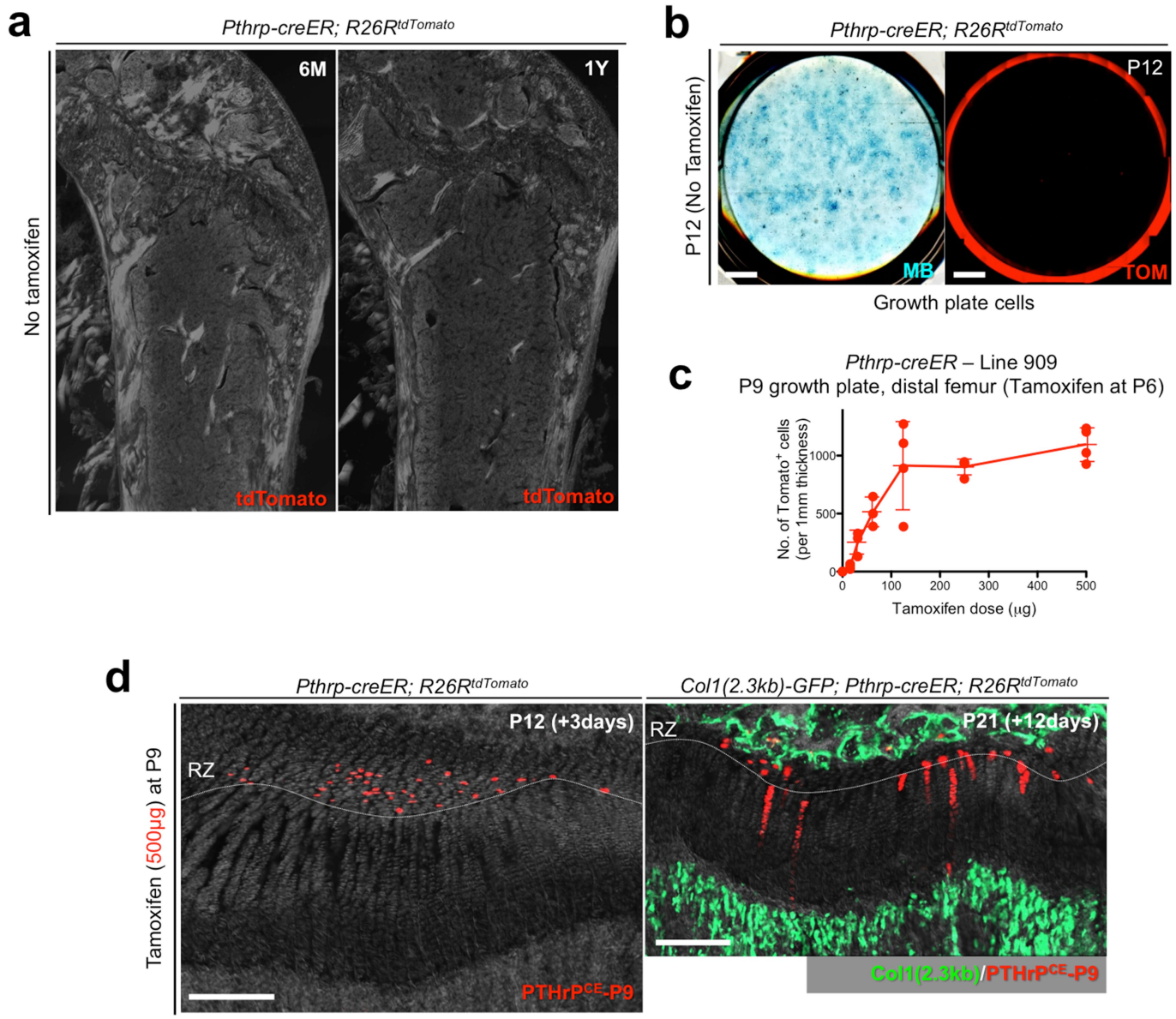

Extended Data Fig. 10 | Absence of tamoxifen-independent recombination in *Pthrp-creER* line. a, No tamoxifen controls of *Pthrp-creER;R26R*^{tdTomato} mice at 6 months (left) and 1 year (right) of age. Red, tdTomato; blue, DAPI; grey, DIC. Scale bars, 500 μm. $n = 3$ mice per group. **b**, No tamoxifen controls of primary colonies (passage 0) isolated from *Pthrp-creER;R26R*^{tdTomato} mice at P12 without tamoxifen injection. Left, methylene blue (MB) staining; right, red tdTomato (TOM). Scale bar, 5 mm. $n = 3$ mice. **c**, Dose–response curve of recombination based on *Pthrp-creER*. Quantification of tdTomato$^+$ cells in resting zone at P9 in *Pthrp-creER;R26R*^{tdTomato} mice upon a single dose of tamoxifen at P6. *x* axis, dose of tamoxifen (μg); *y* axis, the number of tdTomato$^+$ cells per 1-mm thickness. $n = 3$ (0, 31.3 and 62.5 μg), $n = 4$ (15.6, 125, 250 and 500 μg) mice per group, data are presented as mean ± s.d. **d**, Tamoxifen-induced recombination in growth plates pulsed on P9. *Pthrp-creER;R26R*^{tdTomato} distal-femur growth plates at P12 (left) and *Col1a1(2.3kb)-GFP; Pthrp-creER;R26R*^{tdTomato} mice at P21 (right). Tamoxifen (500 μg) was injected at P9. Green, Col1a1(2.3kb)–GFP; red, tdTomato; grey, DAPI and DIC. Scale bars, 200 μm. $n = 3$ mice.

LETTER

https://doi.org/10.1038/s41586-019-0989-6

A radical switch in clonality reveals a stem cell niche in the epiphyseal growth plate

Phillip T. Newton[1,2]*, Lei Li[1], Baoyi Zhou[1], Christoph Schweingruber[3], Maria Hovorakova[4], Meng Xie[1], Xiaoyan Sun[5], Lakshmi Sandhow[6], Artem V. Artemov[1,7], Evgeny Ivashkin[1], Simon Suter[1], Vyacheslav Dyachuk[3,8], Maha El Shahawy[9], Amel Gritli-Linde[9], Thibault Bouderlique[1], Julian Petersen[1,10], Annelie Mollbrink[11], Joakim Lundeberg[11], Grigori Enikolopov[12], Hong Qian[6], Kaj Fried[3], Maria Kasper[5], Eva Hedlund[3], Igor Adameyko[1,10], Lars Sävendahl[2] & Andrei S. Chagin[1,7]*

Longitudinal bone growth in children is sustained by growth plates, narrow discs of cartilage that provide a continuous supply of chondrocytes for endochondral ossification[1]. However, it remains unknown how this supply is maintained throughout childhood growth. Chondroprogenitors in the resting zone are thought to be gradually consumed as they supply cells for longitudinal growth[1,2], but this model has never been proved. Here, using clonal genetic tracing with multicolour reporters and functional perturbations, we demonstrate that longitudinal growth during the fetal and neonatal periods involves depletion of chondroprogenitors, whereas later in life, coinciding with the formation of the secondary ossification centre, chondroprogenitors acquire the capacity for self-renewal, resulting in the formation of large, stable monoclonal columns of chondrocytes. Simultaneously, chondroprogenitors begin to express stem cell markers and undergo symmetric cell division. Regulation of the pool of self-renewing progenitors involves the hedgehog and mammalian target of rapamycin complex 1 (mTORC1) signalling pathways. Our findings indicate that a stem cell niche develops postnatally in the epiphyseal growth plate, which provides a continuous supply of chondrocytes over a prolonged period.

To characterize the generation of epiphyseal chondrocytes, we used clonal lineage tracing by crossing Col2-creERT mice[3] with multicolour R26R-Confetti reporter mice[4]. Initially, we induced recombination by tamoxifen injection on postnatal day 3 (P3). Two days after injection, all types of chondrocytes were labelled (Fig. 1a), whereas one month later only stable clones originating from long-term progenitors in the resting zone were observed (Fig. 1b).

To assess growth-plate dynamics, tracing of chondrocytes for 10 or 14 days at different ages (embryonic day 14.5 (E14.5) to P4, P0 to P10, or P3 to P18) revealed only clones with few cells during the fetal–neonatal period (Fig. 1c, e, Extended Data Fig. 1b, c) whereas clonal size (clonal cell number) increased markedly later (P30–P40 and P30–P44) (Fig. 1d, e, Extended Data Fig. 1a, d). Clones were initially small (few clonal cells) in bones labelled at both P3 and P30, and expanded with time only in the P30 bones (Extended Data Fig. 1e). To ensure visualization of whole clones, entire 150-μm sections were scanned by confocal microscopy, confirming these observations (Supplementary Videos 1, 2). All subsequent clonal analyses involved scanning entire 150-μm sections. Blocking erosion of hypertrophic chondrocytes with axitinib, which inhibits the VEGF receptor[5], for the final nine days of P15–P30 tracing revealed clones containing more than 50 cells (Fig. 1f). By contrast, clonal size was unaffected by axitinib treatment on P10 (Supplementary Table 1). Proliferation of flat chondrocytes was not influenced by axitinib at any stage (Supplementary Table 1).

This increased clonal size after P30 did not reflect changes in chondrocyte proliferation (Extended Data Fig. 1f) or growth rate (Extended Data Fig. 1g). Morphometry and 5-ethynyl-2′-deoxyuridine (EdU) pulse-chase revealed fewer flat cells, but more EdU-labelled hypertrophic chondrocytes at P30 than at P3, indicating that flat cells do not exhibit increased replication, but move to the hypertrophic layer more rapidly in older mice (Supplementary Table 2). Moreover, chondrocyte death cannot account for the altered clonal pattern (Supplementary Table 2). Thus, none of these analysed parameters explained clonal enlargement with age.

Moreover, growth plate columns were multiclonal at the fetal–neonatal stage (Fig. 1g; Extended Data Fig. 1b, c), but became monoclonal after P30 (Fig. 1b, d, f; for orientation, see histological images in Extended Data Fig. 1h). These monoclonal columns remained in renewing cartilage for at least five months (Extended Data Fig. 1i). Multiclonal neonatal columns appear to arise from several progenitors, whereas monoclonal columns originate from a single stable progenitor. To determine whether the same *Col2a1*-expressing ($Col2^+$) cells initially form small, but thereafter large, stable clones, we performed tracing from embryonic time points to adult ages. We observed that the neonatal patchy pattern of clonality (Extended Data Fig. 1b) changed to stable monoclonal columns in mature mice (Fig. 1h; Extended Data Fig. 1j) suggesting the presence, as early as E14.5, of a subset of progenitors that generate large, stable clones in mature mice.

To understand this shift in clonality, we developed web-based modelling of cell kinetics in the growth plate (http://chaginlab.com/sim, see Supplementary Information). This model indicated that obtaining long, stable, monoclonal columns requires the uppermost cells to undergo renewal, whereas stacking of short clones requires constant recruitment (consumption) of round cells into the proliferative pool. These observations led to a model in which the pool of chondroprogenitors is slowly depleted by direct recruitment during fetal–neonatal growth, whereas after the growth plate forms, remaining chondroprogenitors acquire the capacity for self-renewal, each producing many progeny.

Consumption of chondroprogenitors during the fetal–neonatal period was supported by a reduction in the number of clones with time (labelling at E14.5, this number at P30 ($n = 5$) was $42.5 \pm 7.8\%$ of that at P4 ($n = 4$), $P = 0.015$). Pulse-chase labelling with EdU (injected on P3), CldU (injected on P10) and IdU (injected on P12) followed by tissue collection 4 h after IdU injection revealed direct recruitment

[1]Department of Physiology and Pharmacology, Karolinska Institutet, Stockholm, Sweden. [2]Department of Women's and Children's Health, Karolinska Institutet and Pediatric Endocrinology Unit, Karolinska University Hospital, Stockholm, Sweden. [3]Department of Neuroscience, Karolinska Institutet, Stockholm, Sweden. [4]Department of Developmental Biology, Institute of Experimental Medicine, The Czech Academy of Sciences, Prague, Czech Republic. [5]Department of Biosciences and Nutrition and Center for Innovative Medicine, Karolinska Institutet, Huddinge, Sweden. [6]Center for Hematology and Regenerative Medicine, Karolinska Institutet, Huddinge, Sweden. [7]Institute for Regenerative Medicine, Sechenov First Moscow State Medical University, Moscow, Russian Federation. [8]National Scientific Center of Marine Biology, Far Eastern Branch, Russian Academy of Sciences, Vladivostok, Russian Federation. [9]Department of Oral Biochemistry, Sahlgrenska Academy at the University of Gothenburg, Gothenburg, Sweden. [10]Department of Molecular Neurosciences, Center for Brain Research, Medical University Vienna, Vienna, Austria. [11]Science for Life Laboratory, Department of Gene Technology, KTH Royal Institute of Technology, Stockholm, Sweden. [12]Center for Developmental Genetics and Department of Anesthesiology, Stony Brook University, Stony Brook, NY, USA. *e-mail: phillip.newton@ki.se; andrei.chagin@ki.se

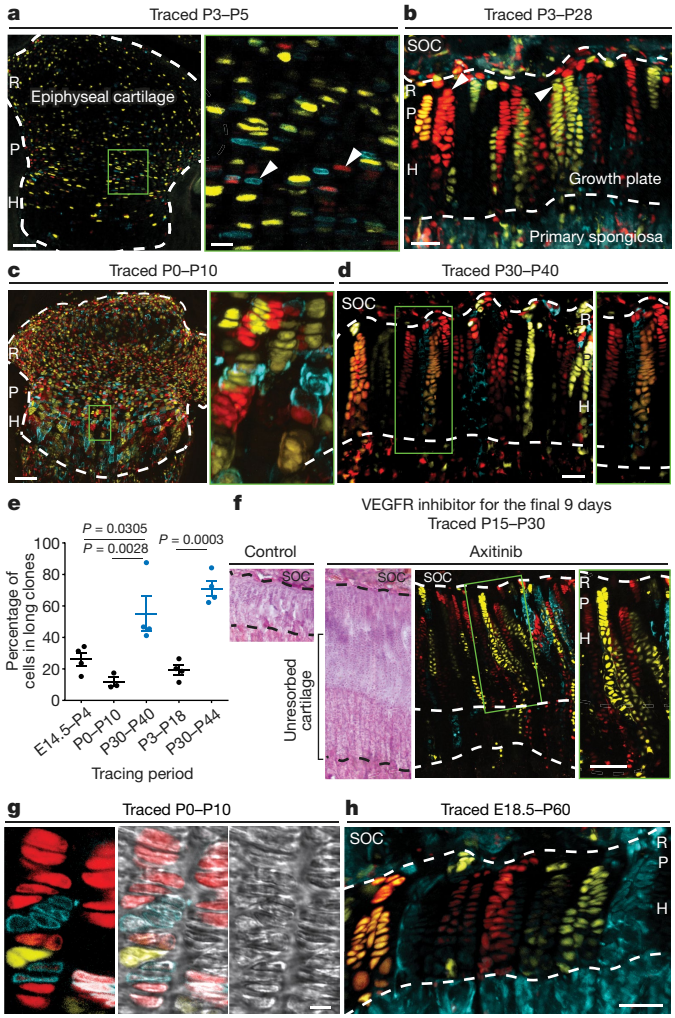

Fig. 1 | A change in clonality occurs in the mouse growth plate at one month of age. Clonal dynamics was analysed in Col2-creERT:*R26R*-Confetti mice by inducing recombination with tamoxifen injected at various time points and traced for different periods. **a**, **b**, Chondrocytes were labelled by injecting tamoxifen on P3 and then traced for two days (**a**) or for 25 days (**b**). All populations of chondrocytes in Col2-creERT:*R26R*-Confetti mice were labelled initially (**a**) and stable clones established with time (**b**). Arrowheads indicate typically labelled cells (**a**) and clones (**b**). **c**, **d**, Tracing for ten days starting either at birth (P0) (**c**) or P30 (**d**) revealed different clonality patterns. **e**, Clonal size was quantified for various tracing periods, with columns containing more than nine cells per clone classified as long columns. Data are mean ± s.e.m., $n = 4$ mice (except for P0–P10 tracing, where $n = 3$); one-way ANOVA with Tukey multiple comparisons. Only separately positioned one-row clones were counted. **f**, The mice were traced from P15 to P30 and injected daily with a VEGFR inhibitor (axitinib) for the last nine days to block cartilage resorption. **g**, Visualization of neonatal columns in combination with clonal tracing from P0 to P10 revealed different clones within single columns (middle and right images were visualized with non-reflected laser light). **h**, Prolonged tracing from E18.5 to P60. The SOC, the growth plate or epiphyseal cartilage, the primary spongiosa and the resting (R), proliferating (P) and hypertrophic (H) zones are indicated for orientation. Cartilage is demarcated by dashed lines. Several mice from a minimum of two independent litters were analysed for each experiment, except in **h**, which shows analysis of mice from a single litter. Scale bars: 100 μm (**a**, (left), **f**), 20 μm (**a**, right), 50 μm (**b**, **d**, **h**), 150 μm (**c**), and 10 μm (**g**).

of label-retaining cells (LRCs) into the proliferative pool and thereafter into the hypertrophic layer (Extended Data Fig. 2a). Futhermore, our web-based model predicted that during the time required for formation of a long column, each colony-forming cell undergoes two to three cell divisions, diluting the label. Indeed, when visualization of slowly dividing chondroprogenitors by H2B–GFP retention (Extended Data Fig. 2b) was combined with R26R-Confetti clonal genetic tracing, only 4 of 118 Confetti$^+$ columns contained H2B–GFP-retaining cells (Extended Data Fig. 2d). By contrast, before renewal (the fetal–neonatal model), on postnatal day 21, direct recruitment of round chondroprogenitors into columnar chondrocytes led to more H2B–GFP-retaining cells in the Confetti$^+$ columns (Extended Data Fig. 2c; $P < 0.0001$, P21 versus P28, Fisher's exact test for count data). This suggests that once renewal begins, colony formation and label retention are mutually exclusive. It is conceivable that only some chondroprogenitors undergo renewal, and there is a separate, dormant population of LRCs (Extended Data Fig. 2d). Even after five months of tracing, some Confetti-labelled cells, not in columns, remained in the resting zone (arrow in Extended Data Fig. 1i″), supporting the existence of two such populations. Similarly, stem cell niches in hair follicles[6,7], bone marrow[8] and intestine[4,9] contain two populations of stem cells with differing proliferation rates.

This shift in clonality coincides with development of the secondary ossification centre (SOC, which matures into epiphyseal bone) and the uppermost clonal cell is always near epiphyseal bone (Fig. 2a). The SOC develops more rapidly in the centre of the epiphysis and clonal size correlated with proximity to the SOC (7.8 ± 0.3 versus 5.7 ± 0.1 cells per clone in central and lateral sections, respectively; $P = 0.0012$, $n = 4$; tracing P6.5–P18; Fig. 2b, c; subsequently, central bone sections were analysed routinely). SOC development depends on angiogenesis, and axitinib administration during P18–P27 delayed this process (Fig. 2d; Supplementary Table 1). Inhibition of SOC maturation delayed development of monoclonality in the growth plate (Fig. 2d). Thus, SOC formation is likely to alter the local microenvironment to support renewal of the chondroprogenitors, providing a stem cell niche[10,11].

To understand acquisition of self-renewal, we combined laser-capture microdissection (LCM) of chondroprogenitors at P2 or P28 with single-cell RNA Smart2 sequencing protocol (LCM–seq[12]) (Extended Data Fig. 3a). This revealed changes in several pathways involved in stem cell and regenerative biology, including upregulation of genes related to the extracellular matrix (ECM), oxidative stress and fibroblast growth factor binding, and downregulation of negative regulators of the canonical Wnt pathway, the ERK1/2 pathway and wound-healing genes (Extended Data Fig. 3b–d). The age-related differences were slightly larger in the resting zone than in the hypertrophic zone, which served as an internal control ($P = 4.931 \times 10^{-5}$; Extended Data Fig. 3e). Expression of ECM genes, related to formation of the stem cell niche[13], showed the most marked change, consistent with alteration of local ECM organization by SOC.

CD73 (encoded by *Nt5e*) was among the most upregulated stem cell surface markers (4.9 ± 1.2-fold; P28 versus P2; $P = 0.018$) and immunohistochemical analysis confirmed de novo expression of CD73 at P28 (Fig. 2e, f; Extended Data Fig. 3f; markers for cell proliferation (Ki67) and differentiation (MEF2C) were controls for developmental changes, Extended Data Fig. 3g, h, respectively). When chondrocytes expressing integrin-α5 (also known as CD49e) and double-positive CD73$^+$CD49e$^+$ chondroprogenitors were sorted by fluorescence-activated cell sorting (FACS) (Extended Data Fig. 4a), the CD73$^+$CD49e$^+$ chondroprogenitors expanded in culture (sevenfold within 12 days), formed colonies (80 ± 20 cells per colony ($n = 7$) versus 19 ± 7 cells per colony for the CD73$^-$CD49e$^+$ population ($n = 4$), $P < 0.05$), and underwent mesenchymal differentiation into chondrocytes, osteoblasts and adipocytes (Extended Data Fig. 4b–i). Thus, upon formation of the niche, this self-renewal and multi-lineage differentiation of chondroprogenitors identifies them as adult stem cells, which are probably unipotent under physiological conditions, but multipotent in vitro.

Asymmetric division of one stem cell produces a new stem cell and a daughter cell that proliferates (a transit-amplifying cell) and thereafter differentiates[14]. In the mature growth plate, flat chondrocytes would correspond to transit-amplifying cells, whereas the spatial organization (that is, clonal cells arranged in columns) and unidirectional differentiation suggest that division of colony-forming cells is primarily

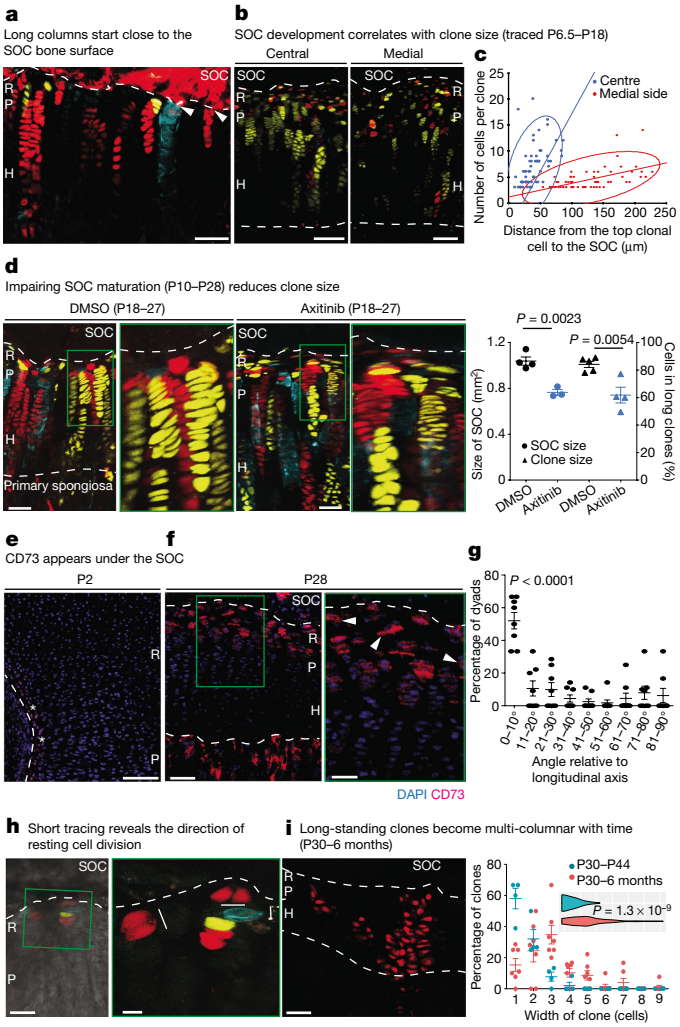

Fig. 2 | Indications that an altered microenvironment facilitates chondroprogenitor renewal. a Col2-creERT:*R26R*-Confetti mice were administered tamoxifen on P30 and analysed on P44. Bone matrix was visualized by xylenol injection 48 h before tissue collection. Arrowheads indicate columns that begin in immediate proximity to the bone surface. **b**, Col2-creERT:*R26R*-Confetti mice were traced from P6.5 ± 1.5 to P18 and sectioned to the centre, where the SOC development is the most advanced, or 750 μm towards the medial side of the bone. Clone size was calculated and plotted against the distance between the top clonal cell and the SOC traced from P8 to P18 (**c**). **d**, Col2-creERT:*R26R*-Confetti mice were traced from P10 to P28 and injected daily with axitinib (from P18 to P27) to delay SOC maturation; analysis includes all clones with more than three cells per clone, beginning within 100 μm of the SOC. $n = 5$ mice (DMSO), $n = 4$ (axitinib); analysed by unpaired two-tailed *t*-test. **e**, **f**, Immunofluorescent staining of CD73 at P2 (**e**; ∗labelled cells in the groove of Ranvier) and P28 (**f**; arrowheads, typical resting-zone cells). **g**, **h**, Col2-creERT:*R26R*-Confetti mice were injected with tamoxifen on P30.5 ± 2.5 and analysed 4 ± 1 days later. The angles between self-standing dyads in the top of the growth plate were measured relative to the longitudinal axis of the bone. $n = 8$ mice, a total of 53 dyads; one-way ANOVA with Tukey multiple comparisons, *P* indicates difference between 0–10° and all other groups. In **h**, white lines indicate the direction of division; the lower magnification panel was visualized with non-reflected laser light. **i**, Col2-creERT:*R26R*-Confetti mice were traced from P30 to six months of age. The width of clones entering the primary spongiosa was analysed using two-sided Wilcoxon signed-rank test ($n = 4$ mice (P30–P40), $n = 7$ mice (P30 to 6 months)). Data in **d**, **g** and **i** are mean ± s.e.m. All data represent several mice from two independent litters, except in **a** and **c**, which represent mice from one litter. Scale bars: 50 μm (**a**, **d**, **e**, **f** (left)), 100 μm (**b**), 25 μm (**f** (right)), 30 μm (**h** (left), **i**), 10 μm (**h** (right)).

asymmetric. Indeed, Confetti tracing during P30.5–P34.5 ± 1 revealed that most resting-zone dyads lie parallel to the longitudinal growth axis, with 13% perpendicular (71–90° angle) (Fig. 2g, h). After tracing for a longer period, most isolated dyads in this zone were also parallel to the longitudinal growth axis (Extended Data Fig. 5a). Cells in the growth plate might also orient as a result of migration or stacking due to tissue polarization[15], which is reflected by the orientation of primary cilia[16]. Cilia on flat chondrocytes, but not on chondroprogenitors, were polarized (with 61.3 ± 4.8% and 32.8 ± 2.2% of cilia, respectively, oriented longitudinally, $P = 0.005$, $n = 3$; Extended Data Fig. 5b). The 13% of dyads that are oriented perpendicularly indicates that some stem cells divide symmetrically, as supported by symmetric distribution of partitioning protein 3 (PAR3), a marker for symmetrical/asymmetrical division, within clonal dyads (Extended Data Fig. 5c). The number of cells expressing PAR3 and atypical protein kinase C-ζ (PKC-ζ), was relatively small and was not enhanced substantially by blocking spindle degradation with Taxol[17], which resulted in both symmetric and asymmetric distribution of PAR3 (Extended Data Fig. 5d–g). These low marker levels probably reflect slow proliferation in the resting zone, visualized by staining for phosphorylated histone H3 (Extended Data Fig. 5h).

To demonstrate symmetric division of colony-forming cells functionally, we monitored changes in clonal width with time. In the growth plate, symmetric division of stem cells would lead to larger multicolumnar clones, as we observed after tracing for 5 months (Fig. 2i). This observation implies symmetric division of chondroprogenitors and thereby loss of some cells. Indeed, blunted columns were observed occasionally (arrows, Extended Data Fig. 5i). Thus, renewal of chondroprogenitors appears to involve both asymmetric and symmetric division.

Disruption of the stem cell niche impairs tissue maintenance, as in microcephaly[18] or hair growth[19]. Thus, disruption of the epiphyseal niche should stop the supply of chondrocytes and cause fusion of the growth plate, a process that is still largely unexplained[20]. Inhibition of the hedgehog pathway causes such fusion[21] and the results of LCM-seq indicated substantial changes in expression (shown in parentheses as a log2 fold-change) of targets of hedgehog signalling[22] upon niche formation, with *Foxf2* (5.2, $P = 0.08$), *Foxd1* (6.5, $P = 0.01$) and *Hey1* (3.2, $P = 0.3$) being upregulated and *Gas1* (−2.0, $P = 0.04$) and *Stil* (−2.4, $P = 0.03$) being downregulated; however, these changes were not statistically significant when adjusted for multiple comparison. Analysis of transgenic mice expressing GFP-tagged Sonic hedgehog (Shh) revealed abundant expression of Shh in the SOC (Extended Data Fig. 6a) by mesenchymal stem cells and their progenitors, as well as endothelial and haematopoietic cells (Extended Data Fig. 7). Accordingly, diffusion of Shh from the SOC, together with diffusion of Indian hedgehog (Ihh) from the hypertrophic zone[23] might lead to maximal hedgehog signalling specifically in the resting zone. Indeed, we detected extensive hedgehog signalling in round chondrocytes, both by in situ staining for *Gli2* (Extended Data Fig. 6b) and from recombination activity of Gli1-creERT (Extended Data Fig. 6c). Blocking hedgehog signalling with the SMO antagonist vismodegib (six administrations at P31–P34, tracing P30–P35) reduced clonal size specifically within the resting zone (Extended Data Fig. 6d) and subsequently caused fusion of the growth plate (Extended Data Fig. 6d).

Proliferation in the resting zone was inhibited by vismodegib (Extended Data Fig. 6e, f), whereas premature hypertrophy was not detected (MEF2C staining, Extended Data Fig. 6g). Of note, stem cells retained expression of the CD73 stem cell marker (Extended Data Fig. 6h), suggesting that the hedgehog pathway helps maintain the cycle of stem cells, but not their identity. Activation of hedgehog signalling with the SMO agonist SAG (six administrations at P31–P34, analysed at P35) increased proliferation within the niche (Extended Data Fig. 6i), but did not expand the CD73-positive domain ($P = 0.3$, $n = 5$ (vehicle), $n = 3$ (SAG), Extended Data Fig. 6k). Even a single intra-articular injection of SAG accelerated proliferation within the niche 24 h later (Extended Data Fig. 6j). Finally, neither stimulation of the hedgehog pathway by Shh nor inhibition by vismodegib or GANT61 (a Gli1 inhibitor) altered the number of colony-forming units of double-positive $CD73^{+}CD49e^{+}$ cells (Extended Data Fig. 6m);

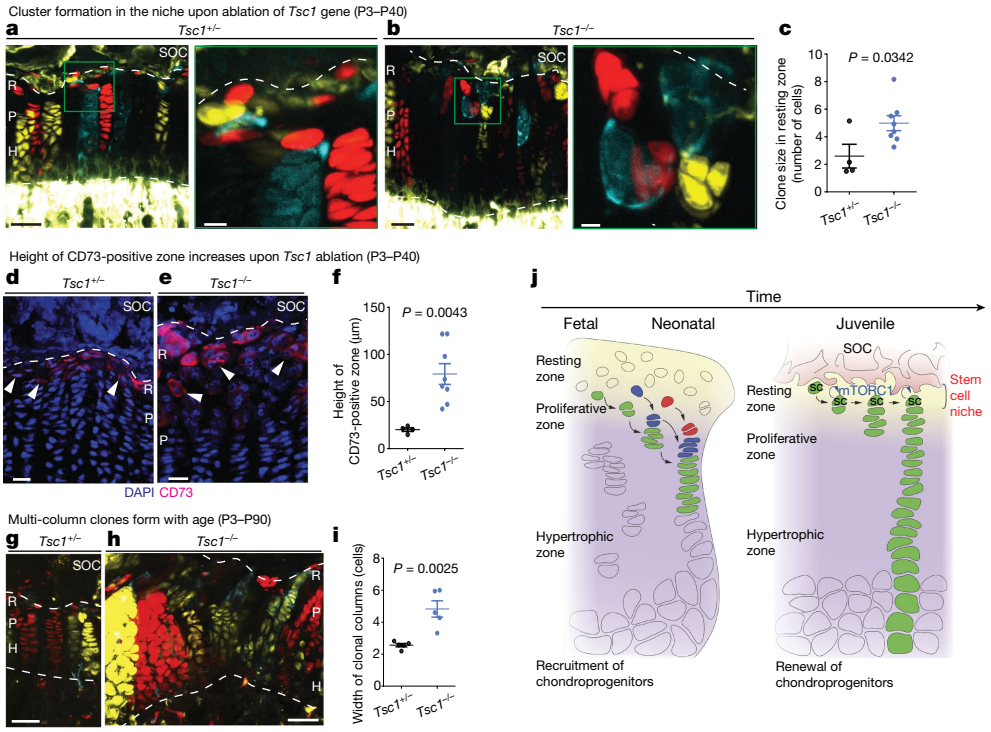

Fig. 3 | Activation of the mTORC1 pathway promotes symmetric cell division in the growth plate. a, **b**, Col2-creERT:*R26R*-Confetti:*Tsc1*$^{fl/+}$ (*Tsc1*$^{+/-}$) (**a**) and Col2-creERT:*R26R*-Confetti:*Tsc1*$^{fl/fl}$ (*Tsc1*$^{-/-}$) (**b**) mice were administered tamoxifen at P3 and analysed at P40. **c**, The clonal size of round cells above the columnar zone was quantified in confocal scans of 150-μm-thick central sections of the tibia using Imaris software. $n = 4$ (*Tsc1*$^{+/-}$), $n = 8$ (*Tsc1*$^{-/-}$). **d**–**f**, Immunofluorescence of CD73 in *Tsc1*$^{+/-}$ (**d**) and *Tsc1*$^{-/-}$ (**e**) mice, quantified (**f**) using Imaris. Arrowheads, typical labelling in the resting zone. $n = 4$ (*Tsc1*$^{+/-}$), $n = 8$ (*Tsc1*$^{-/-}$). **g**–**i**, Mice were injected with tamoxifen as in **a** and **b**, but analysed at P90. The average width of clones entering the primary spongiosa in **g** and **h** was quantified (**i**). $n = 5$ mice per genotype. **j**, Graphical summary illustrating how the growth mechanism changes after the formation of the SOC. Dashed lines demarcate the growth plate, and labels indicating the SOC, and the resting (R), proliferating (P), and hypertrophic (H) zones are included for orientation where appropriate. Data in **a**–**f** represent several mice from two independent litters; **g**–**i** represent three independent litters; data in graphs are mean ± s.e.m. and were analysed by unpaired two-tailed *t*-tests. Scale bars: 50 μm (**a** (left), **b** (left), **g**, **h**), 10 μm (**a** (right), **b** (right)) and 20 μm (**d**).

however, stimulation of the hedgehog pathway increased, and inhibition decreased, the number of cells per colony (Extended Data Fig. 6l), again supporting a role for hedgehog signalling in the proliferation, but not identity, of stem cells. Altogether, these findings indicate that hedgehog signalling is involved in renewal of stem cells in the epiphyseal niche.

The balance between symmetric and asymmetric division of stem cells has implications for niche function. We recently found that activation of mTORC1 by chondrocyte-specific ablation of the *Tsc1* gene disorganizes the resting zone after formation of the SOC[24], without affecting chondrocyte proliferation or differentiation[24] (Supplementary Table 3). To explore further, we crossed Col2-creERT:*Tsc1* floxed mice with R26R-Confetti mice and injected their offspring with tamoxifen on P3. Their resting zone started to become disorganized at P28 (Extended Data Fig. 8a, b) with obvious clonal clusters forming 12 days later (Fig. 3a-c; Extended Data Fig. 8c, d; Supplementary Table 3). There was no detectable expression of the chondrocyte markers *ColX* or *Ihh* in these clusters (Extended Data Fig. 8e–g), but *Gli2* (Extended Data Fig. 8h) and the stem cell marker CD73 (Fig. 3d–f) were expressed. Notably, CD73 was expressed by all cells in isolated Confetti-labelled dyads within the resting zone of both *Tsc1*$^{+/-}$ ($n = 7$) and *Tsc1*$^{-/-}$ ($n = 7$) mice traced at P3–P40. Activation of the mTORC1 pathway was confirmed by an increased level of phosphorylated S6 restricted to cells in the hypertrophic and resting zones (Extended Data Fig. 8i).

Surprisingly, when proliferation of slowly dividing cells was assessed by injecting EdU (daily for four days before tissue collection at P40), the number of EdU-positive epiphyseal stem cells increased (62.4 ± 7.5 ($n = 7$) versus 24.7 ± 3.7 ($n = 3$) per section; mean ± s.e.m.; $P = 0.014$), with no change relative to the total number of resting-zone cells (Extended Data Fig. 9a–c). The percentage of EdU-positive flat cells and their migration to the hypertrophic zone were also unaltered (Extended Data Fig. 9c). This unchanged proliferation of stem cells was confirmed by immunostaining for Ki67 and phosphorylated histone H3 (Extended Data Fig. 9d, e, Supplementary Table 3). The proliferation of underlying flat chondrocytes (Extended Data Fig. 9f, EdU labelling for 4 h on P40, immediately before tissue collection) and expression of the chondrocyte marker SOX9 (Extended Data Fig. 9g) were also unaffected by mTOR activation. The cilia on cells above the columns were distributed irregularly, suggesting lack of tissue polarization (Extended Data Fig. 9h). Thus, neither proliferation of chondroprogenitors nor their recruitment into the proliferative layer changed detectably, whereas clones in the resting zone grew gradually.

We hypothesized that alteration of mTORC1 signalling slightly shifts cell division from asymmetric to symmetric. Indeed, PAR3 was distributed symmetrically in a larger proportion of stem cell clonal dyads in Tsc1 conditional-knockout mice (P3–P40, Extended Data Fig. 10a). Furthermore, the number and thickness of multi-columnar clones in these mice increased with time (during P3–P90, Fig. 3g–i), indicating accelerated expansion of colony-forming cells. Clusters of chondroprogenitors in these mice (P3–P40) retain hedgehog dependence, as vismodegib (eight doses, twice daily for four days before analysis on P45) forced them to differentiate directly into columnar cells and form multi-columnar clones (Extended Data Fig. 10b; Supplementary Videos 3, 4), resembling those that develop with age (Fig. 3h). Upon vismodegib treatment, some CD73-positive cells detached from the niche and entered the columnar layer without starting to proliferate (Extended Data Fig. 10b), again suggesting that hedgehog signalling regulates stem cell renewal, but not identity. Finally, inhibition of mTORC1 by tissue-specific ablation of Raptor slightly enhanced loss of clones in otherwise phenotypically normal growth plates (arrowheads,

Extended Data Fig. 10c), resulting in fewer Confetti-labelled columns in the growth plate and mild growth retardation (Extended Data Fig. 10c; Supplementary Table 4). This suggests a slight shift towards lineage-restricting division, a phenotype opposite to that in the *Tsc1* conditional-knockout mice. Thus, the mTORC1 pathway modulates the balance between symmetric and asymmetric division of stem cells in this niche. Given that mTORC1 is closely connected with metabolic signalling in cells, mTORC1 may link stem cell renewal to local energy and oxygen levels, which are known to regulate stem cell behaviour[8].

In summary, a stem cell niche develops in the postnatal epiphyseal growth plate, facilitating self-renewal of chondrocyte progenitors and enabling a continuous supply of chondrocytes for bone elongation (summarized in Fig. 3j). Formation of a niche for maintenance of slowly dividing stem/progenitor cells appears to be common to tissues requiring continuous generation of terminally-differentiated progeny, such as skin, intestine, blood or germ-line cells[11,14]. These insights may help to improve the treatment of children with growth disorders.

Online content

Any methods, additional references, Nature Research reporting summaries, source data, statements of data availability and associated accession codes are available at https://doi.org/10.1038/s41586-019-0989-6.

Received: 29 September 2017; Accepted: 1 February 2019;
Published online 27 February 2019.

1. Hall, B. K. *Bones and Cartilage: Developmental and Evolutionary Skeletal Biology* 2nd edn (Academic Press, Cambridge, MA, 2015).
2. Moss-Salentijn, L., Moss, M. L., Shinozuka, M. & Skalak, R. Morphological analysis and computer-aided, three dimensional reconstruction of chondrocytic columns in rabbit growth plates. *J. Anat.* **151**, 157–167 (1987).
3. Nakamura, E., Nguyen, M. T. & Mackem, S. Kinetics of tamoxifen-regulated Cre activity in mice using a cartilage-specific CreERT to assay temporal activity windows along the proximodistal limb skeleton. *Dev. Dyn.* **235**, 2603–2612 (2006).
4. Snippert, H. J. et al. Intestinal crypt homeostasis results from neutral competition between symmetrically dividing Lgr5 stem cells. *Cell* **143**, 134–144 (2010).
5. Gerber, H.-P. et al. VEGF couples hypertrophic cartilage remodeling, ossification and angiogenesis during endochondral bone formation. *Nat. Med.* **5**, 623–628 (1999).
6. Joost, S. et al. Single-cell transcriptomics reveals that differentiation and spatial signatures shape epidermal and hair follicle heterogeneity. *Cell Syst.* **3**, 221–237 (2016).
7. Rompolas, P. et al. Spatiotemporal coordination of stem cell commitment during epidermal homeostasis. *Science* **352**, 1471–1474 (2016).
8. Suda, T., Takubo, K. & Semenza, G. L. Metabolic regulation of hematopoietic stem cells in the hypoxic niche. *Cell Stem Cell* **9**, 298–310 (2011).
9. Clevers, H. The intestinal crypt, a prototype stem cell compartment. *Cell* **154**, 274–284 (2013).
10. Schofield, R. The relationship between the spleen colony-forming cell and the haemopoietic stem cell. *Blood Cells* **4**, 7–25 (1978).
11. Morrison, S. J. & Spradling, A. C. Stem cells and niches: mechanisms that promote stem cell maintenance throughout life. *Cell* **132**, 598–611 (2008).
12. Nichterwitz, S. et al. Laser capture microscopy coupled with Smart-seq2 for precise spatial transcriptomic profiling. *Nat. Commun.* **7**, 12139 (2016).
13. Gilbert, S. F. *Developmental Biology* 11th edn (Sinauer Associates, Sunderland, MA, 2017).
14. Hsu, Y. C., Li, L. & Fuchs, E. Emerging interactions between skin stem cells and their niches. *Nat. Med.* **20**, 847–856 (2014).
15. Li, Y. & Dudley, A. T. Noncanonical frizzled signaling regulates cell polarity of growth plate chondrocytes. *Development* **136**, 1083–1092 (2009).
16. de Andrea, C. E. et al. Primary cilia organization reflects polarity in the growth plate and implies loss of polarity and mosaicism in osteochondroma. *Lab. Invest.* **90**, 1091–1101 (2010).
17. Rowinsky, E. K. & Donehower, R. C. Paclitaxel (Taxol). *N. Engl. J. Med.* **332**, 1004–1014 (1995).
18. Lancaster, M. A. et al. Cerebral organoids model human brain development and microcephaly. *Nature* **501**, 373–379 (2013).
19. Rompolas, P. et al. Live imaging of stem cell and progeny behaviour in physiological hair-follicle regeneration. *Nature* **487**, 496–499 (2012).
20. Emons, J., Chagin, A. S., Sävendahl, L., Karperien, M. & Wit, J. M. Mechanisms of growth plate maturation and epiphyseal fusion. *Horm. Res. Paediatr.* **75**, 383–391 (2011).
21. Kimura, H., Ng, J. M. Y. & Curran, T. Transient inhibition of the Hedgehog pathway in young mice causes permanent defects in bone structure. *Cancer Cell* **13**, 249–260 (2008).
22. Everson, J. L., Fink, D. M., Chung, H. M., Sun, M. R. & Lipinski, R. J. Identification of sonic hedgehog-regulated genes and biological processes in the cranial neural crest mesenchyme by comparative transcriptomics. *BMC Genomics* **19**, 497 (2018).
23. Maeda, Y. et al. Indian Hedgehog produced by postnatal chondrocytes is essential for maintaining a growth plate and trabecular bone. *Proc. Natl Acad. Sci. USA* **104**, 6382–6387 (2007).
24. Newton, P. T., Xie, M., Medvedeva, E. V., Sävendahl, L. & Chagin, A. S. Activation of mTORC1 in chondrocytes does not affect proliferation or differentiation, but causes the resting zone of the growth plate to become disordered. *Bone Rep.* **8**, 64–71 (2018).

Acknowledgements We thank H. M. Kronenberg (MGH) for critical reading of this manuscript, O. Dobre (Blue Insight) for programming the web simulator, O. Kharchenko for graphical work (Fig. 3j), and M. E. Kastriti and O. Podgorny for methodological advice. This work was supported financially by the Swedish Research Council (A.S.C., K.F., L. Sävendahl, E.H., M.K., I.A., V.D., J.P., A.G.-L.), Karolinska Institute (A.S.C., L.L., M.K., I.A.), StratRegen KI and Stiftelsen Konung Gustaf V:s 80-årsfond (A.S.C.), Swedish Cancer Society (M.K.), the Swiss National Science Foundation (C.S.), EMBO (M.X.), Stiftelsen Frimurare Barnhuset and Sallskapet Barnavard (P.T.N.) and the Grant Agency of the Czech Republic (#14-37368G, M.H.). We also acknowledge support from the National Genomics Infrastructure in Stockholm funded by Science for Life Laboratory, the Knut and Alice Wallenberg Foundation, the Swedish Research Council, and SNIC/Uppsala Multidisciplinary Center for Advanced Computational Science for assistance with massively parallel sequencing and access to the UPPMAX computational infrastructure.

Reviewer information *Nature* thanks Ophir Klein, Michael Longaker and the other anonymous reviewer(s) for their contribution to the peer review of this work.

Author Contributions P.T.N. and A.S.C. conceived the study. P.T.N. performed the majority of the experiments with the help of L.L., B.Z., L. Sandhow, M.X., S.S., X.S., H.Q., M.H., T.B., M.E.S., A.G.-L., J.P., J.L., A.M., C.S., V.D. and E.I. A.V.A. carried out all the bioinformatics analysis. I.A., G.E., L. Sävendahl, E.H., K.F. and M.K. contributed intellectually throughout the project. P.T.N. and A.S.C. wrote the manuscript. All of the authors critically reviewed this manuscript and approved the final draft. More details are provided in the Supplementary Information.

Competing interests The authors declare no competing interests.

Additional information
Extended data is available for this paper at https://doi.org/10.1038/s41586-019-0989-6.
Supplementary information is available for this paper at https://doi.org/10.1038/s41586-019-0989-6.
Reprints and permissions information is available at http://www.nature.com/reprints.
Correspondence and requests for materials should be addressed to P.T.N. or A.S.C.
Publisher's note: Springer Nature remains neutral with regard to jurisdictional claims in published maps and institutional affiliations.

METHODS

Mouse experiments. All mouse work was approved by the Ethical Committee on Animal Experiments (Stockholm North Committee/Norra Djurförsöksetiska Nämd) and conducted in accordance with The Swedish Animal Agency´s Provisions and Guidelines for Animal Experimentation. The sample size was chosen on the basis of expense of data collection and the need for sufficient statistical power. The null hypothesis was tested with a minimum of 3 (usually 3–7) independent observations (that is, mice), and if rejected with a statistical power 0.95 or above, the number of observation was retained as tested. If a statistical power was below 0.95, power analysis was performed to determine the sample size required to reject the null hypothesis. If the outcome was more than 30 observations required to reject the null hypothesis, such a rejection was considered below biological significance. All observations were done on samples from different mice, where each mouse was considered as an individual observation unless stated otherwise. For every experiment, mice were collected from at least two independent litters, and usually three or more unless otherwise specified. No data were presented in the manuscript, which cannot be reproduced. Randomization was performed blindly among mice of the same genotype. For example, out of 10 mice of each genotype obtained from two litters, for initial hypothesis testing, 3–5 mice were chosen randomly for each genotype. Analysis was performed by a blinded observer whenever possible. An exception was made only for comparing groups with obvious changes in phenotype where the observer could identify the groups on the basis of their appearance. Mice were used regardless of their sex and the majority of the experiments were performed before sexual maturation.

Mouse strains. In the Col2-creERT strain, developed by S. Mackem (NIH), expression of CreERT protein is controlled by *Col2a1*[3]. The Gli1-creERT2 strain is available from Jackson Laboratories (JAX#007913)[25]. Cre-mediated DNA recombination is dependent on tamoxifen in both of these strains. Rosa26R-Confetti (referred to as *R26R*-Confetti[4] or Confetti, and obtained from the laboratory of H. Clevers (Hubrecht Institute)) is a reporter mouse strain that contains the brainbow 2.1 construct[26]. Upon Cre-mediated DNA recombination, one of four different fluorescent proteins (nuclear green, cytoplasmic red, cytoplasmic yellow and membrane-bound cyan) is expressed in a stochastic manner from each allele, allowing clonal identification[4]. Importantly, in our system we almost never (less than 1% of the time) observed the appearance of green fluorescence of Confetti colours, which allowed us to combine Confetti with the H2B-GFP mouse; in such experiments, mice with only one Confetti allele were used (below). In the Tsc1-floxed mice (JAX#005680), developed by Kwiatkowski and colleagues, Cre-mediated recombination excises the essential exons 17 and 18[27]. Raptor-floxed mice (JAX#013188), in which exon 6 is excised by Cre-mediated recombination[28], were generated by Sabatini and colleagues. In the tdTomato reporter strain, Cre-mediated deletion of a stop codon in the Rosa-tdTomato gene (JAX #007908)[29] produces a red fluorescent protein. For clonal genetic tracing, the R26R-Confetti strain was crossed with Col2-creERT mice to produce the Col2-creERT:Confetti strain. Col2-creERT:Confetti stain were given a single intraperitonial injection of tamoxifen at a dose of between 25–100 μg per g body weight, to achieve recombination of varying efficiency for the spatial separation of individual clones. Neighbouring cells that expressed the same fluorescent protein were considered to be clonal. If this was unclear, based on morphology or the clonal pattern elsewhere on the section, these clones were excluded from quantification. For clonal genetic tracing of chondrocytes in embryogenesis, pregnant Col2-creERT:Confetti mice received a single intraperitoneal dose of 1.5–2.0 mg tamoxifen (Sigma, T5648) when pregnancy reached E14.5. Tamoxifen was dissolved in corn oil (Sigma, C8267). In mice homozygous for Confetti, differential recombination can occur on each allele, sometimes leading to the expression of two different fluorescent proteins; for example, cells expressing both RFP and YFP appear orange. Gli1-creERT2:tdTomato reporter mice were treated with 3 mg tamoxifen on P29 and analysed on P33. The Col2-creERT strain was crossed with Tsc1-floxed and R26R-Confetti mice to obtain inducible, chondrocyte-specific loss of Tsc1 in the developing epiphyseal cartilage. Gene ablation/tracing was induced on P3 by intraperitoneal injection of 400 μg tamoxifen. Note that the dose of tamoxifen used in the current study was reduced by 20% in order to decrease the efficiency of recombination and visualize individual clones, as compared to our previous report on these mice[24]. The Col2-creERT strain was crossed with Raptor-floxed and R26R-Confetti mice to obtain inducible, chondrocyte-specific loss of Raptor in the developing epiphyseal cartilage. Gene ablation and tracing was induced on P3 by intraperioneal injection of 500 μg tamoxifen. Cre-mediated recombination of the floxed allele in the cartilage was verified by PCR. H2B-GFP Tet-On mice, created by crossing Tg(tetO-HIST1H2BJ/GFP)47Efu/J mice (JAX #005104) with the B6.Cg-*Gt(ROSA)26Sor*$^{tm1(rtTA*M2)Jae}$/J (JAX #006965) strain, accumulate H2B histone conjugated with GFP upon exposure to doxycycline. Following cessation of treatment, the level of H2B–GFP is diluted out by every cell division so that slowly dividing cells can be identified based on their retention of GFP. The Shh-GFP reporter mouse strain (JAX #005622; Shhtm1(EGFP/cre)Cjt/J) expresses GFP under the transcriptional control of the Shh promoter. Antibodies were used to detect GFP in all cases.

Pharmacological modulation in vivo. To reduce the resorption of terminal hypertrophic chondrocytes and to block SOC development, mice were injected intraperitoneally with axitinib (Sigma, 25 mg per kg body weight, an inhibitor of VEGFR (as described[30])) once daily, and tissues were collected one day after the final dose. To assess the ability of axitinib to inhibit SOC development, SOC area was measured in the central section of the tibia using ImageJ. Vismodegib, an antagonist of the hedgehog pathway (100 mg/kg, LC Labs) or DMSO vehicle, was injected intraperitoneally twice daily[21]. With the Col2-creERT:*Tsc1* Confetti model, vismodegib (or the DMSO vehicle) was injected as follows: once on P40, twice daily on P41–P43 and once on P44; during this same experiment, single daily doses of axitinib were administered on P41–P44 to prevent fusion of the growth plate; and tissues were collected on P45. To block the separation of dividing cells, Taxol (Sigma, 10 mg per kg body mass) or the DMSO vehicle was injected once daily for 3 days before tissue collection.

Tissue processing. After tissue collection, the samples were placed into freshly prepared 4% formaldehyde in phosphate-buffered saline (PBS) and fixed for 6 h at 4 °C with mixing on a roller. Samples were then transferred to 30% sucrose (VWR, C27480) and rolled again overnight at 4 °C. Following embedding in OCT medium (Sakura, 102094-104), sections of between 10 μm and 150 μm in thickness were prepared with a cryostat (Leica, CM3050). For tissue subjected to in situ analysis, the fixation time was extended to 24 h. For bones from mice aged three months and over, brief decalcification was performed with 10% EDTA/4% formaldehyde solution, mixed on a roller for several days at 4 °C, and changed twice daily.

Confocal microscopy and image analysis. Confocal imaging and clonal analysis were performed with a Zeiss LSM710 fluorescence microscope, and Imaris and ImageJ software, as described previously[31]. In brief, the entire thickness of 10–150-μm sections of frozen samples was scanned, and 3D *z* stacks were constructed. The number of cells per clone was counted manually using Imaris software in 3D. Some analysis was performed without all colours when quantification recombination levels were extremely high. 3D confocal images were analysed in surpass and slice modes of Imaris. Typically, sections at the centre of the tibial growth plate (as determined from the position of the cruciate ligament) were used for quantification. The angle of cell division was measured in the 3D reconstructions with Imaris and a protractor. The images displayed are 3D reconstructions using Imaris or maximal projection, unless otherwise stated. Contrast, brightness and gamma adjustment have been altered to improve visualization in pseudocoloured confocal scans. The orientation of primary cilia was assessed in 3D by measuring the angle of the cilia to the nucleus, relative to the longitudinal axis of the bone using Imaris and a protractor.

EdU labelling and detection. EdU (Life Technologies, E10187) was injected to mice intraperitoneally at a dose of 65 μg per g body weight. After sample preparation, EdU was detected using a click reaction for 30 min at room temperature in a mixture containing 0.1 M Tris (pH 7.5), 2 mM $CuSO_4$, 0.1 M ascorbic acid and 2 μM Alexa Fluor azide 647, that was protected from light[32]. Quantification was conducted either manually using Imaris, or automatically using ImageJ.

Triple S-phase labelling protocol. Mice were injected with EdU (52 μg per g body weight) twice on P3, with 5-chloro-2′-deoxyuridine (CldU, 130 μg per g body weight) on P10, and finally with 5-iodo-2′-deoxyuridine (IdU 90 μg) on P12, 4 h before tissue collection. Bones were fixed overnight in ice-cold 4% formaldehyde/PBS, before being incubated overnight in 30% sucrose and then embedded in OCT. Sections 30 μm thick were prepared.

The method for the detection of the three BrdU analogues were based on ref. [33] but modified to reduce its duration in the following ways: the sections were incubated with 4% Triton X100/PBS for one hour. EdU was detected with the click reaction using Alexa Fluor azide 488, as described above. Blocking of non-specific reactions, DNA denaturation, and neutralization were performed as described[33]. After washing, blocking was performed with 5% normal horse serum in PBS containing 0.1% Triton X100 (PBST) for one hour at room temperature. To detect IdU, sections were incubated with mouse monoclonal anti-BrdU antibodies (clone B44, BD Biosciences, catalogue no. 347580), diluted 1:1,000 in blocking buffer, and incubated overnight with gentle shaking at room temperature in a humidified chamber. After washing sections three times with PBST, IdU was visualized by incubating sections with secondary anti-mouse antibodies conjugated to Cy3, diluted 1:400 in blocking buffer, with gentle shaking at room temperature in a humidified chamber for 2 h. Sections were washed three times with PBST, then CldU was visualized by incubating sections with anti-BrdU antibodies conjugated to Alexa Fluor 647 (clone BU1/75 (ICR1); Novus Biologicals, catalogue no. NB500-169AF647), diluted 1:1,000 in blocking buffer, for 2 h with gentle shaking at room temperature in a humidified chamber. Sections were washed 3 times in PBST, then once in PBS before mounting in Fluoroshield, and visualizing by confocal microscopy.

Histology and immunohistochemistry protocols. Samples were cut into 10–30-μm-thick sections for immunofluorescence. Antibodies used are listed in Supplementary Table 5. For primary antibodies of murine origin, additional blocking with Vectorshield mouse-on-mouse kit (Vector labs, MKB-2213) was performed. Antigen retrieval was achieved as follows: no retrieval (anti-pS6, anti-MEF2C, anti-PAR3), 0.1% trypsin for 30–45 min at room temperature (anti-phospho histone H3, anti-acetylated tubulin, anti PKC-ζ, anti-CD73, anti-Sox9), or boiling DAKO antigen retrieval buffer (anti-GFP, anti-Ki67). After blocking with 3% horse serum in PBS containing 0.1% Triton X100 (to detect cell surface markers, Triton X100 was excluded) for 30–60 min, slides were incubated with primary antibody overnight at 4 °C, washed with PBST (PBS, 0.1% Tween 20) and subsequently incubated with the appropriate secondary antibody for 60–90 min at room temperature under protection from light. Following counterstaining with DAPI, detection and imaging were carried out using a confocal Zeiss LSM710 fluorescence microscope. For Shh or Ihh immunohistochemistry, paraffin sections were processed as described previously[34]. Assessment of even or uneven distribution of PAR3 was performed by manually assessing the staining of dyads after 3D reconstruction using Imaris. When neighbouring cells within a Confetti-positive clone were both PAR3-positive, we assumed that this represented a symmetrically labelled dyad, whereas if only one cell in a clonal dyad was PAR3-positive we assumed asymmetrical division.

Immunofluoresence to screen for surface markers. Screening for surface stem cell markers was performed using antibodies against CD73 (TY/11.8, BioLegend, 127206), CD54 (BioLegend, clone YN1/1.7.4), CD90 (BioLegend, clone Ox-7), CD44 (BioLegend, clone IM7), CD29 (BioLegend, clone ebioHMB1-1), CD105 (BioLegend, clone MJ7/18), CD39 (BioLegend, 143807). For all antibodies except anti-CD73, positively-labelled cells could be detected in surrounding tissues but not in the growth plate. During FACS experiments, less than 2% of $CD73^{+}C49E^{+}$ cells were found to be SCA1-positive (BD Bioscience, clone E13-161.7).

In situ hybridization. In situ hybridization was performed as previously reported for *ColX*[35], and using the same protocol for *Gli2* and *Ihh*, but with probes provided by T. Kobayashi (Massachusetts General Hospital) and B. Lanske (Harvard School of Dental Medicine).

Labelling with calcein or xylenol. Mice were injected intraperitoneally with xylenol (0.09 mg per g body weight) or calcein (10 mg per kg body weight), 24 h or 48 h before tissue collection. The samples were collected, placed into 4% paraformaldehyde for 12–24 h at 4 °C on a roller, cryopreserved and sectioned as described above. The ImageJ software was used to measure the distance between mineralization front and the metaphyseal side of the growth plate.

Morphometric analysis. In connection with quantification of clone size in Figs. 1e, 2c, 2d and Extended Data Fig. 1e, only cells in clones with more than three cells were included, whereas all clones were included for Fig. 3c, Extended Data Fig. 6d‴, Extended Data Fig. 8b and Supplementary Table 3 to quantify resting-zone clone size. In Supplementary Tables 1–3, proliferating zone (flat) cells in histological sections were defined as those that were at least twice as wide as high and located within stacked columns.

Modelling cell kinetics. We created a web-based tool (http://www.chaginlab.com/sim) in which all the different parameters of cellular kinetics can be manipulated, including the rate of proliferation and number of cells in each zone. We also incorporated two models for the behaviour of round chondrocytes. In the first model (referred to as fetal), a new row of round cells is added at the top of the growth plate in connection with each cell division (according to the specified rate of proliferation for this zone). In the second model (juvenile) the uppermost-labelled cell in the column remains stable. Please see Supplementary Information for further information on using the web tool.

Isolation of growth-plate chondrocytes for FACS. Hind limbs of one-month-old wild-type mice (on a mixed background) were dissected into ice-cold PBS. Microdissection was performed to gently clean the tibia of muscle and ligaments in ice-cold dissection medium (DMEM/F-12-HEPES + 0.1 mg/ml gentamycin). Using a scalpel, the growth plate was cut through the hypertrophic zone and then the blunt side of the scalpel was used to carefully scrape out the cartilage until the blade reached the hard surface of the SOC. The pieces of cartilage were collected and treated with 0.15% collagenase II in dissection medium for 90–120 min at 37 °C on a roller and the digestion process was terminated by adding FBS to make up 20% of the volume. The cell suspension was centrifuged at 300*g* for 7 min and the supernatant discarded. The pelleted cells were resuspended in pre-FACS buffer (20% FBS, 0.05 mg/ml gentamycin and 5 mM EDTA in PBS).

Immunofluorescence staining and multi-colour FACS of resting-zone cells. The resting-zone cells were identified by combination staining of fluorescence-conjugated CD73 (1:100, FITC-conjugated, clone TY/11.8, BioLegend) and CD49e (1:100, PE-conjugated, clone 5H10-27, BioLegend). Dead cells were excluded by propidium iodine staining. Negative fractions were defined by the fluorescence minus one (FMO) method. $CD49e^{+}CD73^{+}$ and $CD49e^{+}CD73^{-}$ cells were sorted in FACS buffer (50% FBS, 0.05 mg/ml gentamycin and 5 mM EDTA in PBS) for subsequent culture. Analysis and sorting were performed on a FACSAria II (BD Biosciences). The data was analysed using FlowJo v.9.9.6 (TreeStar).

Differentiation potential of resting-zone cells. All differentiation experiments were performed after two passages of cell expansion. Pellets of 300,000 cells were cultivated for 3 weeks in the presence of chondrogenic differentiation medium. Chondrogenic differentiation medium consisted of DMEM with 4.5 g/l glucose, 1% penicillin/streptomycin (10,000 U/ml), 1% HEPES supplemented with 2 mM pyruvate, 0.35 mM L-proline, 1% of 'ITS +3 liquid media supplement' (insulin/transferrin/selenium supplement, 100×), 10^{-7} M dexamethasone, 5 μg/ml ascorbic acid and 10 ng/ml TGF-β3, control medium was DMEM with 4.5 g/l glucose, 1% penicillin/streptomycin (10,000 U/ml), 1% HEPES and 20% FBS. Medium was changed twice a week. On day 21, pellets were fixed in 4% formaldehyde for 48 h, embedded in OCT and stained with safranin O and Fast Green to assess chondrogenic differentiation. The protocols for adipogenic and osteogenic differentiation were applied as described[36]. In brief, cells were treated for 21 days with either adipogenic or osteogenic differentiation medium, respectively, and stained with oil red O (for lipids) and alizarin red (for mineralization), respectively, after fixation.

FACS and characterization of bone marrow cells from Shh-GFP mice. Hind limbs were collected from one-month-old Shh-GFP mice and transported from Prague to Stockholm in PBS containing 10% FBS on ice. Bone marrow cells were isolated and analysed by FACS analysis, as described[36]. In brief, femurs and tibias from one-month-old mice were crushed in PBS containing 10% FBS (PAA). The marrow cells were collected with a 70-μm cell strainer. The cells from bone were obtained by subsequent treatment of bone fragments with 0.1% collagenase II (CLS II Worthington Biochemical) for 30–45 min and with 0.05% trypsin-EDTA for 10 min at 37 °C. The bone and marrow cells were spun down at 300*g* for 5–10 min and resuspended in PBS containing 10% FBS. The cells were then incubated with purified anti-mouse CD16/32 antibody to block background staining, followed by anti-mouse CD31–PECY7, CD51–PE, CD45–PECY5, CD150–Alexa Fluor 647, CD117-APC/Cy7, TER119-PE/Cy5, SCA1–Alexa Fluor 700 and CD41–brilliant violet 421 antibodies. All samples were stained with the vital marker propidium iodide to exclude dead cells before analysis on a FACS Aria II (BD). Data analysis was carried out with FlowJo software (TreeStar). See Supplementary Table 5 for detailed information about the antibodies used in the study. The gates for each cell population were defined on the basis of FMO controls, in which one of the conjugated antibodies was omitted.

Laser-capture microdissection. We adapted LCM-seq[12,37] for cartilaginous tissue of the epiphyseal growth plate. Mouse bones were embedded in OCT medium by submerging in hexane, and pre-cooled in an ethanol bath containing dry ice. Tissues were sectioned at 10 μm thickness at −20 °C using a Microm cryostat, placed onto chilled PEN 1.0 Membrane Slides (Zeiss), dried (during optimisation, slides were dried directly in air, dried in air after passing through an ethanol gradient, or dried in air after passing through an ethanol gradient to xylene; as all methods were equally effective, samples from all drying methods were pooled for analysis (see Metadata file, GSE113982)) and stored at –80 °C until further use. To visualize the different cell populations in the epiphyseal growth plate for LCM, we conducted histological staining accordingly: slides were placed at room temperature for 30 s, the sections were sequentially submerged in 70% ethanol for 30 s, then in ultrapure water (Life Technologies) for 30 s, and stained in in Histogene Staining Solution (Arcturus) for 30–50 s. Sections were then washed in ultrapure water for 30 s, and fixed in 70% ethanol for 30 s, 95% ethanol for 30 s, and finally in 99.7% ethanol for 30 s. LCM was carried out on a Leica DM6000R/CTR6500 microscope using the Leica LMD7000 system to collect pools of cells from the resting and hypertrophic zones. A minimum of 12 cells was collected per pool (sample). In total, nine pools were collected from seven mice at P2 (for two mice, a pool was collected from each leg) and seven pools were collected from seven mice at P28. The collected cell pools were lysed in 5 μl ice-cold lysis buffer (0.2% Triton X-100, Sigma Aldrich, and 2 U/μl Recombinant RNase Inhibitor (Takara/Clontech), in ultrapure water) and instantly snap-frozen on dry ice.

cDNA library preparation and sequencing. Smart-Seq2 library preparation[38,39] was performed from the crude lysates with modifications as described[12] for LCM-seq, except for the tagmentation step, for which the Nextera XT DNA library Prep Kit (Illumina) was used.

LCM -seq data analysis. Illumina Casava v.1.7 software was used for base calling and demultiplexing. Adapters were trimmed from the 3′ end of the sequenced reads with Cutadapt software.

Single-end alignment to the mm10 genome was performed with STAR v.2.5.2b using default parameters. Read counts per gene were counted with the FeatureCounts tool (v.1.5.3) from the Subread package. Samples with fewer than 200,000 aligned reads were excluded during quality control. Overall, analysed samples had on average 689,000 aligned reads (ranging from 415,000 to 1,542,000 aligned reads), with 50.15% average mapping efficiency (ranging from 33.12% to 80.39%).

Even though RNA-seq data did not come from single cells, the small amount of cells in each sample (10–30 cells per sample) and the potentially high level of RNA degradation caused similar challenges in data analysis, such as high dropout rate: there was a high probability that a gene with non-zero expression had zero coverage in the RNA-seq experiment. To overcome these challenges, we applied PAGODA/SCDE[40,41] computational tools specifically designed to handle single-cell transcriptomic data.

We first investigated similarities between sequenced samples. To deal with dropouts, we investigated similarities of samples in the pathway space. We calculated the matrix of expression values for non-redundant PAGODA aspects constructed from gene sets (gene ontology categories and cluster of genes co-expressed in the analysed dataset) with PAGODA software[40]. We calculated the similarity between every pair of samples as Pearson's correlation between columns in this matrix. The resulting correlation matrix is shown in Extended Data Fig. 3e.

To find the genes differentially expressed between P28 and P2 time points, we aggregated the samples obtained from the mice of the same genotype of a given age from a given spatial region (for example, the resting zone). Only samples having more than 100,000 reads mapped to genes were considered for the analysis, yielding five mice per time point for the resting zone suitable for differential-expression analysis. We applied DESeq2[42] with default parameters. Gene expression of significantly up- and downregulated genes (false discovery rate (FDR) cut-off 0.005) normalized by DESeq2 is shown in Extended Data Fig. 3b, c. Differentially expressed genes were visualized on a heat map (shown in Extended Data Fig. 3d).

To determine which gene categories were enriched with upregulated and downregulated genes at P28 as compared to the P2 time point, we used gene ontology annotation from ENSEMBL BioMart. For each pathway, we performed Fisher's exact test to estimate the association between the presence of a gene in the given pathway and the presence of a gene among the significantly upregulated (or downregulated) genes (FDR cutoff 0.005). The calculated logarithmic *P* values of association for the most enriched pathways are shown in Extended Data Fig. 3b, c.

Statistical analysis. Data are presented as mean ± s.e.m., unless otherwise indicated. The unpaired Student's *t*-test was used to compare two groups, and one-way ANOVA with Tukey's multiple-comparison test was used to calculate *P* values when more than two groups were compared, unless otherwise specified. Excel and GraphPad Prism were used to calculate statistics, unless otherwise specified. The DESeq2 test with Benjamini–Hochberg multiple-testing correction was used for assessment of differentially expressed genes in LCM-seq data[42]. The violin plot was calculated as described[43]. Graphs were drawn with GraphPad Prism or Oriana software and Venn diagrams were constructed using the online tool provided by the United States Department of Transportation (https://www.usgs.gov/software/vbvenn-visual-basic-venn-diagram-software-page).

Code availability. The custom code build for the web tool (http://www.chagin-lab.com/sim) is available upon request from the corresponding author without restrictions.

Reporting summary. Further information on experimental design is available in the Nature Research Reporting Summary linked to this article.

Data availability

The LCM-seq dataset generated during the study has been deposited at the Gene Expression Omnibus with accession number GSE113982. Numerical source data for the figures are provided in the Supplementary Information and all original confocal scans are available upon request to the authors.

25. Ahn, S. & Joyner, A. L. Dynamic changes in the response of cells to positive hedgehog signaling during mouse limb patterning. *Cell* **118**, 505–516 (2004).
26. Livet, J. et al. Transgenic strategies for combinatorial expression of fluorescent proteins in the nervous system. *Nature* **450**, 56–62 (2007).
27. Kwiatkowski, D. J. et al. A mouse model of TSC1 reveals sex-dependent lethality from liver hemangiomas, and up-regulation of p70S6 kinase activity in Tsc1 null cells. *Hum. Mol. Genet.* **11**, 525–534 (2002).
28. Sengupta, S., Peterson, T. R., Laplante, M., Oh, S. & Sabatini, D. M. mTORC1 controls fasting-induced ketogenesis and its modulation by ageing. *Nature* **468**, 1100–1104 (2010).
29. Madisen, L. et al. A robust and high-throughput Cre reporting and characterization system for the whole mouse brain. *Nat. Neurosci.* **13**, 133–140 (2010).
30. Hall, A. P., Westwood, F. R. & Wadsworth, P. F. Review of the effects of anti-angiogenic compounds on the epiphyseal growth plate. *Toxicol. Pathol.* **34**, 131–147 (2006).
31. Kaucka, M. et al. Analysis of neural crest-derived clones reveals novel aspects of facial development. *Sci. Adv.* **2**, e1600060 (2016).
32. Salic, A. & Mitchison, T. J. A chemical method for fast and sensitive detection of DNA synthesis *in vivo*. *Proc. Natl Acad. Sci. USA* **105**, 2415–2420 (2008).
33. Podgorny, O., Peunova, N., Park, J. H. & Enikolopov, G. Triple S-phase labeling of dividing stem cells. *Stem Cell Reports* **10**, 615–626 (2018).
34. Reibring, C.-G. et al. Expression patterns and subcellular localization of carbonic anhydrases are developmentally regulated during tooth formation. *PLoS ONE* **9**, e96007 (2014).
35. Chagin, A. S. et al. G-protein stimulatory subunit alpha and Gq/11α G-proteins are both required to maintain quiescent stem-like chondrocytes. *Nat. Commun.* **5**, 3673 (2014).
36. Xiao, P. et al. *Sipa1* deficiency-induced bone marrow niche alterations lead to the initiation of myeloproliferative neoplasm. *Blood Adv.* **2**, 534–548 (2018).
37. Nichterwitz, S., Benitez, J. A., Hoogstraaten, R., Deng, Q. & Hedlund, E. LCM-seq: a method for spatial transcriptomic profiling using laser capture microdissection coupled with polyA-based RNA sequencing. *Methods Mol. Biol.* **1649**, 95–110 (2018).
38. Picelli, S. et al. Smart-seq2 for sensitive full-length transcriptome profiling in single cells. *Nat. Methods* **10**, 1096–1098 (2013).
39. Picelli, S. et al. Full-length RNA-seq from single cells using Smart-seq2. *Nat. Protoc.* **9**, 171–181 (2014).
40. Fan, J. et al. Characterizing transcriptional heterogeneity through pathway and gene set overdispersion analysis. *Nat. Methods* **13**, 241–244 (2016).
41. Kharchenko, P. V., Silberstein, L. & Scadden, D. T. Bayesian approach to single-cell differential expression analysis. *Nat. Methods* **11**, 740–742 (2014).
42. Love, M. I., Huber, W. & Anders, S. Moderated estimation of fold change and dispersion for RNA-seq data with DESeq2. *Genome Biol.* **15**, 550 (2014).
43. Hintze, J. L. & Nelson, R. D. Violin plots : a box plot–density trace synergism. *Am. Stat.* **52**, 181–184 (1998).

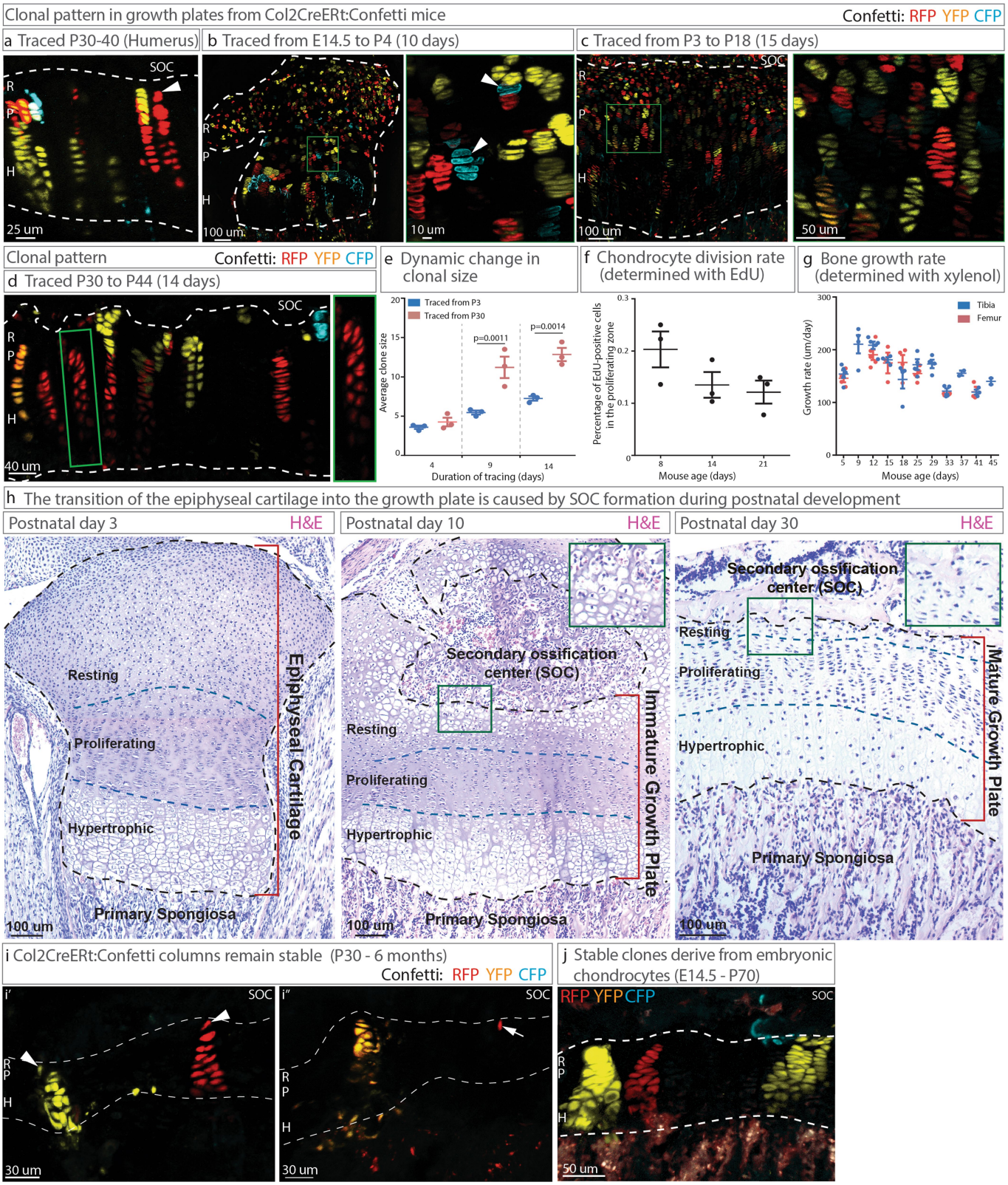

Extended Data Fig. 1 | See next page for caption.

Extended Data Fig. 1 | Clonality and growth rate dynamics during maturation of the growth plate. a–d, Clonal pattern in Col2-creERT:*R26R*-Confetti mice traced from P30 to P40 (**a**; the humerus is shown, all other images throughout the manuscript show tibial growth plates), from E14.5 to P4 (**b**), from P3 to P18 (**c**) and from P30 to P44 (**d**). Arrowheads in **a** and **b** show typical clones. **e**, Col2-creERT:*R26R*-Confetti mice received tamoxifen at either 3 or 30 days of age and were traced simultaneously for 4, 9 or 14 days. Clone size was quantified using Imaris. $n = 3$ mice per age per time point; mean ± s.e.m.; one-way ANOVA with Tukey multiple comparisons. **f**, Chondrocyte proliferation rate (single EdU injection, 24 h before analysis) was quantified at different ages. Data are mean ± s.e.m.; $n = 3$ mice per age. **g**, The rate of bone formation under the growth plate of proximal tibia or distal femur was assessed by xylenol pulse-chase bone labelling. $n = 2$–4 mice per time point; mean ± s.e.m. **h**, Representative histological images (haemotoxylin and eosin staining) of the proximal tibial growth plate before (P3, left), during (P10, middle) and after (P30, right) SOC formation. Blue dashed lines demarcate borders between the resting, proliferating and hypertrophic zones. The junction between SOC and the resting zone is magnified in inserts. **i**, Col2-creERT:*R26R*-Confetti mice traced from P30 to 6 months of age. Arrowheads indicate stable clones and the arrow indicates a labelled resting-zone cell, which did not form a column during the tracing period. **j**, Col2-creERT:*R26R*-Confetti mice traced from E14.5 to P70. The black or white dashed lines demarcate the growth plate from the surrounding tissues. Data in **a**–**d** and **j** represent two independent experiments or litters, data in **e**–**h** represent one experiment per time point (with the number of mice per data point indicated above), whereas data in **i** represent 3 independent experiments or litters.

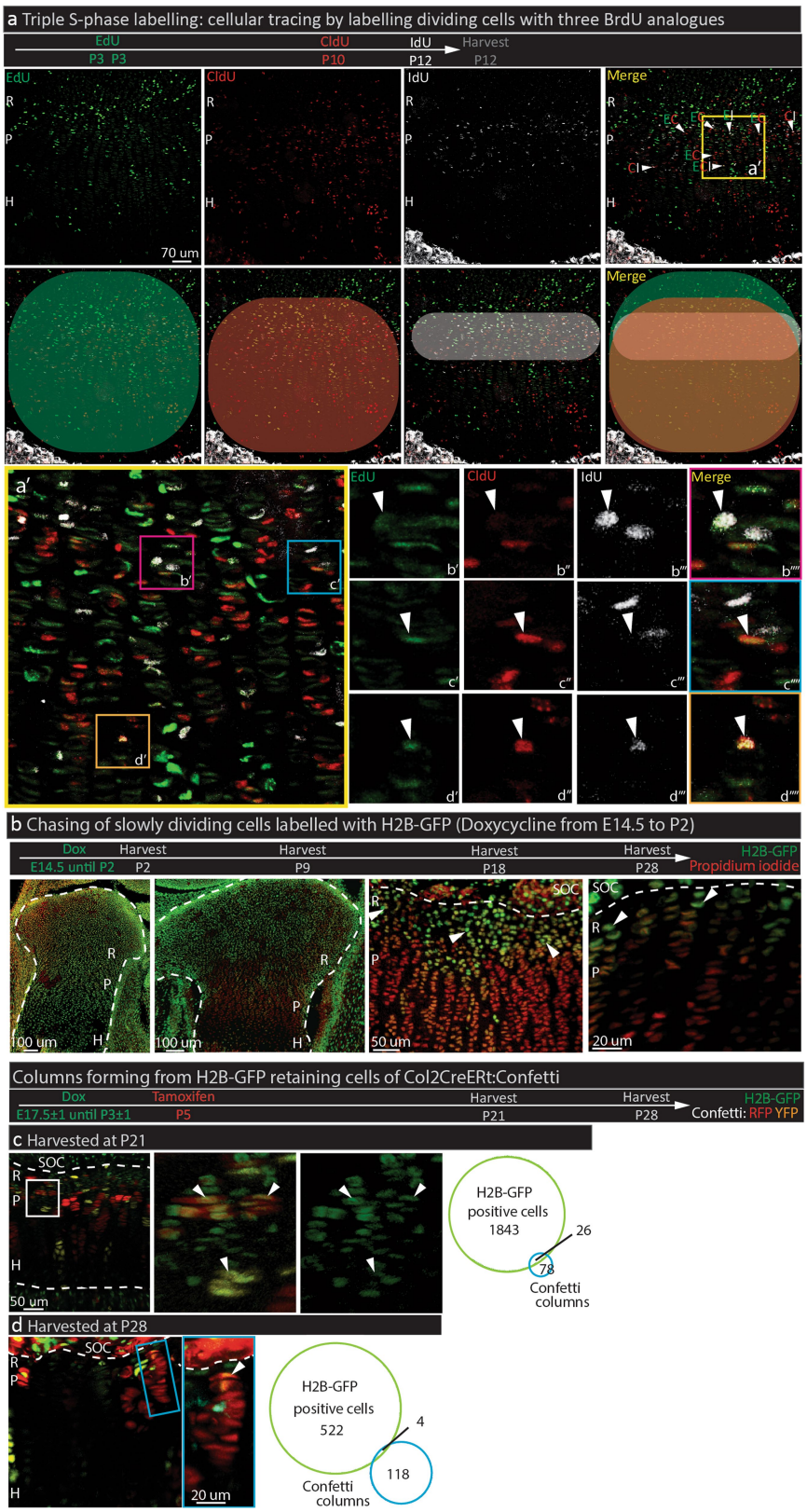

Extended Data Fig. 2 | See next page for caption.

Extended Data Fig. 2 | Contribution of slowly dividing resting-zone cells to the underlying growth-plate zones. a, Mice were injected with EdU on P3 (two doses), CldU on P10 and IdU on P12, 4 h before tissue collection. Confocal images of stained sections are presented, with individual channels shown in the top row, and channels merged to the right. The merged image is labelled with arrowheads indicating double positive cells (E, EdU; I, IdU; C, CldU) and area in **a′** expanded below to show a close-up image of double- and triple-positive cells (**b′**–**d′**). The second row in **a** shows domains containing each label and the overlapping areas. **b**, LRCs were identified in H2B-GFP mice (Tg(tetO-HIST1H2BJ/GFP)47Efu/J mice crossed with B6.Cg-*Gt(ROSA)26Sor*$^{tm1(rtTA*M2)Jae}$/J), exposed to doxycycline from E14.5 to P2, and chased until P2, P9, P18 or P28. LRCs appear green, whereas nuclei were visualized with propidium iodide (red). Arrowheads indicate typical GFP-retaining cells in the resting zone. Laser power was enhanced for older mice in order to obtain comparable GFP intensity in confocal scans. **c**, **d**, H2B-GFP mice were crossed with Col2-creERT:*R26R*-Confetti mice and column-forming LRCs were visualized with doxycycline being administered from E17.5 ± 1 day until P3 ± 1 and tamoxifen on P5. Colocalization of GFP-retaining cells with Confetti clones (arrowheads) were quantified at P21 (**c**) and P28 (**d**). Dashed lines in **b**–**d** demarcate the border between cartilage and the surrounding tissues. The SOC, resting (R), proliferating (P), and hypertrophic (H) zones are labelled for orientation. Data in **a** represents two independent experiments, data in **c** and **d** represent one experiment per time point.

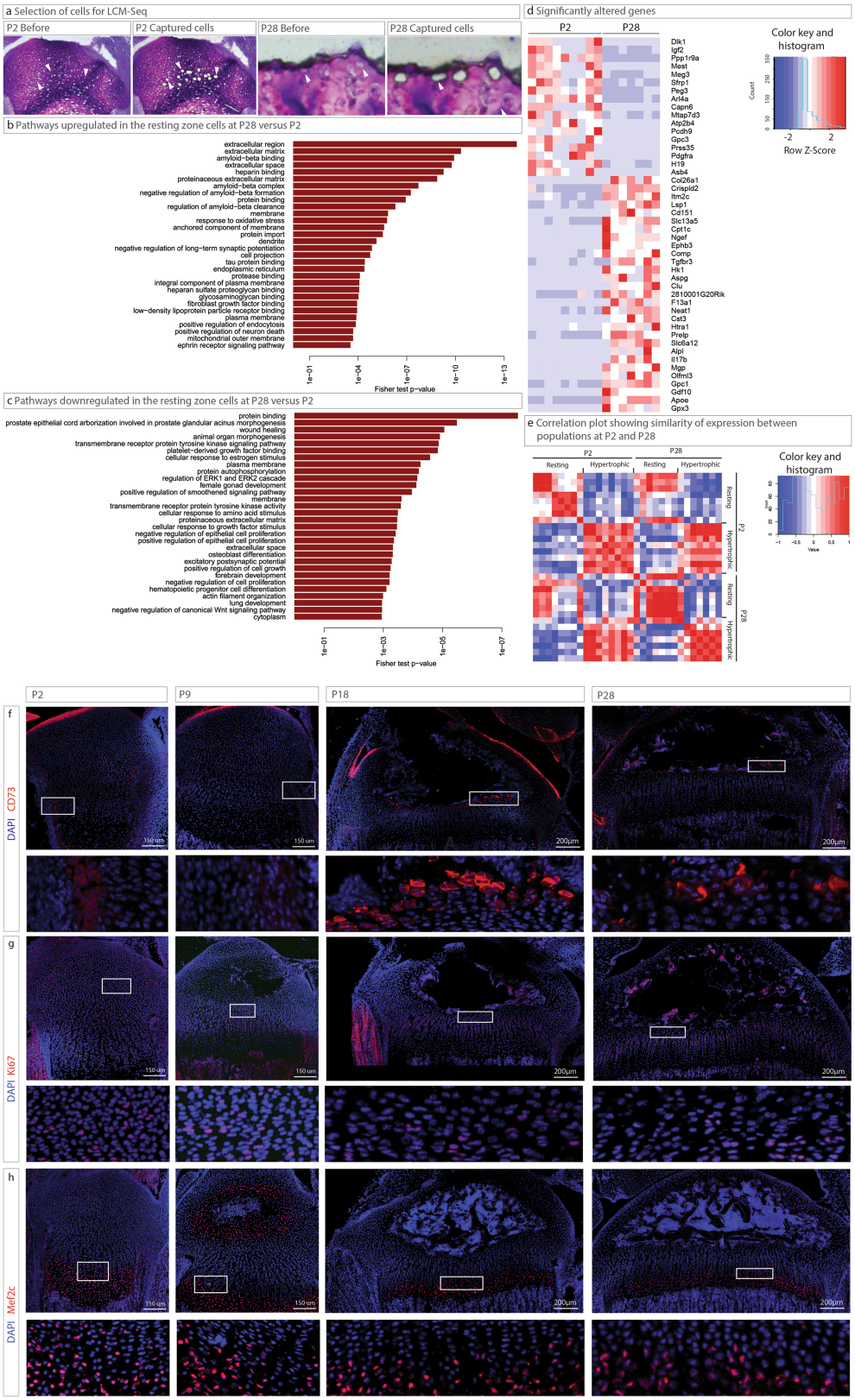

Extended Data Fig. 3 | See next page for caption.

Extended Data Fig. 3 | Changes in the expression profile of the resting zone upon niche formation. a, Sections of cartilage at P2 and P28 were imaged before and after cells were captured by LCM for subsequent RNA-seq analysis. **b**, **c**, Gene ontology categories enriched by genes significantly upregulated (**b**) or downregulated (**c**) in the resting zone at P28 compared to P2. Logarithmic *P* values of significance are indicated on the *x* axis. **d**, Expression heat map for the genes most significantly up- and downregulated between P2 and P28 time points in the resting zone (DESeq2 test with multiple testing correction, FDR < 0.005). **e**, Heat map of similarities in gene expression between individual samples from the resting and hypertrophic zones from P2 and P28 time points. For each sample, expression of non-redundant PAGODA aspects was calculated and similarity between samples was defined as correlation of aspect expressions (see Methods for details). **f**–**h**, Proximal tibial growth plates from P2, P9, P18 and P28 mice were immunostained for CD73 (**f**), Ki67 (**g**) or MEF2C (**h**) and counterstained with DAPI. For **a**–**e**, a total of 8 pools of cells from 7 mice were collected at P2 and 7 pools of cells from 7 mice were collected at P28. For **f**–**h**, staining was performed in a single experiment (minimum 3 mice) per time point.

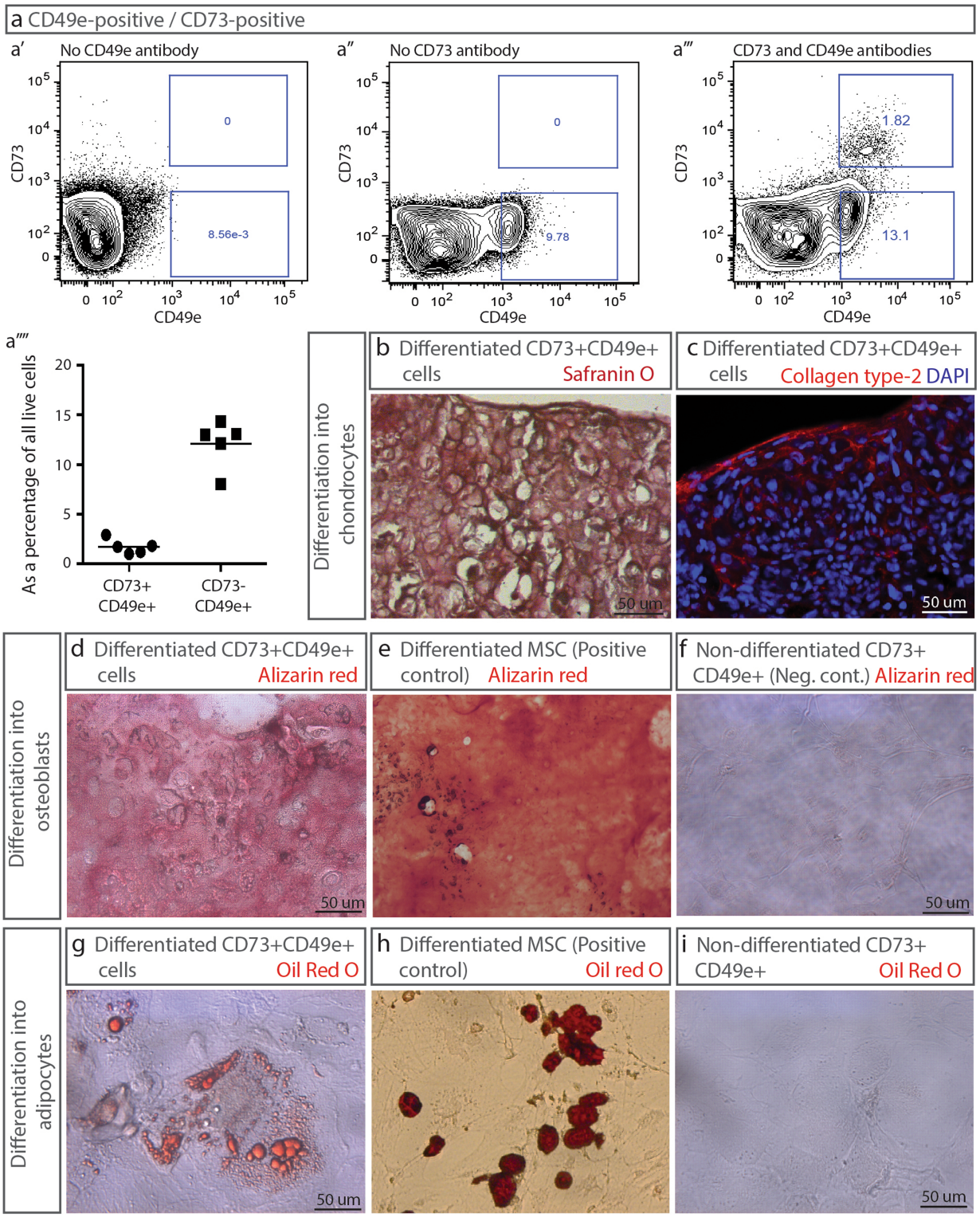

Extended Data Fig. 4 | Isolation and ex vivo differentiation of CD49e$^+$CD73$^+$ resting-zone stem cells. a, Isolated growth-plate chondrocytes were analysed by FACS and the live cells were sorted for expression of both CD73 and CD49e. FMO control for CD49e (**a′**), FMO control for CD73 antibody (**a″**) and gating strategy for both CD49e and CD73 (**a‴**); percentage of single (CD49e$^+$CD73$^-$) and double (CD49e$^+$CD73$^+$) positive cells among all live cells. **b**, **c**, The CD49e$^+$CD73$^+$ cells were grown in chondrogenic conditions in pellets ex vivo, and thereafter stained either with safranin-O (**b**) or for type-II collagen by immunofluorescence (**c**). **d**–**f**, Alizarin red staining (**d**) indicated that CD49e$^+$CD73$^+$ cells cultured in osteoblastic-differentiation medium differentiated to osteoblasts similarly to mesenchymal stem cells (MSCs) (**e**), but not in the absence of differentiation medium (**f**). **g**–**i**, Oil red O staining indicated that CD49e$^+$CD73$^+$ cells cultured in adipogenic-differentiation medium differentiated to adipocytes (**g**), albeit to a lesser extent than MSCs (**h**), but not in the absence of differentiation medium (**i**). Data represents two independent experiments.

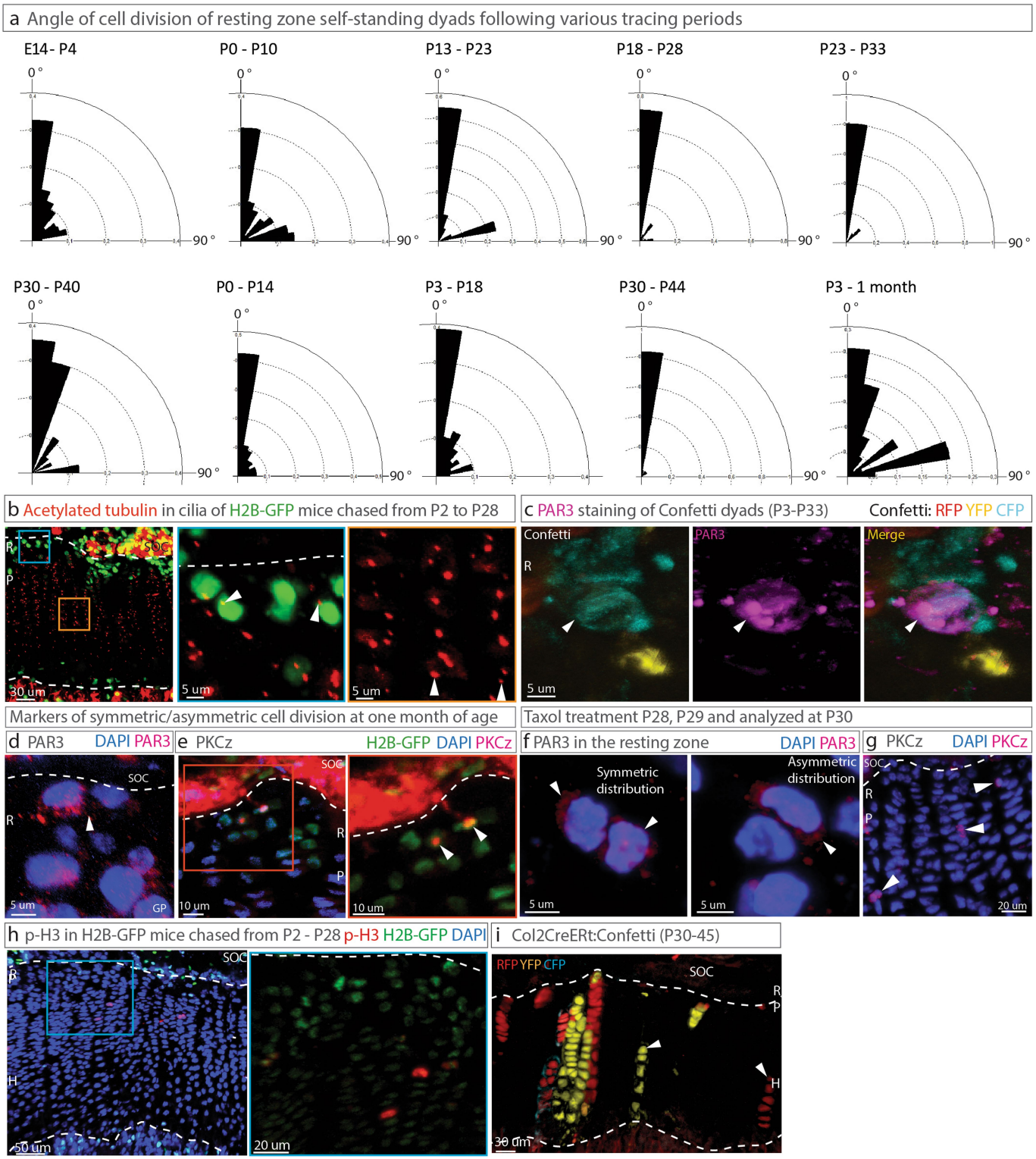

Extended Data Fig. 5 | Orientation of cell divisions in the epiphyseal niche. a, Col2-creERT:*R26R*-Confetti mice were traced as indicated above each plot. The angle between cells in self-standing dyads within the resting zone was measured relative to the longitudinal axis of the bone (2–5 mice per tracing period, with a total of 559 dyads analysed). **b**, H2B-GFP mice were labelled with doxycycline from E14.5 to P2 and chased until P28 to visualize slow-dividing cells (green). Cilia were visualized by immunostaining for acetylated tubulin (arrowheads). **c**, Col2-creERT:*R26R*-Confetti mice were traced from P3 to P33 and immunostained for PAR3. Arrowhead indicates a PAR3-positive clonal dyad. **d**, Growth plates from 28-day-old mice were immunostained for PAR3. **e**, H2B-GFP mice chased as in **b** were immunostained for PKC-ζ. Arrowheads indicate positively stained cells in the resting zone. **f**, **g**, To block spindle degradation, mice were treated with Taxol (10 mg kg^{-1}) for two days before tissue collection at P30 and subsequently immunostained for PAR3 **(f)** or PKC-ζ **(g)**. Arrowheads in **f** highlight even (left panel) and uneven (right panel) distribution of PAR3. Even with Taxol treatment, staining for PKC-ζ in the resting zone was minimal (arrowheads indicate positive cells). **h**, Growth plates from 28-day-old H2B-GFP mice chased as in **b** were stained for phosphorylated histone H3 (p-H3). **i**, Blunted columns (arrowheads) in Col2-creERT:*R26R*-Confetti mice traced from P30 to P45. The dashed lines demarcate the growth plate from surrounding tissues. The resting (R), proliferating (P), hypertrophic (H) zones and SOC are indicated for orientation. Data in **b**, **e**–**h** each represent one experiment (minimum 3 mice per experiment); data in **c**, **d** and **i** represent two independent experiments.

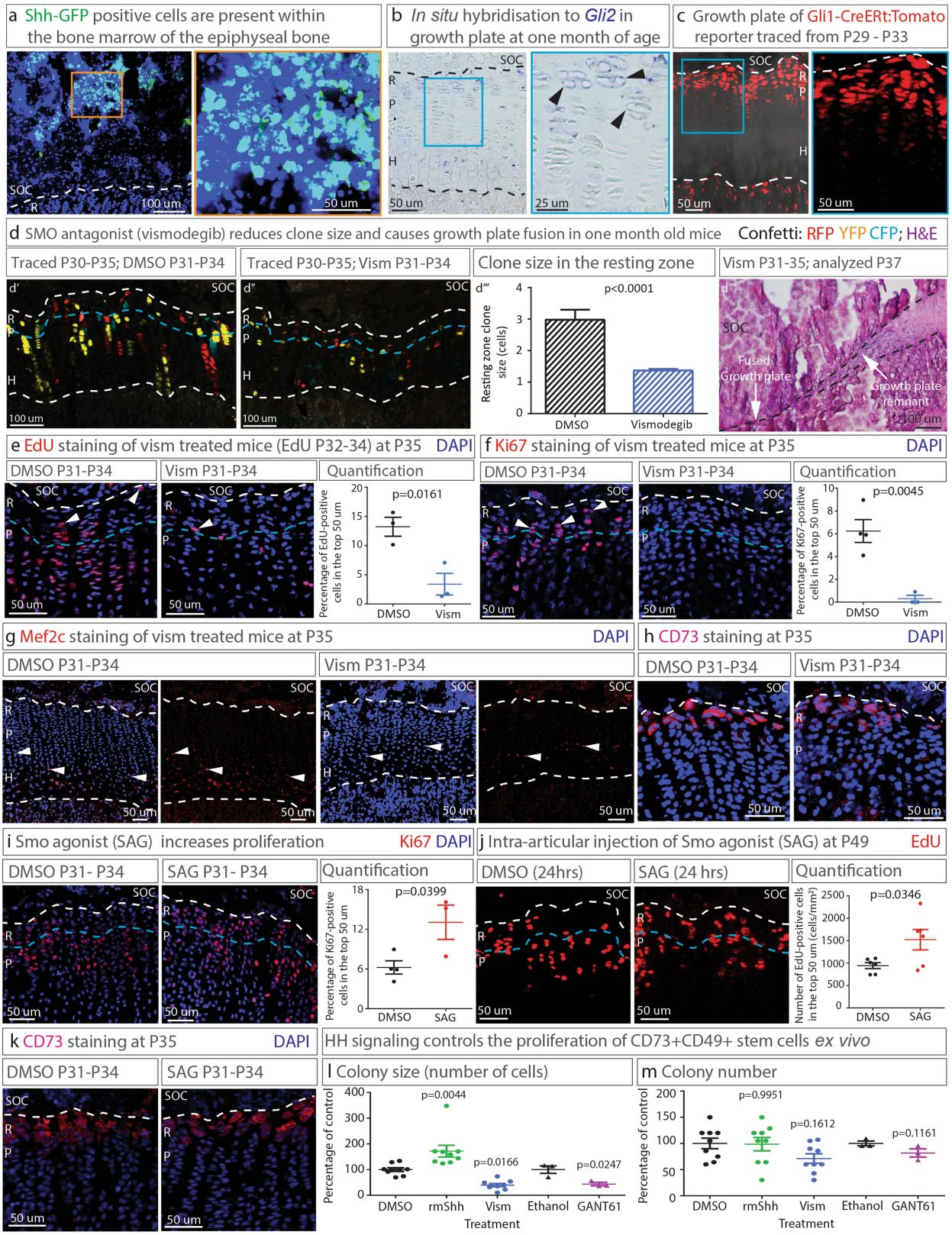

Extended Data Fig. 6 | See next page for caption.

Extended Data Fig. 6 | Indications that hedgehog signalling controls stem cell renewal in the epiphyseal niche. a, Shh-GFP reporter mice revealed Shh expression within the SOC at P30 (blue staining, DAPI). **b**, In situ hybridization for *Gli2* mRNA at P30 (arrowheads point towards typical labelling). **c**, Gli1-CreERT2:tdTomato mice traced from P29 to P33 to reveal Gli1 activity. **d**, Col2-creERT:*R26R*-Confetti mice were traced at P30–P35, and received six injections of either DMSO or the SMO antagonist vismodegib (Vism, 100 mg per kg(body weight) per injection) between P31 and P34. Blue dashed lines indicate the top 50 μm, where the clone size was quantified (**d‴**, mean ± s.e.m., $n = 123$ clones from 8 mice (vismodegib); $n = 49$ from 4 mice (DMSO)). When vismodegib treatment was extended by two extra injections, the growth plate fused at P37 (**d⁗**; haemotoxylin and eosin staining). **e**–**h**, Growth plates from mice treated as in **d′** and **d″** were analysed for proliferation within the top 50 μm (demarcated by blue dashed line) by means of EdU incorporation (**e**; injected daily P32–P34; $n = 4$ for each treatment) and KI67 immunolabelling (**f**; $n = 4$ (DMSO) or 3 (Vism) mice) and for expression of differentiation marker MEF2C (**g**) and stem cell marker CD73 (**h**). Arrowheads in **e**–**g** indicate typical positively-stained cells. **i**, Mice received six doses of either DMSO or SMO agonist (SAG, 25 mg per kg(body weight) per injection) between P31 and P34 and proliferation was analysed by Ki67 immunolabelling at P35 and quantified in the top 50 μm (depicted by blue dashed lines, $n = 4$ (DMSO) or 3 (SAG) mice). **j**, Mice at 7 ± 1 weeks of age received a single intra-articular administration of either SAG or DMSO followed by intraperitoneal EdU injection 4 h later. EdU incorporation was quantified 20 h later in the top 50 μm of the growth plate ($n = 6$). **k**, CD73 was immunodetected in mice treated as in **i**. $CD73^+CD49e^+$ cells were sorted by FACS as in Extended Data Fig. 4a and colony size (**l**) and number (**m**) were assessed following 10 days of culture in the presence of vehicle (DMSO (or ethanol for GANT61)), recombinant mouse sonic hedgehog (rmShh, 1 μg ml^{-1}), vismodegib (1 μM) or the Gli1 inhibitor GANT61 (5 μM). Data in **l** and **m** are mean ± s.e.m., $n = 9$ wells from 3 independent experiments for rmShh and Vism, and $n = 3$ wells from one experiment (GANT61). All white dashed lines demarcate the growth plate. The SOC, the resting (R), proliferating (P) and hypertrophic (H) zones are indicated for orientation. Data in **a** and **j** represent two independent experiments, data in **b**, **c**, **d⁗**, **e** and **k** each derive from one experiment and those in **d′**–**d‴** are pooled from three independent experiments with the number of mice in each experiment indicated above. Plots represent mean ± s.e.m. and were analysed by unpaired two-tailed *t*-test, except the comparison between DMSO, rmShh and Vism groups (**l** and **m**), which was by one-way ANOVA with Tukey's multiple comparisons.

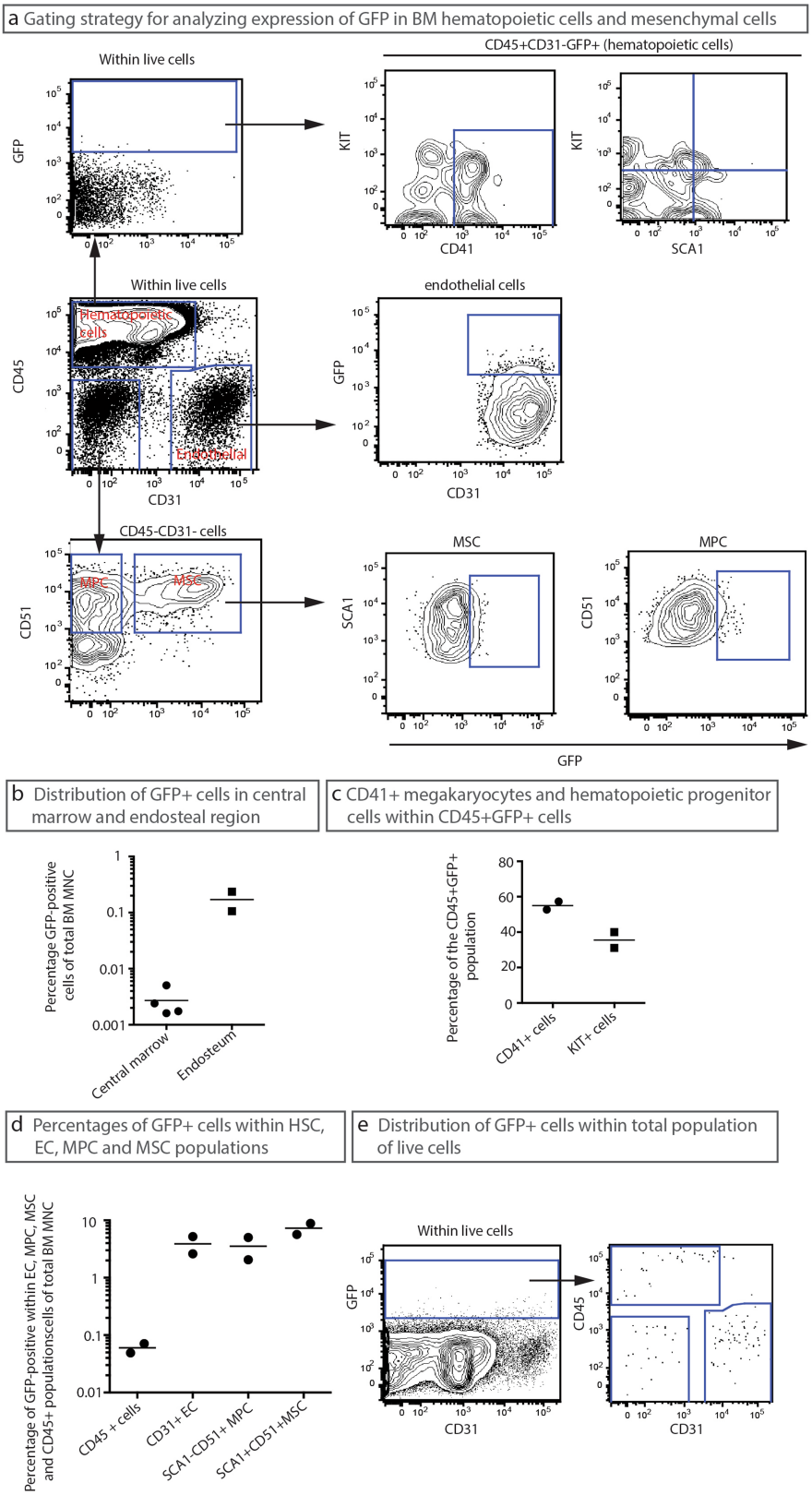

Extended Data Fig. 7 | Identification of Shh-positive cell populations within the bone marrow. a, Representative FACS profile showing gating strategy for analysing expression of Shh–GFP$^+$ cells in bone marrow. The cells were gated within propidium iodide-negative live cells. **b**, Distribution of GFP$^+$ cells in central marrow and endosteal region. The cells from central marrow were obtained by gently crushing bones and the endosteal cells were obtained by enzyme dissociation of bone fragments. **c**, Percentages of CD41$^+$ megakaryocytes and haematopoietic progenitor (KIT$^+$) cells among CD45$^+$GFP$^+$ cells. **d**, Percentages of GFP$^+$ cells within haematopoietic cells (CD45$^+$), endothelial cells (CD31$^+$), mesenchymal progenitor cells (MPC, CD45$^-$CD31$^-$SCA1$^-$CD51$^+$) and MSCs (CD45$^-$CD31$^-$SCA1$^+$CD51$^+$). **e**, Representative FACS profile showing GFP$^+$ cells among total live cells. In **b**–**d**, each data point represents one mouse, and the mean is shown as a line. Two independent analysis were performed for **b**–**e** with at least 3 GFP$^+$ mice for each experiment.

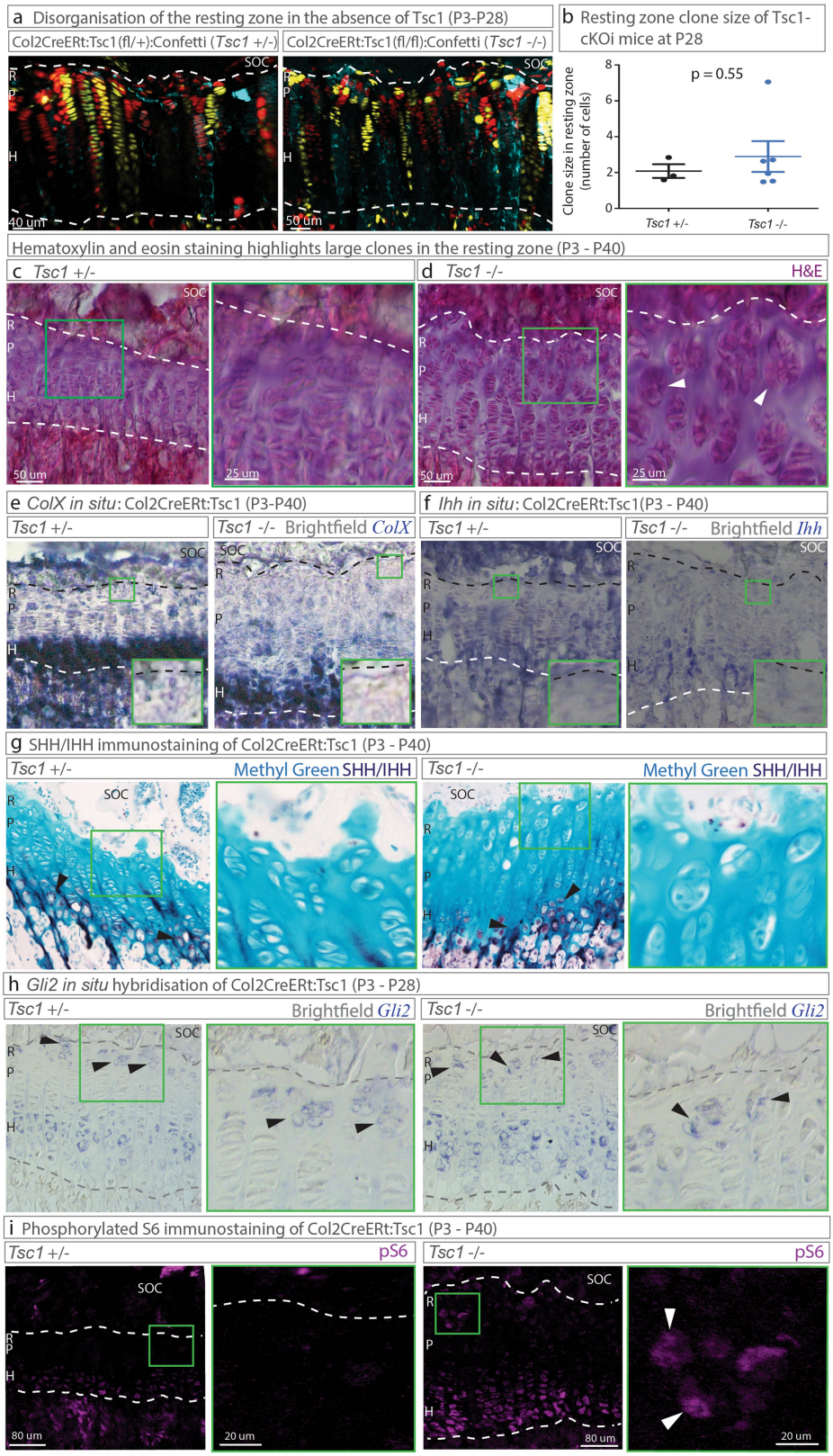

Extended Data Fig. 8 | See next page for caption.

Extended Data Fig. 8 | Postnatal cartilage-specific Tsc1 ablation does not promote hypertrophic differentiation in the resting zone. All Col2-creERT:*R26R*-Confetti:*Tsc1* mice were injected with tamoxifen on P3 and analysed either on P28 (**a**, **b**, **h**) or P40 (**c**–**g**, **i**). The central sections of the tibial growth plates of Col2-creERT:*R26R*-Confetti:$Tsc1^{fl/+}$ ($Tsc1^{+/-}$, left) and Col2-creERT:*R26R*-Confetti:$Tsc1^{fl/fl}$ ($Tsc1^{-/-}$, right) mice were imaged on P28 (**a**) and the clonal size of round cells above the columnar zone quantified with Imaris (**b**; mean ± s.e.m.; $n = 3$ ($Tsc1^{-/+}$) and 6 ($Tsc1^{-/-}$), unpaired two-tailed *t*-test). **c**, **d**, Haemotoxylin and eosin staining of the sections depicted in Fig. 3a, b. Arrowheads indicate typical clusters in the resting zone of $Tsc1^{-/-}$ mice. **e**–**g**, In situ hybridization for *ColX* (**e**) and *Ihh* (**f**), and immunostaining for Shh/Ihh (**g**). Insets in **e** and **f** show a magnified view of the outlined area in the resting zone, showing absence of staining. **h**, In situ hybridization for *Gli2*. **i**, Immunostaining for phosphorylated S6 (readout for mTORC1 activity). Typical positive cells in **g**–**i** are indicated by arrowheads. The dashed lines demarcate the growth plate. The SOC, the resting (R), proliferating (P), and hypertrophic (H) zones are labelled for orientation. Data in **a**, **b** and **i** derive from 2 independent experiments, whereas **c**–**h** represent one experiment with several mice stained at least twice.

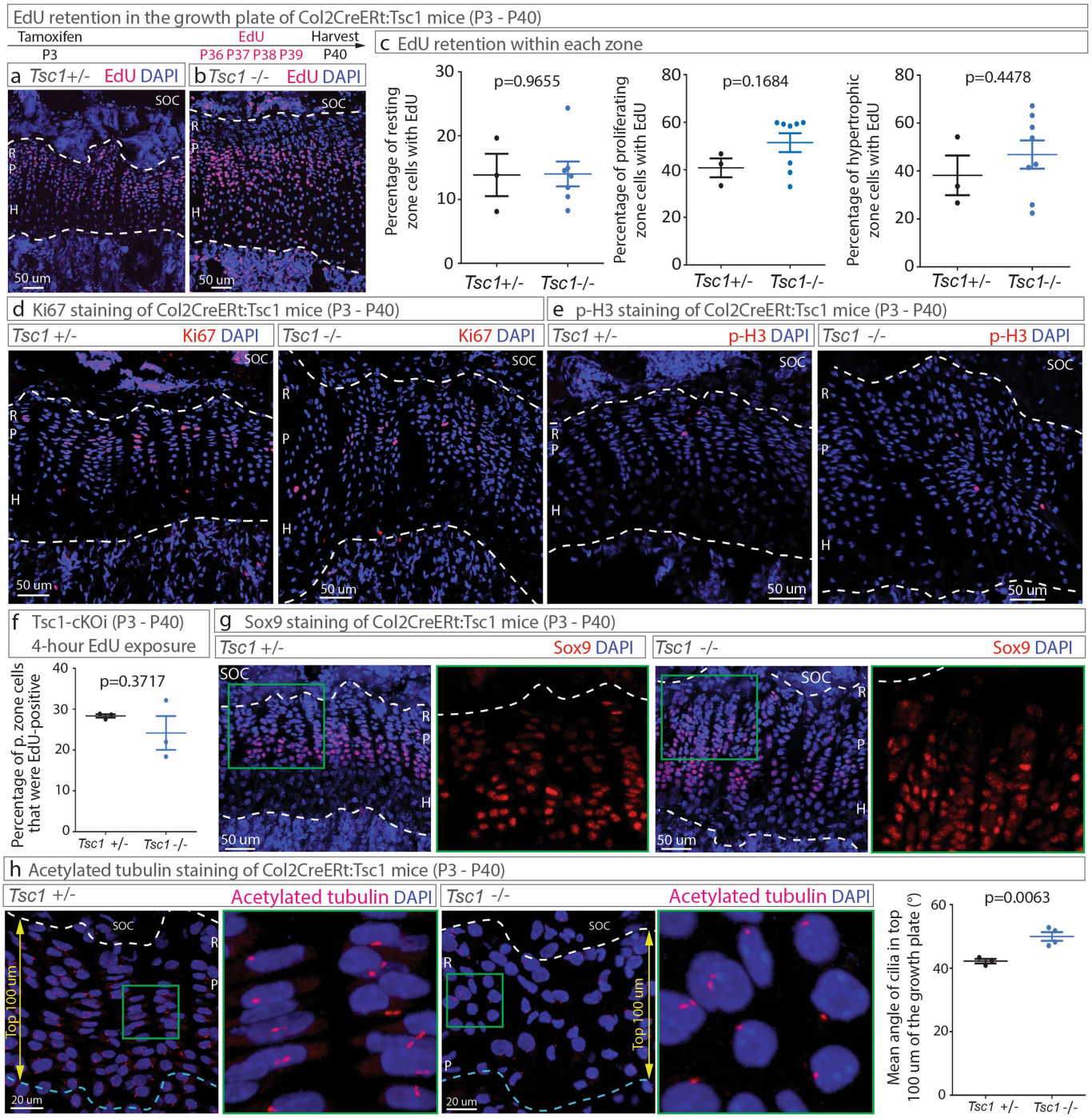

Extended Data Fig. 9 | Postnatal cartilage-specific Tcs1 ablation does not elevate proliferation in the resting zone. One (*Tsc1*$^{+/-}$) or two (*Tsc1*$^{-/-}$) copies of the *Tsc1* gene were deleted in Col2-creERT:*R26R*-Confetti:*Tsc1*-floxed mice by tamoxifen injection on P3, and mice were analysed on P40. **a**–**c**, EdU was injected once daily for four days before tissue collection, and EdU-positive cells in the resting (**c**, left), proliferating (**c**, middle) and hypertrophic (**c**, right) zones were quantified (mean ± s.e.m.; $n = 3$ (*Tsc1*$^{+/-}$) and 7 or 8 (*Tsc1*$^{-/-}$)). **d**, **e**, Immunostaining for Ki67 (**d**) and phospho-histone H3 markers of proliferation (**e**). **f**, Mice were injected with a single dose of EdU 4 h before tissue collection, and the percentage of EdU-positive cells in the proliferating zone was calculated (mean ± s.e.m.; $n = 3$). **g**, Immunostaining for Sox9 (enlarged images on the right of each pair are shown without the DAPI channel, to improve visualization). **h**, Immunostaining for acetylated tubulin (the panels to the right are close up images of a single plane, to aid visualization of the cilia), with the mean angle of cilia in the top 100 μm indicated in the graph (mean ± s.e.m.; $n = 3$ (*Tsc1*$^{+/-}$) and 4 (Tsc1$^{-/-}$)). Counterstaining with DAPI (blue) and two-tailed unpaired *t*-test were used throughout experiments presented. The SOC, resting (R), proliferating (P) and hypertrophic (H) zones are labelled for orientation. The white dashed lines demarcate the growth plate. The blue dashed lines in **h** indicate the top 100 μm of the growth plate. Data from **a**–**e** and **h** each derive from 2 independent experiments, and **f** and **g** are from a single experiment each with $n = 3$ mice.

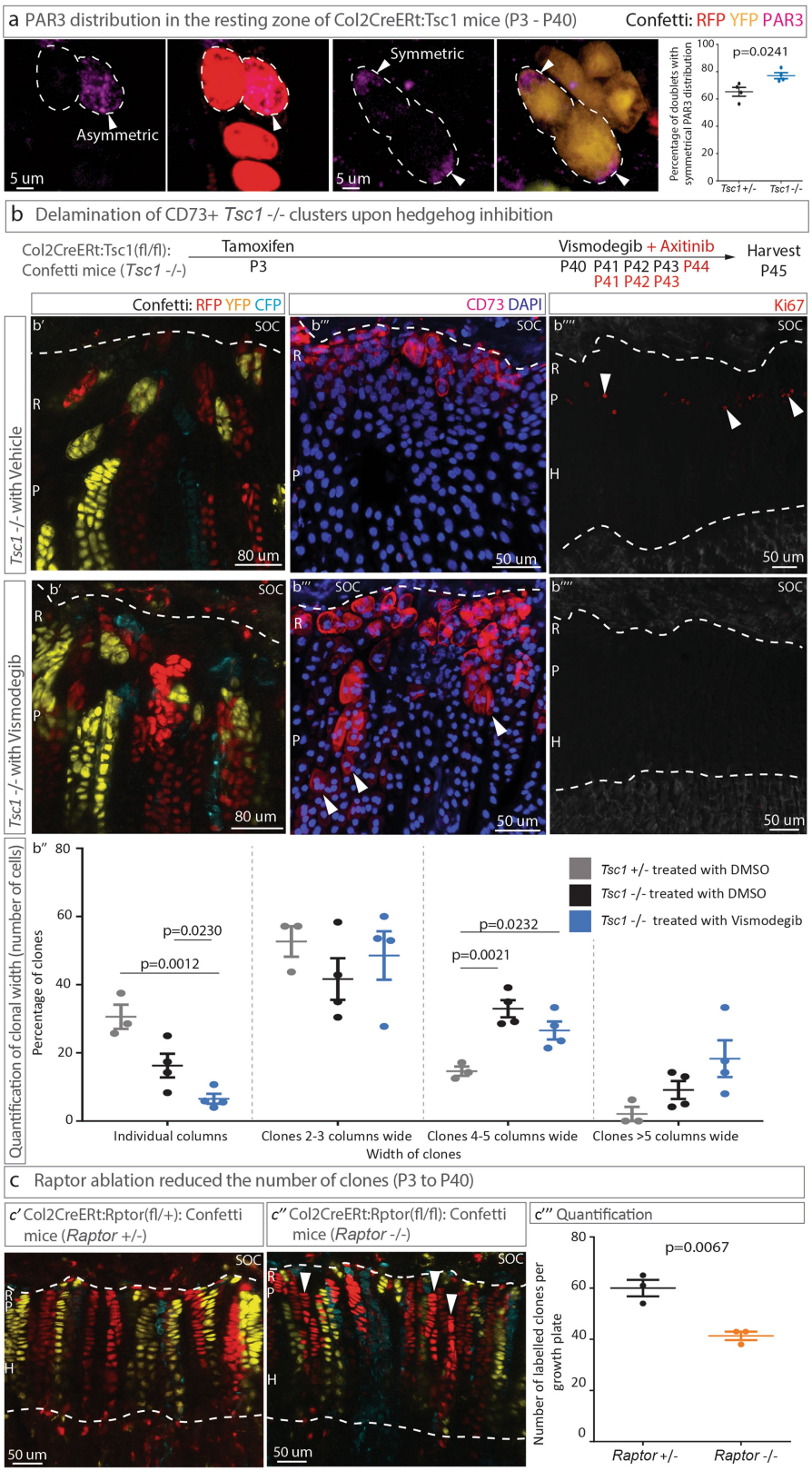

Extended Data Fig. 10 | See next page for caption.

Extended Data Fig. 10 | mTORC1 signalling controls symmetric versus asymmetric division of resting zone cells. a, Immunostaining for PAR3 combined with confocal visualization of Confetti clones in the resting zone of Col2-creERT:*R26R*-Confetti:*Tsc1*$^{fl/+}$ (*Tsc1*$^{+/-}$) or Col2-creERT:*R26R*-Confetti:*Tsc1*$^{fl/fl}$ (*Tsc1*$^{-/-}$) mice injected with tamoxifen at P3 was performed at P40. Representative images for asymmetric and symmetric distribution of PAR3 within clones are shown (arrowheads) and distribution within the resting zone clones was quantified (mean ± s.e.m., $n = 4$ mice; unpaired two-tailed *t*-test). Dashed lines demarcate PAR3–Confetti double-positive dyads. **b**, Tsc1 was ablated by tamoxifen injection on P3, and from P40, mice were given either vehicle (DMSO) or the SMO antagonist vismodegib (8 doses, twice daily) before analysis at P45. All mice were injected daily with axitinib to prevent growth plate fusion. The growth plates were imaged for Confetti proteins (b′), or immunostained for CD73 (**b‴**, arrowheads indicate CD73-positive cells within the proliferative zone) and Ki67 (**b⁗**, arrowheads indicate typical Ki67-positive cells). **b″**, The width of Confetti-labelled clones at 100 μm from the SOC surface was quantified (mean ± s.e.m.; *Tsc1*$^{+/-}$ with DMSO ($n = 3$ mice), *Tsc1*$^{-/-}$ with DMSO ($n = 4$ mice), *Tsc1*$^{-/-}$ with Vism ($n = 4$ mice); one-way ANOVA with Tukey's multiple comparisons). The data derives from 1 (*Tsc1*$^{+/-}$ group) or 3 (*Tsc1*$^{-/-}$ groups) independent experiments. **c**, Col2-creERT:*R26R*-Confetti:*Raptor*$^{fl/+}$ (*Raptor*$^{+/-}$) or Col2-creERT:*R26R*-Confetti:*Raptor*$^{fl/fl}$ (*Raptor*$^{-/-}$) mice received tamoxifen on P3 and were analysed on P40. The clonal pattern revealed blunted columns (arrowheads) and a decreased number of labelled clones within the growth plate of *Raptor*$^{-/-}$ mice as counted at the horizontal midline (**c‴**; mean ± s.e.m., $n = 3$ mice from 1 (*Raptor*$^{+/-}$) or 2 (*Raptor*$^{-/-}$) independent litters; unpaired two-tailed *t*-test). The dashed lines in **b** and **c** demarcate growth plates. The SOC, the resting (R), proliferating (P), and hypertrophic (H) zones are labelled for orientation.